The Thesis Committee for Jorge Andres Navas Guzman, Sr.
Certifies that this is the approved version of the following thesis:

Chemical Enhanced Oil Recovery Simulation in Highly Stratified Heterogeneous Reservoir. A Field Case Study.

APPROVED BY
SUPERVISING COMMITTEE:

Supervisor:

Mojdeh Delshad

Co-Supervisor:

Kamy Sepehrnoori

Chemical Enhanced Oil Recovery Simulation in Highly Stratified Heterogeneous Reservoir. A Field Case Study.

by

Jorge Andres Navas Guzman, Sr.

Thesis

Presented to the Faculty of the Graduate School of

The University of Texas at Austin

in Partial Fulfillment

of the Requirements

for the Degree of

Master of Science in Engineering

The University of Texas at Austin

December 2019

Dedication

To my **Lord JESUS**, my beautiful and brave wife **Claudia** and my beloved kids **Martina**, **Julieta** and **Esteban**.

Acknowledgements

I am truly grateful with Dr. Delshad for her valuable support as my supervisor during the last two years. I am thankful for her confidence in my capabilities, her accurate technical advices, her helpful attitude and kindness. I would also like to express my sincere gratitude to my co-supervisor Dr. Sepehrnoori. From the first day he has shown me his willingness and availability to answer any doubt. His patient and calm teach me to put in practice these qualities in my life. Additionally, I am really thankful to Dr. Fernandes and his company for supplying the UTCHEMRS simulator at the requirements of the original sector model. His relevant contribution has made this research possible. I gained great practice and understanding through his recommendations for my research work. His collaborative attitude is admirable and greatly appreciated.

From the bottom of my heart I want to express my special appreciation to my dear wife Claudia. This academic achievement belongs to her as well. This work would not have been possible without her priceless help, her courage to accept this challenge and her encouragement during difficult times. To my beautiful children Martina, Julieta and Esteban all my love and gratitude for keeping me strong and happy with their joy and innocence. Additionally, I would like to recognize my incredible parents Alcibiades and Clara for their continuous encouragement to pursue my dreams. To my sister Daisy and my brothers Oscar, Alcibiades and Luis all my gratitude and love.

I am thankful with the staff of the Hildebrand Department of Petroleum and Geosystems Engineering. Specially, I have gratitude to Amy Stewart for her willingness to help. As my graduate coordinator she facilitated our life in Austin as family of an international student.

I would also like to recognize Fabio Bordeaux, Mehran Mehrabi, Mauricio Fiallos, Jose Salazar and Hector Barrios for their helpful collaboration, knowledge and assertive comments for my work and my research. I would also to express my gratitude to my friends in Christ for their priceless and wisdom advices, their inspiration and words of encouragement which keep me firm in my faith in GOD.

Finally, I am truly grateful with my employer who decided to believe in me through this great investment in my career and the future of my family. This opportunity has marked my life positively. Thanks.

Abstract

Chemical Enhanced Oil Recovery Simulation in Highly Stratified Heterogeneous Reservoir. A Field Case Study.

Jorge Andres Navas Guzman, Sr., MSE

The University of Texas at Austin, 2019

Supervisor: Mojdeh Delshad

Co-Supervisor: Kamy Sepehrnoori

Oil and gas companies are looking for proven hydrocarbon reserves from their existent drained reservoirs with the objective to extend the production and economical life of their fields. The chemical enhanced oil recovery (CEOR) has raised with a myriad type of process that goes beyond the primary and secondary recovery. The polymer flooding (PF) is a widely applied process in reservoirs with low swept efficiency after the water flooding (WF) process. Colombian field has one of the first polymer pilots in the region with positive results of oil recovery in "A" sands. Thus, the operator is interested in the expansion of PF for the same reservoir and even in deeper reservoir sands.

This thesis focuses in the evaluation of different scenarios of PF and surfactant polymer flooding (SPF) for the producer layers A and B with a mechanistic model, thus obtaining new recommendations for the recovery strategy in the field. Therefore, a sector model was constructed from a full field commercial simulator to the in-house simulator:

UTCHEMRS. In addition, this sector model was migrated to a second commercial simulator allowing a performance comparison for three simulators. UTCHEMRS model was validated with the commercial simulators through the history matching (HM) phase. The primary and waterflood history match was in agreement with the field data.

Simulation results suggested that PF for the base case in "A" sands presented an incremental oil recovery of up to 12% additional to water flooding. Additionally, PF was extended to the lower layer "B" sand to investigate the potential of polymer injection. The PF injection in both reservoirs simultaneously loses swept efficiency and decreases the oil recovery in 3%. However, a hypothetical case of new infill producer wells with the objective of testing the individual reservoir performance has revealed that PF is having important raises in oil recovery for B sands as well. Though, further research should be developed in order to strengthen this interpretation.

Finally, the results of SPF case for A sands are inconclusive because a laboratory tests of surfactant phase behavior is needed to ensure the lowest IFT in reservoir conditions.

Table of Contents

List of Tables xii

List of Figures xiv

Chapter 1. Introduction 1

1.1 Objective 1

1.2 Limitations 2

1.3 Description of chapters. 2

Chapter 2. Literature Review 4

2.1 Rheology of Fluids 4

2.2 Enhanced Oil Recovery (EOR) 5

2.2.1 Mobility Ratio 5

2.2.2 Capillary Number 6

2.3 Definitions of Efficiency in Polymer Injection 7

2.4 Polymer Injection In a Heterogeneous Sandstone Reservoir 9

2.5 Capillary Number And Interfacial Tension 11

2.6 Surfactant 12

2.7 Surfactant Polymer (SP) – Flooding 15

Chapter 3. Field Background and Polymer Pilot Context 16

3.1 Colombian Field 16

3.1.1 Reservoir Characterization 16

3.1.2 Field History 19

3.2 Polymer Pilot Background 19

3.1.2 Polymer Features 21

3.2.2 Injectors Condition 22

3.2.3 Reservoir heterogeneity 23

3.2.4 Challenges of PF to Overcome and Initial Results of Polymer Pilot 24

Chapter 4. Base Model and Methodology 26

4.1 Sector Model 26

4.2 Methodology 28
Step 1. Migration of the base case to UTCHEMRS 28
Static and dynamic model migration 29
Polymer viscosity dependence at shear rate 33
Polymer adsorption 35
Step 2. History Match models 36
Step 3. Water Flooding HM and Base Case Forecast 39
Step 4. Polymer Flooding Base Case Forecast in A2 and A2i 42
Step 5. Perform scenario for polymer injection in A2, A2i, B2c, and B2d. 42
Step 6. Comparison of oil recovery performance of PF for A and B sands 45
Step 7. Base case Simulation for surfactant polymer injection 47
Step 8. Evaluate and compare the results 56
Chapter 5. Results and Discussions 57
5.1 Polymer Flooding in A Sands 57
5.1.1 Base case forecast in A2 and A2i sands 57
5.2 Polymer Flooding in A and B Sands 62
5.2.1 Base case forecast in A2, A2i, B2c and B2d sands. 63
5.3 Polymer Flooding Performance in A sands versus B sands 70
5.3.1 Results 71
5.3.2 Discussion 74
5.3.2.1 Well 443 75
5.3.2.2 New infill wells 79
5.4 Surfactant Polymer Flooding in A Sands 88
5.4.1 Base case forecast in A2 and A2i sands 88
5.4.1.1 Well 1159 analysis 91
5.4.1.1 Well 01PO analysis 95
5.5 Economical Evaluation For Base Cases with PF and SPF. 98
5.5.1 Polymer flooding base case evaluation 99
5.5.2 Surfactant Polymer flooding base case evaluation 101

Chapter 6. Conclusions and Future Work....104
6.1 Summary and Conclusions....104
6.2 Future Work....106
Glossary....107
Nomenclature/ Abbreviations....107
SI Metric Conversion Factors....108
Bibliography....109

List of Tables

Table 3.1. Rock properties of A, B and C sands and sub sands of A in Colombian Field 18
Table 3.2. Polymer properties – Flopaam 5115 22
Table 4.1. Relative permeability parameters for RT 1, 2 and 3. 32
Table 4.2. Relative permeability parameters for RT 4 33
Table 4.3. Comparative oil volumes at January 2018 what time. 39
Table 4.4. Comparative oil volumes HM and forecast simulations for WF as of December 2023. 42
Table 4.5. Rock properties of A, B and C sands and sub sands of B in Colombian Field 43
Table 4.6. Reservoir and fluid data for A and B reservoirs. 45
Table 4.7. Injection rates for A and B sands. 47
Table 4.8. Surfactant retention parameters. 48
Table 4.9. Microemulsion viscosity parameters 49
Table 4.10. Capillary desaturation parameters for phases 1, 2 and 3. 51
Table 4.11. Surfactant phase behavior parameters. 54
Table 4.12. Chun Huh IFT parameters. 55
Table 4.13. Parameters of the SP injection sequence. 56
Table 5.1. Comparative PF oil volumes forecast for each simulator as of December 2023 59
Table 5.2. Comparative PF oil volumes forecast for ECLIPSE as of December 2023. 60

Table 5.3. Comparative PF oil volumes forecast for INTERSECT as of December 2023.....61
Table 5.4. Comparative PF oil volumes forecast for UTCHEMRS as of December 2023.....62
Table 5.5. Comparative oil volumes for to PF in A vs. both A and B sands as of December 2023. 64
Table 5.6. Oil recovery by Well 443 associated to PF in cases Only A sands versus Only B sands as of December 2023. 71
Table 5.7. Oil recovery by Well NW01 associated to PF in cases Only A sands versus Only B sands as of December 2023. 72
Table 5.8. Oil recovery by Well NW02 associated to PF in cases Only A sands versus Only B sands as of December 2023. 73
Table 5.9. Oil recovery by Well NW04 associated to PF in cases Only A sands versus Only B sands as of December 2023. 74
Table 5.10. Comparative oil volumes for PF vs. SPF base case in A sands as of December 2023. 90
Table 5.11. Parameters for the NPV calculation for the base case of PF. 99
Table 5.12. NPV results for different crude oil prices. 101
Table 5.13. Parameters for the NPV calculation for the base case of SPF. 101
Table 5.14. NPV results per crude oil scenario. 103

List of Figures

Figure 2.1 Different type of shear/stress rate behavior found in polymer fluids (Sorbie, 1991). 5

Figure 2.2. Schematic diagram comparison in a five-spot pattern between (a) areal sweep with water (b) areal sweep with polymer.....8

Figure 2.3. Schematic diagram of the improvement in vertical sweep efficiency caused by polymer flooding at different permeabilities (from Sorbie, 1991). (a) Water injection profile, (b) Polymer injection profile y (c) Schematic of crossflow phenomena.....10

Figure 2.4. Capillary desaturation curve for Berea sandstone (normalized residual oil saturation vs. capillary number). (From Chatzis and Morrow, 1984.)11

Figure 2.5. Schematic of the microemulsion phase behavior according to Winsor (1954).....13

Figure 2.6. Interfacial tensions and solubilization parameters (Reed and Healy, 1977). 14

Figure 3.1. Location map of Colombian Field (modified from Gheneim et al, 2017) 16

Figure 3.2. Illustration of: (a) seismic profile and (b) field division of Colombian Field (modified from Gheneim et al, 2017).....17

Figure 3.3. Log profile example of well in Colombian field. (a) A formation (b) B and C formations. (2017).....18

Figure 3.4 Location of each well of the polymer pilot pattern at A2 formation....21

Figure 3.5. Well 1292 (a) Target of injection zone (b). Injection rate, pressure and polymer concentration. 23

Figure 4.1. Illustration of the sector model in Block VI. (a) Layers are displayed vertically (b) Polymer pilot area 27
Figure 4.2 Flowchart of the proposed methodology. 28
Figure 4.3. Grid properties migrated to UTCHEMRS. (a) Porosity (fraction) (b) Pressure (kPa) (c) Permeability (mD) (d) Water saturation (fraction).30
Figure 4.4. Relative permeability curves of rock type 1, 2, and 3. 31
Figure 4.5. Relative permeability curves of rock type 4. 32
Figure 4.6. Model of polymer viscosity behavior (a) Polymer concentration at 500 ppm with reservoir water (b) Polymer concentration at 1000 ppm with injection water. 35
Figure 4.7. Polymer adsorption plot based on the lab results. 36
Figure 4.8. Liquid rate History Match comparison. 37
Figure 4.9. Oil rate History Match comparison. 37
Figure 4.10. Cumulative Oil recovery during the HM. 38
Figure 4.11. Liquid rate for base case WF. 40
Figure 4.12. Oil rate for base case WF. 41
Figure 4.13. Cumulative oil recovery for base case WF. 41
Figure 4.14. Schematic comparison of the activate at different depths (a) Active wells at A sands (b) Active wells at B sands. 44
Figure 4.15. Schematic of the new wells for the selective polymer injection in A or B sands. Map at A sands depth. 46
Figure 4.16. Solubilization ratio vs. salinity with 50% oil volume. 54
Figure 4.17. SPF sequence. 56
Figure 5.1. Liquid rate for base case PF. 57
Figure 5.2. Oil rate for base case PF. 58

Figure 5.3. Cumulative oil recovery for base case PF. 58
Figure 5.4. Comparative results of WF vs PF simulation of ECLIPSE. (a) Oil rate (b) Liquid rate (c) Oil cumulative (d) Water cut 60
Figure 5.5. Comparative results of WF vs PF simulation of INTERSECT. (a) Oil rate (b) Liquid rate (c) Oil cumulative (d) Water cut.....61
Figure 5.6. Comparative results of WF vs PF simulation of UTCHEMRS. (a) Oil rate (b) Liquid rate (c) Oil cumulative (d) Water cut.....62
Figure 5.7. Polymer concentration injected in A and B sands (a) Polymer concentration at March 2018 (b) Polymer concentration as of December 2023.....64
Figure 5.8. Oil rate comparison between PF in A sands and PF in both A and B sands. 65
Figure 5.9. Comparative results of WF vs PF simulation of UTCHEMRS. (a) Oil rate (b) Water cut (c) cumulative Oil (d) Oil cut 66
Figure 5.10. Comparative results at Sept. 2022. (a) Water saturation map for A sands (b) Water saturation map for B sands. 67
Figure 5.11. Comparison of liquid production of Well 417. 68
Figure 5.12. Comparative results at Sept 2022. (a) Pressure (kPa) map at A sands (b) Pressure (kPa) map at B sands. 69
Figure 5.13. Location map of evaluation case for comparing performance A vs. B (a) Area location at A sands (b) Area location at B sands. 70
Figure 5.14. Performance comparison of WF vs PF in Well 443. (a) Oil rate only in A sands (b) Oil rate only in B sands (c) Cumulative oil only in A sands (d) Cumulative oil only in B sands.....71

Figure 5.15. Performance comparison of WF vs PF for Well NW01. (a) Oil rate only in A sands (b) Oil rate only in B sands (c) Cumulative oil only in A sands (d) Cumulative oil only in B sands 72
Figure 5.16. Performance comparison of WF vs PF in Well NW02. (a) Oil rate only in A sands (b) Oil rate only in B sands (c) Cumulative oil only in A sands (d) Cumulative oil only in B sands 73
Figure 5.17. Performance comparison of WF vs PF in Well NW04. (a) Oil rate only in A sands (b) Oil rate only in B sands (c) Cumulative oil only in A sands (d) Cumulative oil only in B sands 74
Figure 5.18. Simulation maps for case “Only A sands” (a) Polymer concentration at 03-2018 (wt%) (b) Polymer concentration at 12-2023 (wt%) (c) S_w at 03-2018 (d) S_w at 12-2023 (c) Pressure at 03-2018 (kPa) (d) Pressure at 12-2023 (kPa).....76
Figure 5.19. Comparison of water cut of the Well 443. 77
Figure 5.20. Simulation maps for case “Only B sands” (a) Polymer concentration at 03-2018 (wt%) (b) Polymer concentration at 12-2023 (wt%) (c) S_w at 03-2018 (d) S_w at 12-2023 (c) Pressure at 03-2018(kPa) (d) Pressure at 12-2023 (kPa).....78
Figure 5.21. Water saturation maps for Only A at 03-2018 (a) Surface view at A sands for WF (b) Surface view at A sands for PF (c) Cross-section SE-NW for WF (d) Cross-section SE-NW for PF 80
Figure 5.22. Water saturation maps for Only A at 12-2023 (a) Surface view at A sands for WF (b) Surface view at A sands for PF (c) Cross-section SE-NW for WF (d) Cross-section SE-NW view for PF. 81

Figure 5.23. Water cut plots for WF vs PF only A sands (a) Well NW01, (b) Well NW02F, (c) Well NW04.....82
Figure 5.24. Vertical view maps for Only A at 12-2023 (a) Polymer concentration (b) Water saturation for PF.....83
Figure 5.25. Water cut plots WF vs PF only B sands (a) Well NW01 (b) Well NW02F (c) Well NW04.....85
Figure 5.26. Water saturation maps for Only B at 05-2018 (a) Surface view at B sands for WF (b) Surface view at B sands for PF (c) Cross section SW-NE for WF (d) Cross section SW-NE for PF.....86
Figure 5.27. Water saturation maps for Only B at 12-2023 (a) Surface view at B sands for WF (b) Surface view at B sands for PF (c) Cross section SW-NE for WF (d) Cross section SW-NE for PF.....87
Figure 5.28. Vertical view maps for Only A at 12-2023 (a) Water saturation for PF (b) Polymer concentration.....88
Figure 5.29. Liquid rate for base case PF vs SPF. 89
Figure 5.30. Oil rate for base case PF vs SPF.....89
Figure 5.31. Cumulative oil recovery for base case PF vs SPF.....90
Figure 5.32. Well 1159 comparison PF vs SPF (a) Oil rate (b) Water cut. 91
Figure 5.33. Water cut comparison and ME rate 92
Figure 5.34. (a) ME saturation at Nov 2022 (b) Cross-section SW-NE with ME saturation between wells 1222 and 1159. 93
Figure 5.35. Vertical view of permeability in z direction.....94
Figure 5.36. Optimum water salinity and water salinity of Well 1159.....95
Figure 5.37. Oil rate comparison of PF vs SPF and ME rate for Well 01PO. 95
Figure 5.38. Oil rate comparison of PF vs SPF and ME rate for Well 01PO. 96

Figure 5.39. Oil saturation maps at A sands (a) 0.013 PVI (b) 0.016 PVI (c) 0.017 PVI (d) 0.018 PVI (e) 0.021 PVI (f) 0.025 PVI. 97
Figure 5.40. West Texas Intermediate (WTI) crude oil price and NYMEX confidence intervals (U.S. EIA, 2019) 98
Figure 5.41. Net cash flow plot for PF base case with crude oil price of 55 USD/Bbl 100
Figure 5.42. Net cash flow comparison for crude oil price of 70, 55 and 30 USD/ Bbl. 100
Figure 5.43. Net cash flow plot for SPF base case with crude oil price of 55 USD/Bbl 102
Figure 5.44. Net cash flow comparison at a crude oil price of 70, 55 and 30 USD/Bbl. 103

Chapter 1. Introduction

Chapter 1 describes the objective of this thesis, limitations and briefly explains the content of each chapter developed in this work.

1.1 OBJECTIVE

Since the 1970's the global consumption of oil has begun to rise dramatically because its particular properties positioned this fossil fuel as a high energy density source in comparison with other energy sources (Bryce, 2010). The scarcity of new discoveries of conventional oil reservoirs and the ambitious task of meeting the growing energy demand has led to the search for novel technologies to improve oil recovery from the existing mature oil fields. As a result, during this same decade, Enhanced Oil Recovery (EOR) began to be applied as a series of advanced technologies that improve the oil production by lowering the mobility ratio (M) and/or the Interfacial Tension (IFT).

Throughout the history of Enhanced Oil Recovery (EOR) technology the injection of polymer has played an unquestionable role as an effective method of improving the mechanism(s) to extract oil from the oil reservoirs. This improved process is usually applied after the secondary recovery method, such as Water Flooding (WF). The characteristics of polymer are well-known in EOR industry. For instance, the viscosity increase of the driving phase (water) improves the sweep efficiency and the mobility control. Consequently, the polymer displacement of the oil phase behaves like a piston sweep, increasing positively the effectiveness of the drive. In this work, the successful pilot of Polymer Flooding (PF) implemented in a heterogeneous reservoir called "A sands" is used as the basis for the optimization of production through EOR methods in A and B reservoirs.

The Colombian Field has one of the PF pilots with positive results in the area of Mid-Magdalena Valley Basin. After four years of continuous polymer injection in four injectors, this pilot has generated possibilities to evaluate the prospects of expansion and/or the implementation of this technology in another reservoir known as "B sands." The main objective of this thesis is to

evaluate different scenarios of PF in the producing layers A and B. In addition, evaluate a scenario of Surfactant Polymer Flooding (SPF) with a mechanistic reservoir simulator, thus obtaining new recommendations for the recovery strategy in the field. The results of these scenarios were evaluated to recommend the most prospective and reliable plan of EOR expansion and/or implementation.

1.2 LIMITATIONS

The constraints and assumptions considered in this work are documented to avoid inaccurate generalizations.

- The geological and petrophysical models employed in this thesis were taken from the Colombian company interpretation. Thus, this work relies on the accurate interpretation of these models.
- The PVT properties of A and B sands are used from the previous fluid model defined in the operator company.
- The current version of UTCHEMRS 2019.2 can only simulate dead oil when using its adaptive implicit and corner point schemes. Subsequently, the gas phase is not included in the scenarios presented in this work.

1.3 DESCRIPTION OF CHAPTERS.

There are six chapters in this thesis. Chapter 2 gives an EOR introduction and provides a contextualization of PF and SPF processes; this background will be useful for the later chapters. Chapter 3 describes the Colombian Field in terms of location, brief history, and reservoir characterization. Additionally, this chapter shows the current polymer pilot characteristics, the pattern configuration and the heterogeneity aspects related to the reservoirs related to this pilot. Chapter 4 shows details of the sector model used for the forecast scenarios and presents seven steps for the methodology applied to generate the different scenarios and the comparisons given in the next chapter. Chapter 5 provides the results and comparisons and suggests the best scenarios

to maximize the production in a cost-efficient manner. Finally, Chapter 6 presents the conclusions and recommendations for future implementations of EOR technology in the Colombian Field.

Chapter 2. Literature Review

Chapter 2 contextualizes the main and basic concepts about Enhanced Oil Recovery (EOR) associated with polymer and surfactant polymer flooding. The purpose of this section is to offer a theoretical background for the next chapters.

2.1 Rheology of Fluids

Rheology of fluids is the study of the deformation behavior of solid materials and liquids under stresses coming from external forces (Schowalter, 1977). For some fluids (example oil or water), the relation between the shear stress and the deformation fluid rate is constant. These fluids are called Newtonian Fluids (Sorbie, 1991) given by.

$$\tau = \mu\left(\frac{dV}{dr}\right) = \mu\gamma \tag{2.1}$$

where $\left(\frac{dV}{dr}\right) = \gamma$ = shear stress and μ is the constant viscosity

On the other hand, there are also non-Newtonian fluids. Myriad types of fluids such as polymers solutions, soap solutions, pastes, emulsions and suspensions belong to this group. These fluids have high molecular weights and their apparent viscosities changes with the shear stress applied to the liquid (Bird, 2002):

$$\tau = \eta\left(\frac{dV}{dr}\right) \tag{2.2}$$

where η is the viscosity which is a function of shear stress (not constant).

The non-Newtonian fluids are divided in three groups: *pseudoplastic* or shear thinning, which is the classification for polymer solutions, are fluids where the apparent viscosity decreases when the shear stress increases. *Dilatant* or shear thickening has the exactly opposite behavior of the pseudoplastic fluids; the apparent viscosity increases as shear stress increases. Finally, the *Bingham fluids* behave as a solid until the shear stress applied to the material is greater than the threshold τo known as minimum yield stress (Sorbie, 1991). The diagram below shows the relation between shear stress τ and shear rate or rate of deformation.

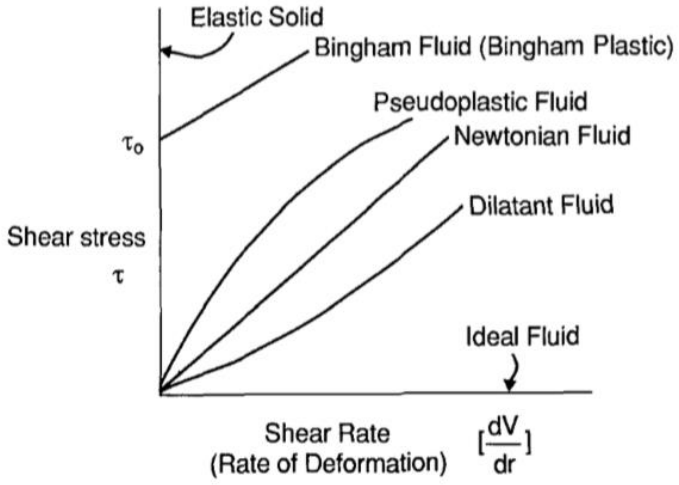

Figure 2.1 Different type of shear/stress rate behavior found in polymer fluids (Sorbie, 1991).

2.2 ENHANCED OIL RECOVERY (EOR)

EOR refers to the oil recovery with the aid of fluids not originally present in the reservoir (Lake, 2014). These injected fluids interact with the rock and/or fluid of the reservoir to create a favorable context for oil extraction to the surface (Green & Willhite, 1998). Therefore, the main purpose of the EOR application is to mobilize the residual oil remaining in the swept zone (Morrow, 1979) to increase the oil recovery factor and consequently to increase the economic and productive life of the reservoirs. The additional oil production achieved through two critical objectives: lower the mobility ratio (M) by adding polymer to injection water and/or increase the Capillary Number (N_c) by adding surfactant and lowering the interfacial tension between oil/water.

2.2.1 Mobility Ratio

The concept of mobility of the fluid phase (λ) is defined by the ratio of permeability of the porous media and the viscosity ratio of the phase (k_i/μ_i) (Lake, 2014). Consequently, the mobility ratio (M) is the relation between two mobilities. In this case, M is the mobility of the driving phase (water) divided by the mobility of the fluid being displaced (oil), (Green & Willhite, 1998).

$$M = \frac{\lambda_w}{\lambda_o} = \frac{\mu_o k_w}{\mu_w k_o} \tag{2.3}$$

Methods, like polymer flooding seek to decrease the mobility ratio (M) of the displacing water phase by increasing its viscosity. The efficiency of the displacement is reached when M is close to one, which intrinsically is when the viscosity of the displacing phase increases. (Zhang, 2007).

2.2.2 Capillary Number

After the process of waterflooding, there are oil spots left behind by capillary forces. This percentage of upswept oil is known as residual oil saturation (ROS) (Green & Willhite, 1998). The bypassed oil is disconnected from the other oil spots (ganglia). Some methods of EOR, such as Surfactant or Alkali, are used with the goal of mobilizing the residual oil trapped by increasing the balance of viscous and capillary forces between the oil and water phases (Sorbie, 1991). The capillary number N_c is the ratio of viscous forces to capillary forces (Chatzis and Morrow, 1984; Hu Guo et al, 2015). In other words, it is the product of superficial velocity (v) and viscosity (μ) of the displacing/wetting phase divided by the interfacial tension (IFT) between the displaced and displacing phases – IFT (σ) (Green & Willhite, 1998).

$$N_c = \frac{v\mu}{\sigma} \tag{2.4}$$

The increase of capillary number would mobilize the trapped oil (Sorbie, 1991). Therefore, there is a relationship between N_c and displacement efficiency (Morrow, 1979). The addition of detergents or surfactants to the injection water phase reduces the IFT (Sheng, 2013). As a result, it mobilizes oil trapped by capillary forces. In Section 2.4 this topic will be explained with more details.

According to the previous paragraphs, the remaining oil is the movable crude that "remains" in the pores after a primary or secondary recovery; the ROS is the unmovable crude due to capillary forces that it cannot be extracted by conventional methods. Polymer flooding is mainly affect the remaining oil due to the improvement in the mobility ratio instead of Capillary number (Needham and Doe, 1987).

2.3 Definitions of Efficiency in Polymer Injection

The polymer injection is a displacement process. In order to evaluate the effectiveness of the process it is necessary to measure the reservoir volume contacted by the displacing fluid including the polymer. (Green & Willhite, 1998). The recovery efficiency (E_R) is represented as the product of volumetric displacement efficiency (macroscopic) (E_v) and the microscopic displacement efficiency (E_D) (Lake, 2014):

$$E_R = E_v E_D \text{ or } E_R = E_A E_I E_D \quad (2.4)$$

Since the addition of polymer to the driving phase decreases its mobility ratio, this reduction influences positively the oil recovery in three different efficiencies: areal and vertical sweep efficiencies and displacement efficiency (Lake, 2014).

The E_v is defined as the product of areal (E_A) and vertical (E_I) sweep efficiencies, which are firmly influenced by the mobility ratio (Green & Willhite, 1998) (Sorbie, 1991) (Lake, 2014) and related to each other (Lake, 2014). The ratio between the swept area by the total reservoir area is the definition of E_A (Green & Willhite, 1998).

$$E_A = \frac{Area\ swept}{Total\ Reservoir\ area} \quad (2.5)$$

The inefficiency in the displacement process is denoted by the case when the viscosity of the displaced phase is larger than the displacing phase viscosity. As a result, the bypassed oil is evidence of poor areal sweep (Sorbie, 1991) due to viscous fingering. The "fingering" is the displacement instability where the less viscous fluid creates "fingers" trying to penetrate the most viscous fluid (Homsy, 1987). The water-soluble polymer addition to the displacing phase (higher viscosity) improves the areal sweep efficiency stabilizing the areal flood (E_A) due to the enhancement (reduction) of the mobility ratio (M) (see Figure 2.2 below). In addition, E_A is also related to the allocation pattern (Sorbie, 1991) (Slater and Farouq Ali, 1970) (Lake, 2014) and the relevant quantitative differences of reservoir permeability (heterogeneity) (Bordeaux, 2016).

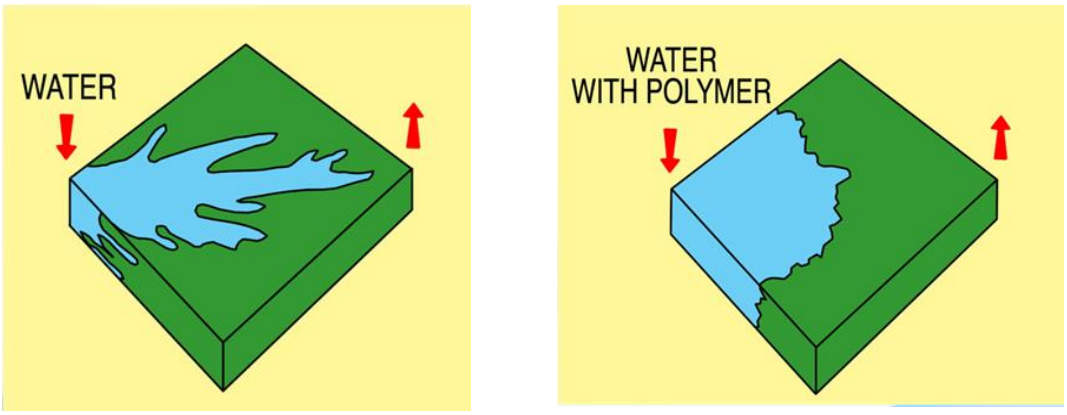

(a) (b)

Figure 2.2. Schematic diagram comparison in a five-spot pattern between (a) areal sweep with water (b) areal sweep with polymer.

Regarding vertical sweep efficiency(E_I), the definition is given by the ratio between the cross-sectional area swept by the displacing fluid and the total cross-sectional area (Lake, 2014).

$$E_I = \frac{Cross\ sectional\ area\ swept}{Total\ cross\ sectional\ area} \tag{2.6}$$

Poor E_I is driven predominantly by widely varying of permeability in the reservoir that may cause early breakthrough in the producer well and consequently reduced oil recovery from the low flow capacity layers (Sorbie, 1991) (Clifford and Sorbie, 1985). The polymer effect on the E_I, through the reduction of M, is the boost of the effect of vertical crossflow. This mechanism allows sweeping better oil from layers with low permeability values (Clifford and Sorbie, 1985). In the next section (2.4) it will be revealed in detail the crossflow phenomena for stratified reservoirs.

On the other hand, the E_D is the volume of oil displaced divided by the volume of oil contacted by displacing fluid (Lake, 2014).

$$E_D = \frac{Volume\ of\ oil\ displaced}{Volume\ of\ oil\ contacted\ by\ displacing\ fluid} \tag{2.7}$$

In other words, the E_D is proportional to the average oil saturation in the porous medium. This displacement is represented in one dimensional medium through fractional flow.

$$f_o = \frac{1}{1 + \frac{\mu_o k_w}{\mu_w k_o}} \tag{2.8}$$

M, which it is in the denominator, leads to raise the oil recovery through an increase in fractional flow of oil when the mobility ratio decrease (Needham and Doe, 1987). This effect of M in f_o is much more evident in the early application of polymer flooding (PF) after the water injection process. This stage of early water flooding may assure the high values of initial oil saturation. Additionally, the adverse high values of μ_o (high M) is also a scenario where is evident the improvement of the displacement process with PF (Needham and Doe, 1987).

2.4 Polymer Injection In a Heterogeneous Sandstone Reservoir

The field-case mentioned in this work is particularly stratified with myriad different permeabilities in the porous medium. For this reason, it is pertinent give some basis about the role played by PF in highly heterogeneous stratified reservoirs.

In the vast majority of cases, the use of polymer in conventional reservoirs is because of unfavorable M and/or predominant heterogeneity in the reservoir (Sorbie, 1991). The goal of the second case is tightly related to E_A and E_I as well. Heterogeneity is the variation in reservoir properties with location that repeatedly appears as random or unpredictable condition due to the facies deposition (Pyrcz and Deutsch, 2014). This condition will always be in the reservoir. The vertical heterogeneity or widely vertical permeabilities are a cause of early arrivals of the water front to the producer wells through “slides” or “thieves” layers with high permeability and/or high flow capacity; leaving behind the tighter layers with unswept oil. This phenomenon in heterogeneous porous media is called channeling (Tavassoli, 2014).

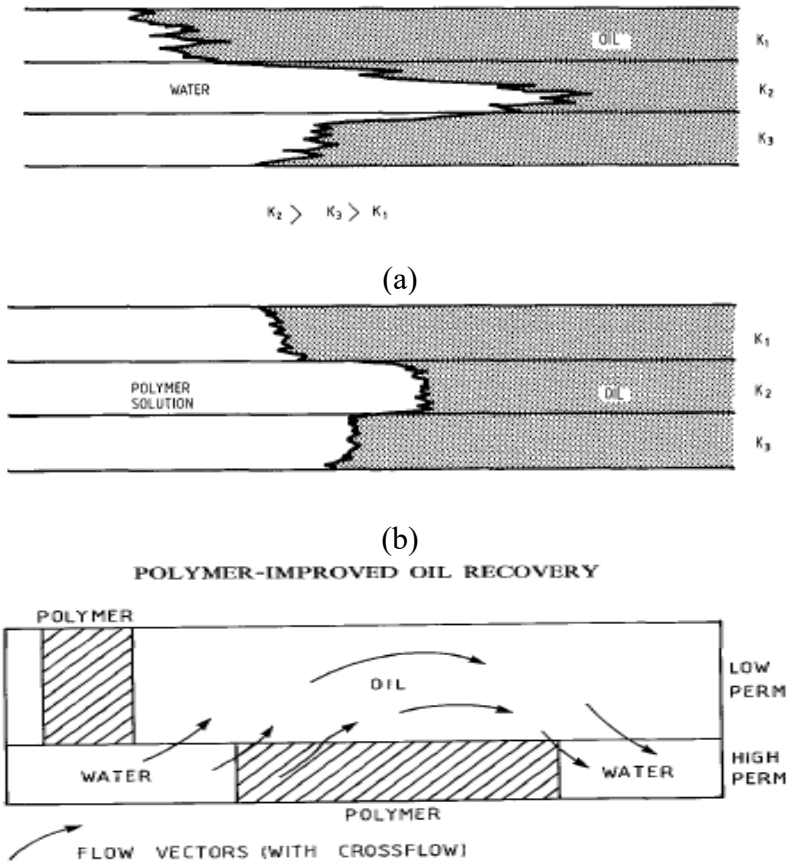

Figure 2.3. Schematic diagram of the improvement in vertical sweep efficiency caused by polymer flooding at different permeabilities (from Sorbie, 1991). (a) Water injection profile, (b) Polymer injection profile y (c) Schematic of crossflow phenomena

As was mentioned in the Section 2.2, the polymer flooding homogenizes the advance front of the displacing fluid on different layers through the crossflow phenomena. (See Figure 2.3.) The nature of the crossflow is explained mostly by difference of pressures. The higher viscosity of the polymer solution compared to water viscosity results in a higher pressure gradient in the more permeable layer swept by the polymer. As a result, it causes the polymer solution to flow into adjacent layers containing water at lower pressure (Sorbie, 1991). Therefore, the improvement of the vertical sweep efficiency is reached through a delay of water arrival to the producer well and the rise of oil production mainly from layers with low permeability. In order to fulfill the crossflow

effect, the boundary between layers must be permeable or semi permeable. (Green & Willhite, 1998).

2.5 Capillary Number And Interfacial Tension

The capillary forces are responsible for trapping fluids in a reservoir (Stegemeier,1976; Lake, 2014). Specifically, oil trapped after a swept process of waterflooding is the main goal of the process, such as surfactant injection. The interrelation between oil and water phases in reservoir creates the interfacial tension (IFT), which is the trigger to the capillary forces (Lake, 2014). One of the EOR efforts is to mobilize the trapped oil overcoming the capillary forces through reduction of the oil/water IFT (Stegemeier,1976). Figure 2.4 shows an experimental data where a Berea sandstone sample answers effectively to the increasing of N_c by decreasing the IFT (Chatzis and Morrow, 1984). Chatzis and Morrow identified a clear correlation between the local capillary number and the residual non-wetting or wetting saturation through this plot known as capillary desaturation curve (CDC) (Lake, 2014).

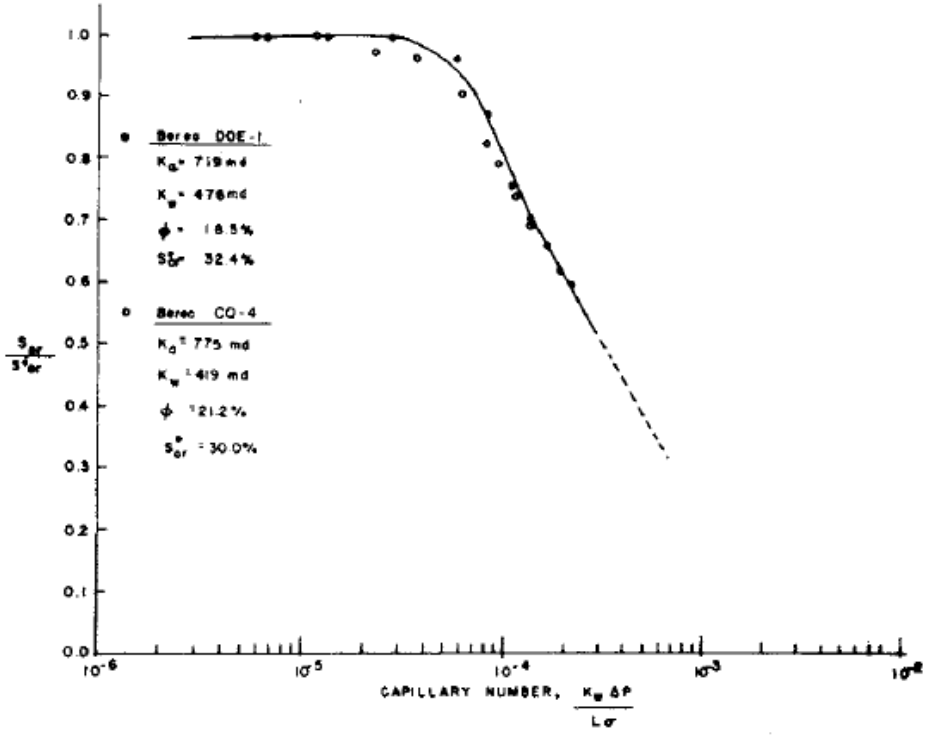

Figure 2.4. Capillary desaturation curve for Berea sandstone (normalized residual oil saturation vs. capillary number). (From Chatzis and Morrow, 1984.)

2.6 SURFACTANT

The most important EOR method for reaching low IFT is the use of surfactants, which are surface active agents that alter the properties of the fluid-fluid interphase (Green & Willhite, 1998). This alteration represents decreasing the energy barrier between the oil and water phases. Surfactant can lead the IFT from 20 dynes/cm to ultra-low values of 0.001 dynes/cm in order to reduce the oil saturation even to values close to zero (Chatzis and Morrow, 1984; Chang et al, 2018).

The structure of a surfactant constitutes two different parts. First, a polar part that is attracted to water (hydrophilic). Second, a non-polar part that is attracted to oil (hydrophobic). According to the polar-group of the surfactant, there are four types. The negative charge in the head group is anionic. The positive charge in the head group is cationic. The non-charge is called nonionic. Finally, the amphoterics which have the both a negative and a positive charge (Lake, 2014).

Ultra-low IFT is strongly related to the optimum solubilization ratio of the surfactant, which happens when both oil and water phases solubilize equally with the surfactant (Baran, 2000). Not all the surfactant can achieve the low IFT and high solubilization ratio desired. The surfactants that have the strongest possible molecular interaction with both oil and water phases are considered the best option to inject. In addition, it is critical to avoid rigid viscous structures in the microemulsion phase since it is necessary for this phase to flow and transport through the pores of the reservoir (Lake, 2014). The mentioned solubility is performed by the micelles, which come from the surfactant, above a critical micelle concentration (CMC). In order to achieve an ultra-low IFT, the surfactant concentration must be greater than CMC because the concentration above the CMC promotes the formation of micelles (Green & Willhite, 1998). The micelles solubilize crude to form a thermodynamically stable fluid called microemulsion. For the purpose of this work, stability explains the ability of the slug or microemulsion to remain in a single phase. Therefore, the microemulsion phase behavior (MPB) has a key role in the Surfactant-Polymer (PF) flooding

because according to experimental data there is a strong agreement in the correlation between IFT and MBP (Reed and Healy, 1977; Huh, 1979).

Microemulsion phase behavior is greatly affected by brine salinity. Winsor (1954) classified the phase behavior transition from low to high salt concentration. Starting from low salinity, there are two phases: an excess of oil phase that is essentially pure oil and a microemulsion phase that contains water plus electrolytes, surfactant and some solubilized oil in swollen micelle. That stage is Winsor Type I or Type II(-). Increasing the salinity, there is a split of three phases in equilibrium, pure oil (excess of oil), pure water (excess of water) and a middle phase microemulsion where the surfactant is part of this phase, which is denser than oil and less dense than water. That phase behavior has the lowest IFT and its name is Winsor Type III or Type III. Finally, the highest salinity concentration has two phases, an excess of water or pure water and a microemulsion phase containing most of the surfactant and oil and some solubilized water exist. As an illustration, see Figure 2.5 (Green & Willhite, 1998; Lake, 2014). In accordance with different stages of the phase behavior, the Type III is desirable for obtaining an ultralow IFT. That environment is the confluence of particular status of parameters such as optimum salinity, three phases at equilibrium, highest solubilization ratio and the oil/surfactant/water close to the invariant point where the boundaries between phases become undifferentiated and therefore display ultralow IFT's among phases (Green & Willhite, 1998).

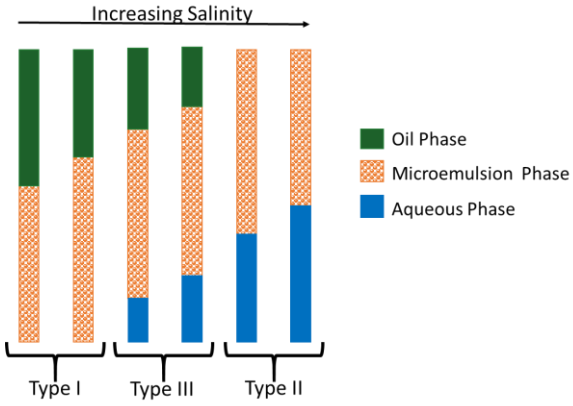

Figure 2.5. Schematic of the microemulsion phase behavior according to Winsor (1954).

The variability of the MPB changes from Type I to Type II, or vice versa, always occurs through the Type III environment (Green & Willhite, 1998). Oil composition is the one of the most important characteristics to change the phase behavior through the alkane carbon number (ACN). Experiment data reveals that while ACN increases, IFT and optimum salinity rises as well (Lake, 2014).

From Reed and Healy (1977), the Figure 2.6 reveals the close relationship among the characteristics mentioned above. The X axis, at the top is split by the three types of environment of the microemulsion phase behavior and at the bottom there is a change by increasing salinity. On the Y axis, on the top there is a measure of IFT; on the bottom there are the solubilization parameters. The correlation in the Type III shows that the IFT is inversely proportional to the solubilization. In addition, at the Type III (shaded region) the optimum salinity is given, the highest σ is seen and the lowest IFT is present.

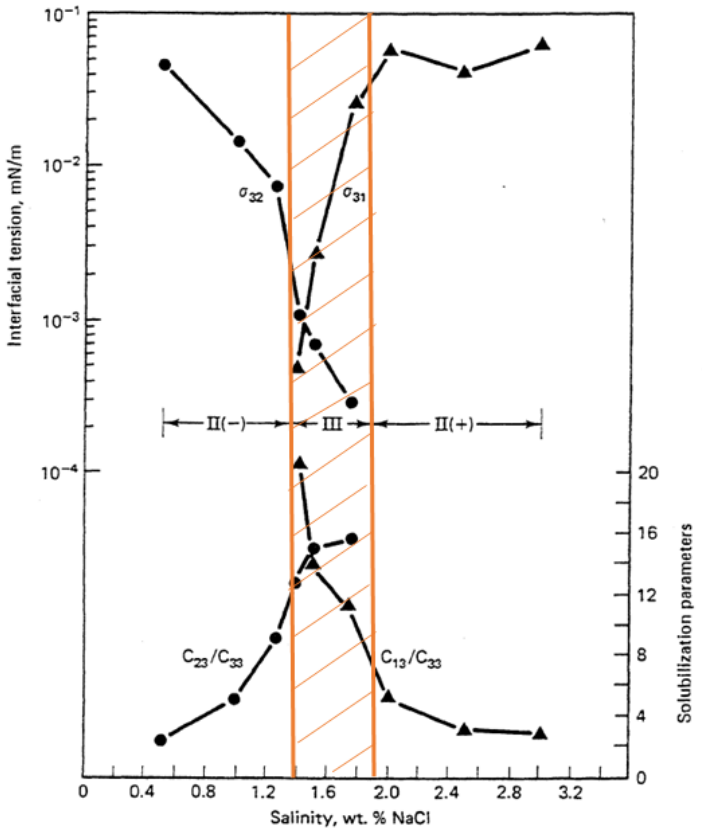

Figure 2.6. Interfacial tensions and solubilization parameters (Reed and Healy, 1977).

2.7 SURFACTANT POLYMER (SP) – FLOODING

Surfactant flooding is any process that adds surfactant with the target of improve the oil recovery in the reservoir. However, the injection of surfactant should be accompanied by the use of polymer because of the crucial role performed by the polymer that is focused on decreasing the mobility in order to keep a stable displacement. The mobility of the surfactant solution without polymer, which is the displacing phase, is greater than the mobility of the oil bank (displaced phase) (Tavassoli, 2014). According to the definition given in the parts 2.2.1 and 2.3, an unfavorable mobility ratio may lead to viscous fingering and poor recovery efficiency (E_R). The recently mentioned hydrodynamic instabilities as fingering phenomena and channeling represented by probable early surfactant arrivals to the producer could be a cause of the low recovery.

With the purpose of improving the efficiencies of the displacement process it is necessary to increase the viscosity of the surfactant solution. Therefore, a mobility control agent is used, which in the vast majority of cases is polymer. Other chemicals would accompany the surfactant solution as co-surfactant, co-solvent or Alkali. The use of these additional components depends on the needs manifested by the fluid-fluid or rock-fluid interaction. For further information of the purpose of using co-surfactant, co-solvent or Alkali, refer to Lake (2014).

In the particular case of SP-flooding, which is object of this study, the surfactant injection in the porous media is through the aqueous solution known as “slug” that contains surfactant and polymer (Lake, 2014). The volume percentage of this slug depends on the floodable pore volume of the reservoir. However, according to experimental data, the range is between 10 to 50% of this pore volume (Lake, 2014). The addition of polymer to the solution will depend on the mobility reduction required for a stable displacement.

Chapter 3. Field Background and Polymer Pilot Context

Chapter 3 outlines the background of the Colombian field and the history of the production and the impact associated with the water flooding as a secondary project. Additionally, this chapter describes the framework of the first field pilot of polymer flooding.

3.1 Colombian Field

The reservoir characteristics of the Colombian Field are presented. The geological features and production history will be discussed.

3.1.1 Reservoir Characterization

The Colombian field is located at the center-north of Colombia in the Mid-Magdalena Valley between the eastern and central mountain ranges, bordered by the Magdalena River. Figure 3.1 gives an schematic of the location.

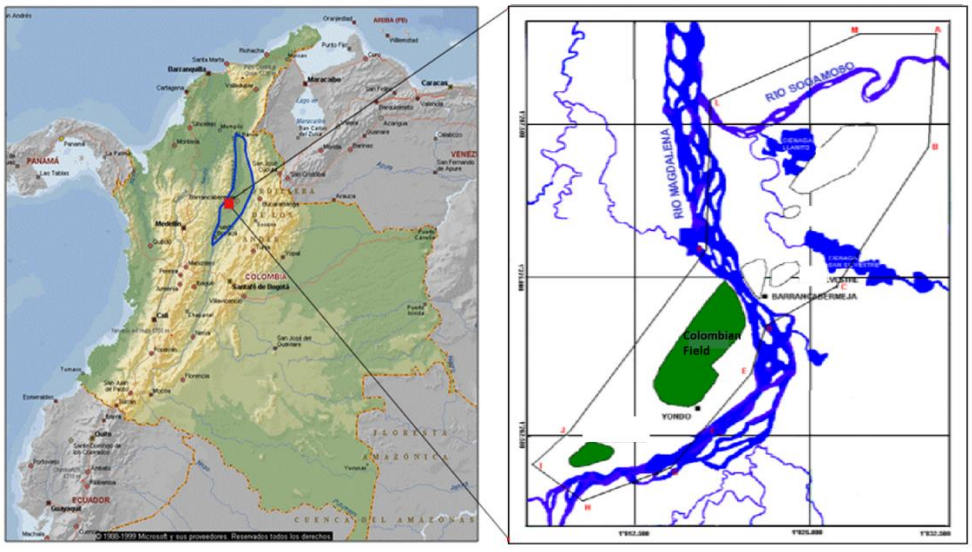

Figure 3.1. Location map of Colombian Field (modified from Gheneim et al, 2017)

The seismic profile shown in the Figure 3.2 (a) represents the structure from the whole Colombian asset from the south on the left and north on the right. The Colombian field is located at the first collection of transpressional faults in the northeast part. From the north as well, the

structure has a low inclination to the east. The numbers from 1 to 8 represent the segmentation of the field by eight different operational blocks: Block VIII being the northernmost and Block I the southernmost (Figure 3.2 (b)). The first polymer injection pilot is being executed in Block VI, which is the largest area with oil reserves in the Colombian field and the block with more wells perforated as well.

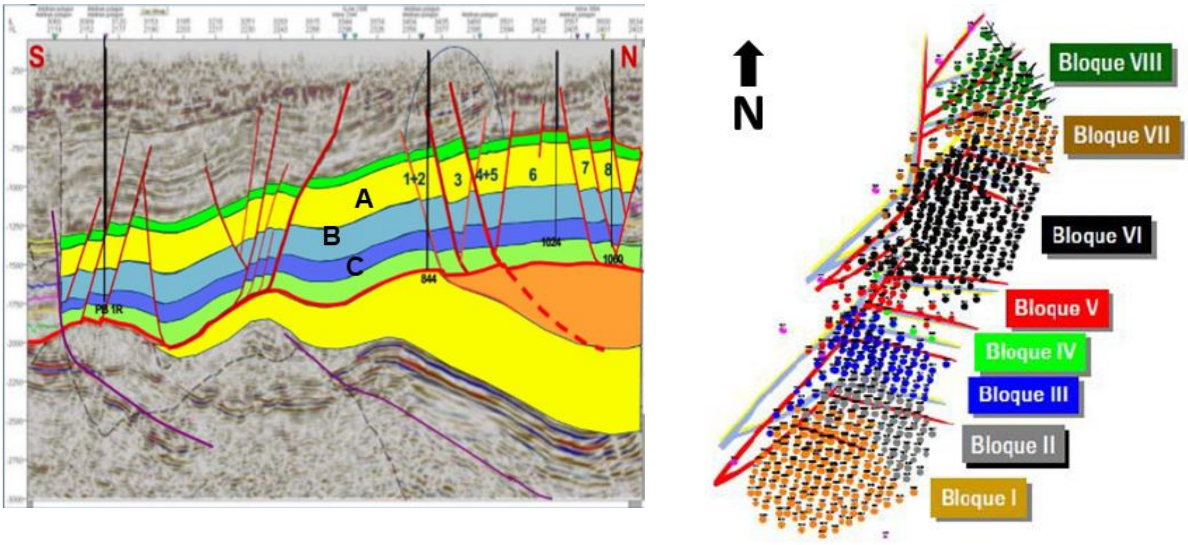

(a) (b)

Figure 3.2. Illustration of: (a) seismic profile and (b) field division of Colombian Field (modified from Gheneim et al, 2017)

The main natural drive is solution gas with a weak water drive in the basal sands. The major reservoirs, which belong to the Tertiary age, are called Sands A the shallowest production layers, the Sands B and C the deeper production reservoirs (see Figure 3.3). Those producing formations are product of fluvial currents of anastomosed type with high heterogeneity, mainly vertical and to a lesser extend laterally. The depths of the formations vary between 2200 and 5500 ft in True Vertical Depth (TVD). From A to C sands there are 23 identified reservoirs with an approximate column of 3000 ft. Each formation is divided in sub-sands differentiated by shale bodies between them, as shown with details in Figure 3.3.

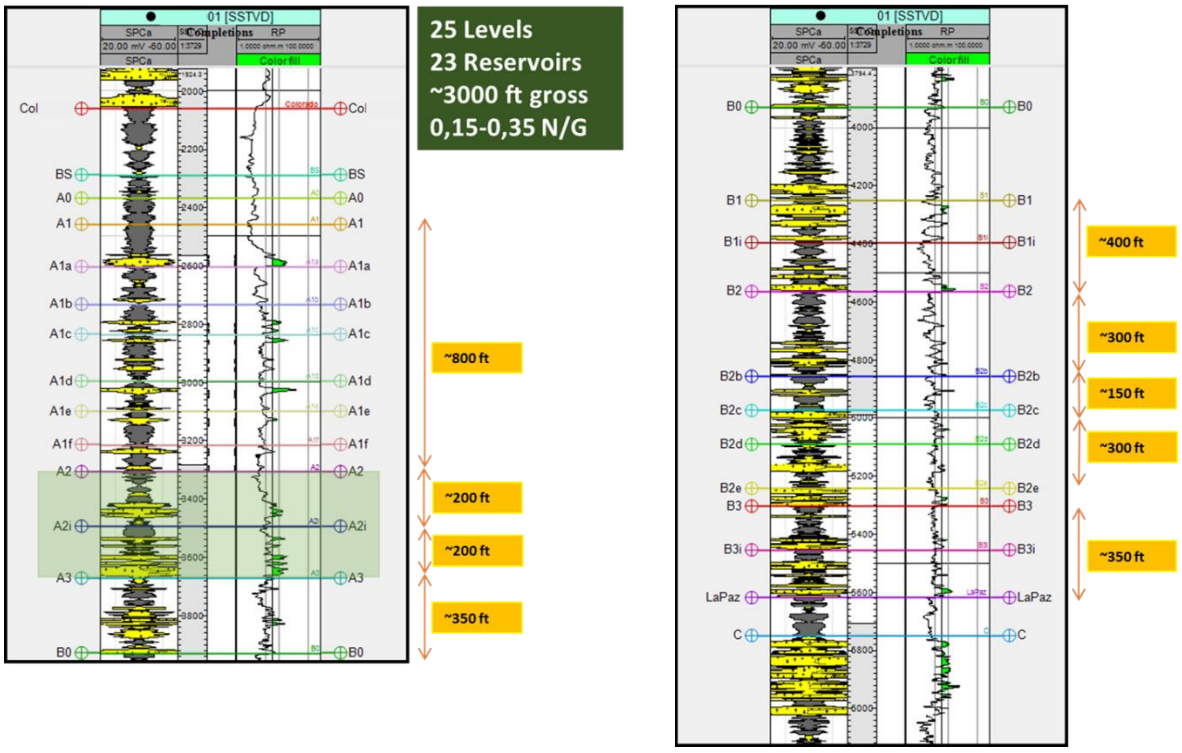

(a) (b)

Figure 3.3. Log profile example of well in Colombian field. (a) A formation (b) B and C formations. (2017)

The reservoir A is composed of intercalations between sand and shale. The ranges of rock properties such as porosity and permeability have a considerable positive difference above the deeper B and C sands. The current EOR pilot, which is developed in the north area of Block 6, has polymer injection in the sub sands A2 and A2i due to the acceptable lateral continuity and good reservoir rock properties (see Table 3.1).

Sands	Gross h (ft)	Net h (ft)	Net to Gross	Avg Porosity of Net sand (%)	Permeability Range of Net sand (mD)
A	1100	220	0.20	22	100-1000
→ A2	145	73	0.50	21.5	110-1000
→ A2i	184	102	0.55	22	115-1000
B	1300	350	0.27	20	50-500
C	200	60	0.30	20	50-600

Table 3.1. Rock properties of A, B and C sands and sub sands of A in Colombian Field

3.1.2 Field History

The Colombian Field was discovered by the perforation of the well C-01 in 1941. The maximum historical peak of production was reached in 1953 with 46,000 Bopd under primary depletion mechanism. In 1979, an Oil and Gas Company from Colombia started the first pilot of water injection in the northern area. As a consequence, the expansion of waterflooding in the field began in Blocks VI, VII and VIII in 1985. Subsequently, the expansion continued in the Blocks I, II, III and V in the year of 1988. A conventional process of injection developed these expansions where each producer and injector were drilled for one formation as target. It means that there were at least 3 different wells at the same location but with different depth and target. Later in 2005 the selective water injection was applied to all the patterns in the field, changing from 3 wells (producers and injectors) to 1 well per location. As well as, the well completion turns to commingle production and the injector wells, which were open in A and B sands, turns to inject selectively. This modification in the well completion has notably improved the production per day and consequently in the recovery factor.

From 1941 to 1985 the recovery factor for primary production was of 11.6%. The conventional waterflooding expansion since 1985 to 2005 had 4.5% of recovery factor and the selective injection from 2005 until now has a 2.9% of oil recovery. As a result, the waterflooding process has supported the most recent production peak in the field turning from 5000 Bopd in 2005 to 20,000 Bopd in 2013, approximately. The previous increase is linked with the drilling of 591 injectors and producers in the whole field. Colombian field with around 1700 perforated wells has produced over 350 MMBbls of oil as of July 2017.

3.2 Polymer Pilot Background

The secondary recovery applied in Colombian field has been a successful project for more than 30 years. However, during these years of waterflooding operation, some limitations and operational issues were identified, such as thief zones or early water irruption, increases of the

water cut and increase in sand production. Mostly the high mobility ratio of ~ 20 and the heterogeneous reservoir are the challenges that may cause issues in the waterflooding process.

The high value of mobility ratio in A sands is mainly by the crude oil viscosity (40-100 cP) and water viscosity (1 cP approx.) at reservoir conditions, which are favorable for an inefficient swept or poor areal sweep. Furthermore, the heterogeneity of the reservoir characterized by stratification and wide variation of permeability could lead to accentuate the low recovery in the displacement process. Consequently, this inefficiency leaves remaining oil represented in large pockets of crude behind. (Sorbie,1991). The challenges associated to the water flooding reveal the need for reservoir management to plan new options that can mitigate these issues that can get worse without any additional effort. As a result, the polymer injection was selected among the different Enhanced Oil Recovery technologies evaluated in a screening process. As Chapter 2 mentions, the polymer itself increases the viscosity of the driving phase, which is generally water, in order to decrease the mobility ratio through the rheological properties of a non-Newtonian fluid (Gogarty, 1967).

In November of 2014, through addition of polymer to the four well existing injectors 1313, 1222, 1304, and 1292, the first pilot of PF in the Colombian field began operation. The well pattern was arranged by 4 injectors and 10 producers: 2 in the center area and 8 producers in the second line. In addition, there are 13 boundary injectors. The figure below shows the configuration of the pattern.

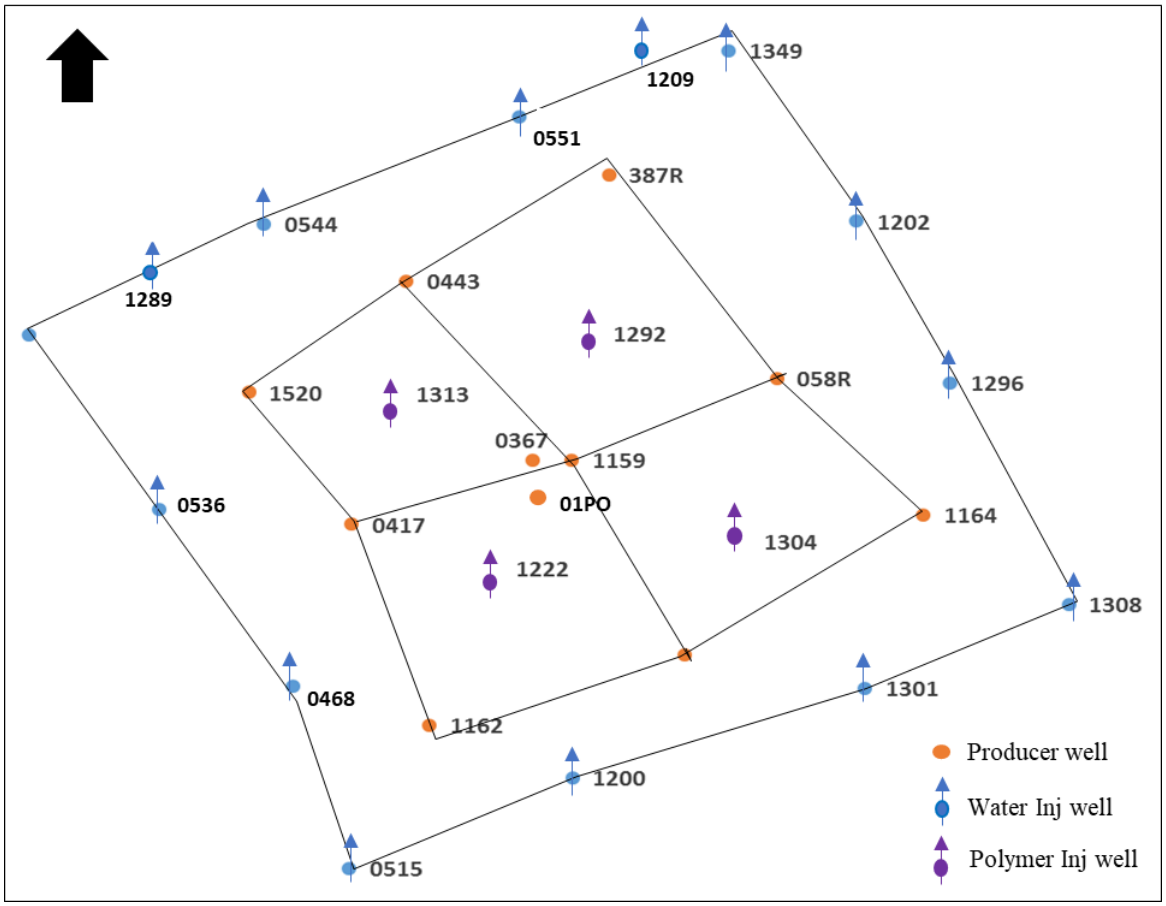

Figure 3.4 Location of each well of the polymer pilot pattern at A2 formation.

3.1.2 Polymer Features

The conventional polyacrylamide HPAM Flopaam 5115 from SNF is the current polymer injected in the A sub-formations, which was preferred after different tests associated with the rheological properties. The polymer screening process included thermal stability, polymer viscosity at different water salinities and polymer filterability. The F-5115 showed the least viscosity change at extreme conditions in comparison with the other polymers in the test. The Table 3.2 displays the properties of F-5115 polymer.

Molecular weight	4 – 6 MM OF DALTONS
Designed viscosity	11.5 cps
Viscosity data at temperature	46 celsius
Filter Ratio	1.1
Goal concentration	312 ppm
pH	5 - 9 @ 5g/L
Relative density	0.8
Thermal stability	> 150 celsius
Total polymer injected daily (Bbl)	1500 (4 Wells)
Total polymer injected daily (Kg)	70 (4 Wells)

Table 3.2. Polymer properties – Flopaam 5115

3.2.2 Injectors Condition

In April of 2014, the upper sands above A2 and the lower sands below A2i were closed in the four injectors of the pilot 1313, 1292, 1304 and 1222. The purpose was to test the effectiveness of polymer injection only in those two sub-sands of A formation. As an illustration, the completion in the target zone of the well 1292 is shown below as well as the plot of injection rates during two years in Figure 3.5.

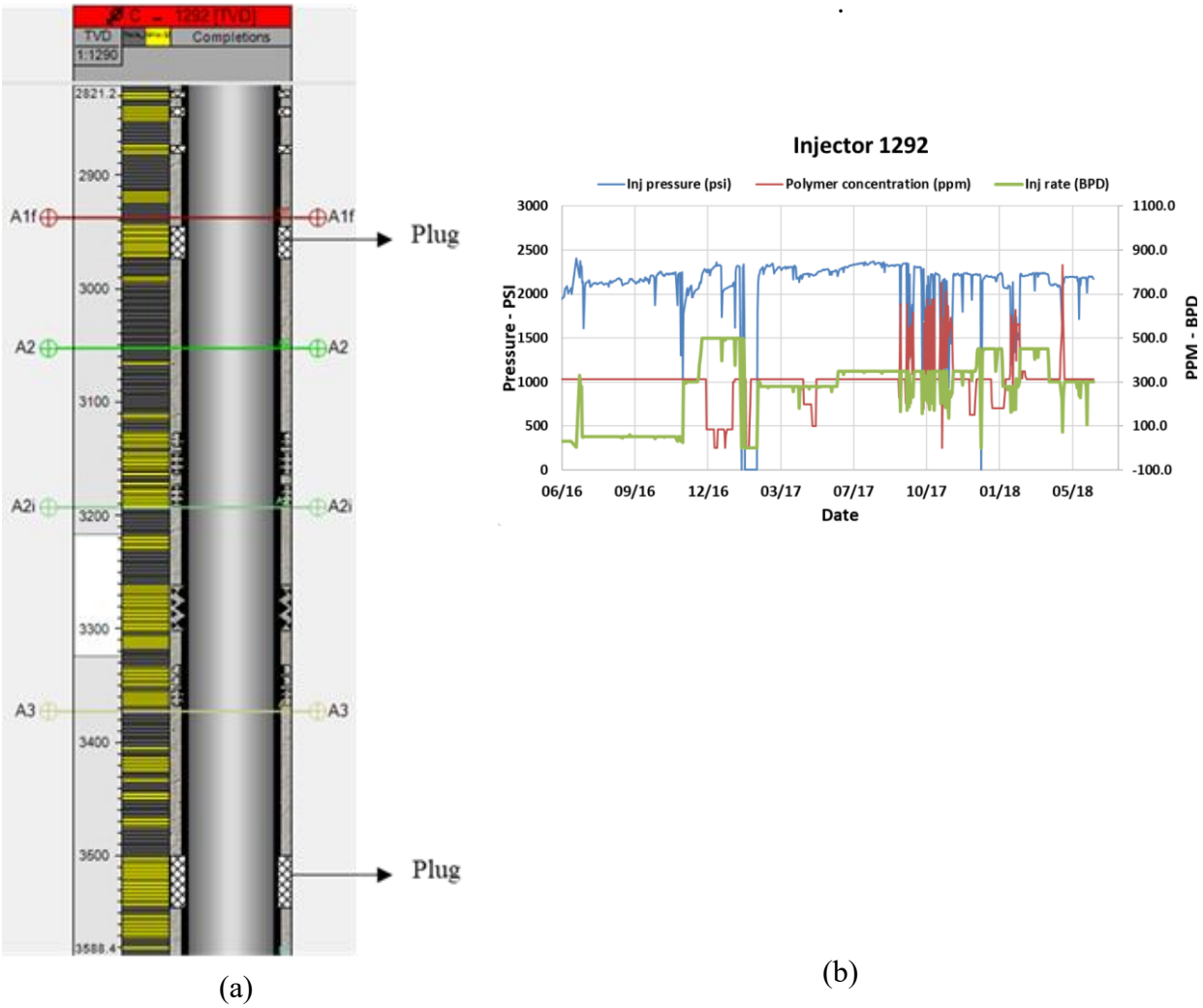

(a) (b)

Figure 3.5. Well 1292 (a) Target of injection zone (b). Injection rate, pressure and polymer concentration.

The four injectors are surveilled for keeping similar injection volumes, injection pressure, and polymer concentration. The injection rates were around 300 and 700 Bopd with an average of 500 Bopd. The injection pressure is between 1500 to 2200 psi and the polymer concentration is close to the target concentration of 312 ppm.

3.2.3 Reservoir heterogeneity

Approximately 300 ft represents the thickness of the sands A2 and A2i. However, the permeabilities range from 0.1 mD to 1 D in less than 30 vertical ft. The flow capacity in each layer

shows that there are high probabilities to find a thief zone or sub-units that can result in early breakthrough.

The process of polymer injection is highly related to the reservoir heterogeneity. In that line, this work is focused on the heterogeneity of permeability, which is the function of the flow capacity (Sahni et al., 2005). Previously, it was mentioned that the effect of heterogeneity during the water injection become a challenge to the sweep efficiency. One method to quantify how heterogeneous is the formation associated with the permeability is through the Dykstra-Parsons Coefficient (VDP) which is indicative of the variance of permeability (Sahni et al., 2005). From 0 to 1 the coefficient represents the most homogeneous close to zero and the most heterogeneous close to 1. For the case of A2 the VDP is around 0.87 and A2i is close to 0.86; for both cases, the permeability was evaluated only at the net pay thickness. Therefore, the wide range of permeability represents the highly heterogeneous sands.

3.2.4 Challenges of PF to Overcome and Initial Results of Polymer Pilot

The Polymer Flooding (PF) in Colombian Field aims to correct three main issues associated with the water flooding process. First, the channeling; according to the heterogeneity aspects, the sub-sands A2 and A2i have high variation of permeability vertically. This heterogeneous formation boosts the water injection to channel quickly through the layers with highest permeabilities and reduced injection in the tight layers. The polymer effect reduces the permeability to water in the layers, triggering the early mentioned cross-flow. In this way, the polymer flooding creates an effect of vertical conformance reducing the early water production and forcing the injection water to move through the layers with less permeability. Second, viscous fingering (mobility ratio); there is a direct relation between the viscous fingering and the mobility ratio. An adverse mobility ratio $M > 1$ boosts the creation of viscous fingers that will channel into the oil. As a consequence, the water breakthrough will arrive early. In addition, the heterogeneity in permeability also influences the formation of viscous fingers (Araktingi, 1993). Adding polymer to water injection in the A sub sands will increases the viscosity of the driving phase in order to suppress the fingering and

consequently improve the areal sweep (Sorbie, 1991). Ultimately, displacement difficulties generated by the capillary forces associated with the waterflooding. The PF will improve the areal efficiency of the displacement process.

Chapter 4. Base Model and Methodology

This chapter describes the sector model used in this work. Following this section, the methodology behind the results at different new scenarios are described. The base model has a relevant role because of the static and dynamic properties, grid characteristics and wells are the basis for the results given in Chapter 5.

4.1 Sector Model

The sector model was built by the reservoir engineering department of a Colombian Oil Company with the goal of simulating polymer injection through sub-sands A2 & A2i using the commercial ECLIPSE-100 from Schlumberger, a black oil, three-dimensional, three phase, chemical flooding and fully-implicit simulator. The area of the sector model covers a northern portion of block VI of Colombian Field. As a result, this base case is the foundation of this work, which will be converted to UTCHEMRS, an in-house chemical flooding reservoir simulator from The University of Texas at Austin. (More details on the simulation deck transfer is presented later.) From the base model, new scenarios are generated and used for the optimization of the production in A sands. A similar study is done for B sands.

The numerical model discretizes the domain with a *corner-point geometry* (CPG) with high vertical resolution due to the vertical heterogeneity presented in Chapter 3. In order to represent reliably the reservoir complexity, 1336 grid cells in the z direction with an average cell thickness of 2.84 ft are considered. In the y direction, there are 85 grid cells with an average cell width of 76.4 ft, and there are 71 grid cells with an average cell length of 91.8 ft along the x direction. A total of 8,062,760 cells are used, which 708,000 are active. Figure 4.1(a) shows the details given to the vertical resolution. In total, there are three geological formations divided into seven zones and subsequently twenty-five layers.

On the other hand, Figure 4.1(b) given below represents the area of the sector model transferred (magenta polygon). In that area, there are a total 56 injectors (blue), 31 producers (green) and 1 observation well (green).

The History Match (HM) of the base case is from February 1985 to February 2018 of about 33 years. This HM includes the Water Flooding (WF) and the Polymer Flooding (PF), performed in the last four years of PF applied in the Colombian Field. During the development of the methodology section the HM results will be displayed including the simulation using another simulator. INTERSECT a new simulator from Schlumberger was also tested using the same sector model to have a comparison among several reservoir simulators. The model was transferred to and simulated with UTCHEMRS and INTERSECT for the HM, WF and PF forecast.

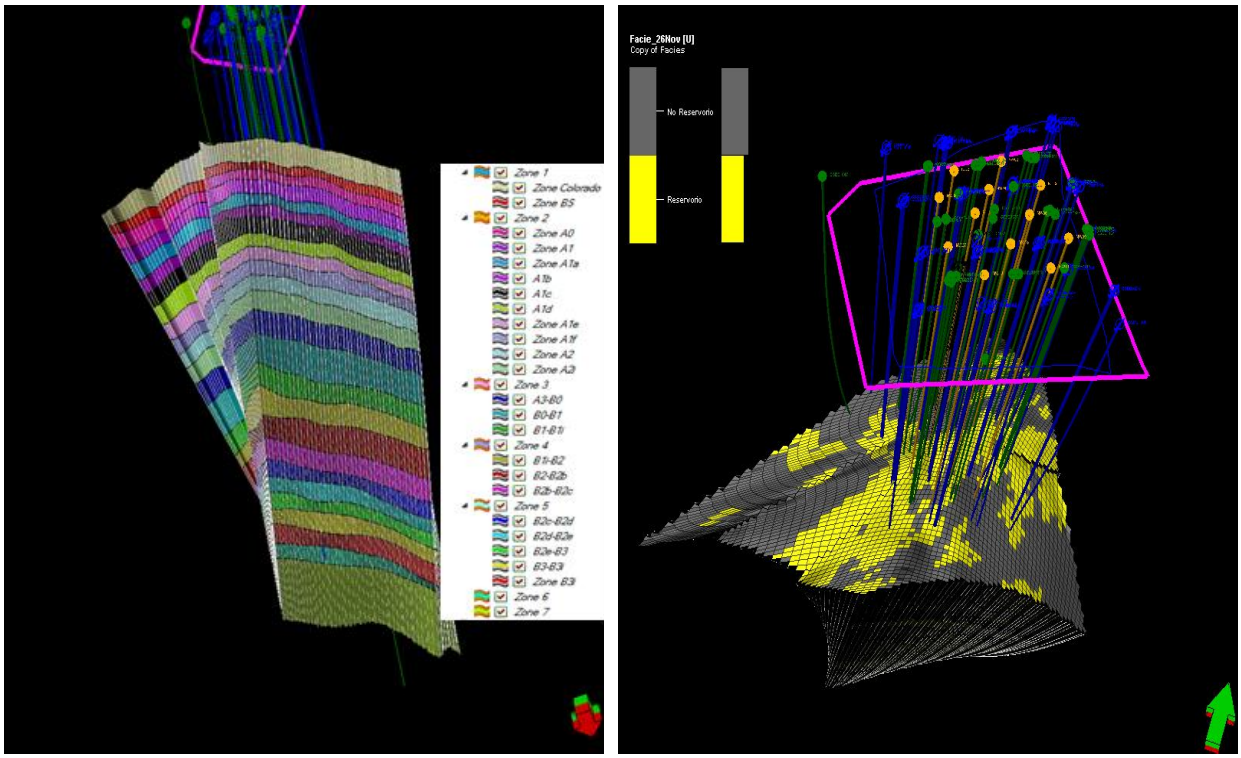

(a) (b)

Figure 4.1. Illustration of the sector model in Block VI. (a) Layers are displayed vertically (b) Polymer pilot area

4.2 METHODOLOGY

The simulation workflow is presented in eight different steps.

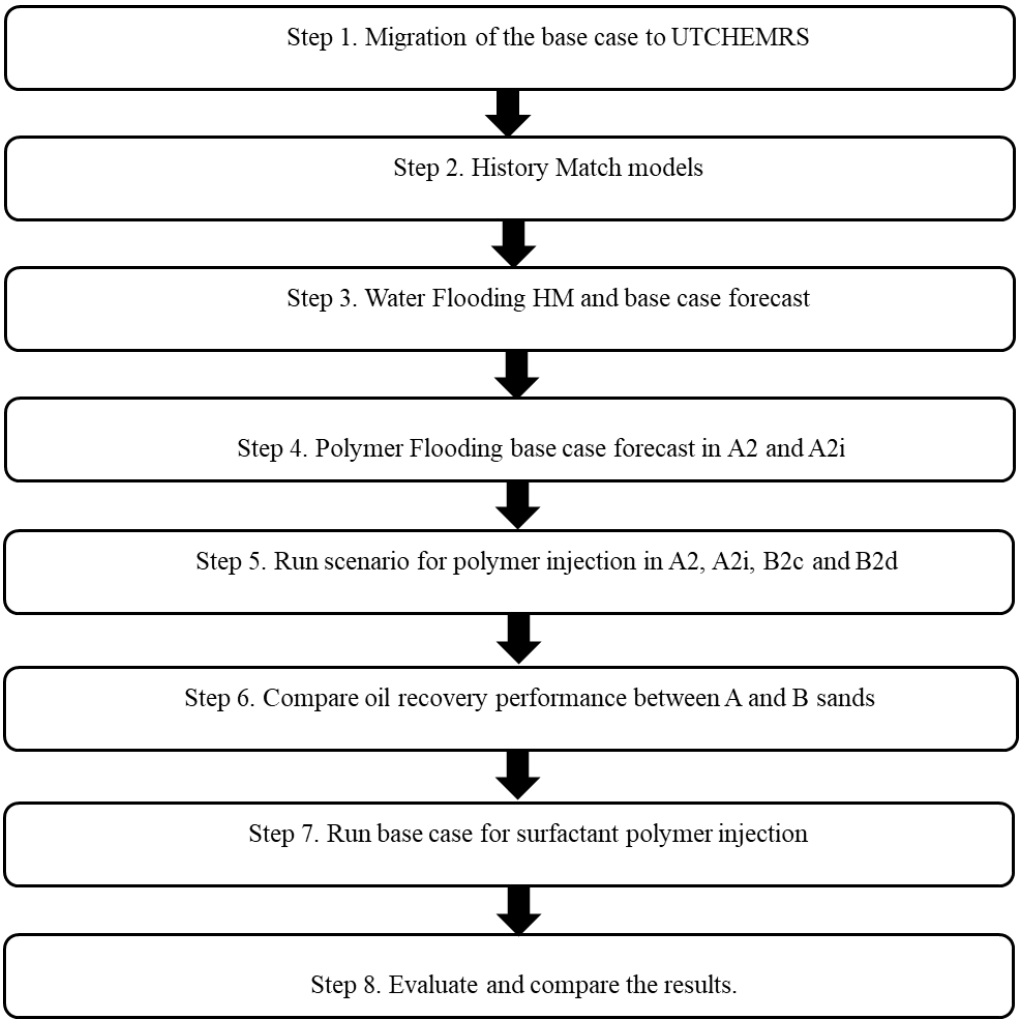

Figure 4.2 Flowchart of the proposed methodology.

Step 1. Migration of the base case to UTCHEMRS

UTCHEMRS Background

In 1978, Pope and Nelson created a chemical flooding compositional simulator. They developed a one-dimensional simulator that considers the polymer shear thinning effect and the micellar phase behavior for three phases mentioned previously in Chapter 2. Later in the decade of 1980's this simulator evolved to UTCHEM (University of Texas Chemical Flooding) as an

Implicit Pressure Explicit Compositions (IMPEC) simulator capable of simulating complex surfactant phase behavior and chemical reactions of different chemical EOR processes. UTCHEMRS (University of Texas Chemical Flooding Reservoir Simulation) is the advanced version of UTCHEM keeping the same robustness of physical modeling, such as three phase microemulsion (ME) phase behavior, polymer injectivity, and effect of hardness and salinity on polymer viscosity and adsorption among others. The key enhancement was the addition of the adaptive implicit method (AIM) which resulted into faster and robust chemical EOR reservoir simulation. The inclusion of a novel grid option that allows transmissibilities for Corner Point Geometry and none-neighbor connection was also considered in this new version. These capabilities allow UTCHEMRS to handle the complex field cases.

Static and dynamic model migration

The data of geological grid, reservoir properties, producers, and injection wells were transferred to UTCHEMRS from the ECLIPSE base case. The initial goal was to compare the capabilities of two simulators. The UTCHEMRS has advanced polymer and surfactant models, such as the effect of hardness (calcium + magnesium) on polymer viscosity and adsorption and improved polymer injectivity model that can add value when making field design recommendations. This migration is the base of new possible scenarios for testing the capabilities in Polymer flooding (PF) and Surfactant Polymer flooding (SPF) in the Colombian Field. Specifically, the transfer of the geological model, the dynamic model, and the polymer properties of the sector model is described as follows.

The conversion of the simulation deck is not restricted to the reformulation of data sets and keywords; it also requires careful analysis of physical models available in both simulators and data regression of raw data to the new simulator. The data reformulation includes the conversion of the reservoir geometry, reservoir properties, and well locations and their completion/perforation data. There are reservoir properties that do not change with time, such as porosity or permeability (see Figures 4.3(a) and 4.3(c)); these collections of attributes are known as static model. On the other

hand, the dynamic model is integrated by attributes that change according to production time, such as reservoir pressure or oil/water saturation (see Figures 4.3b and 4.3d).

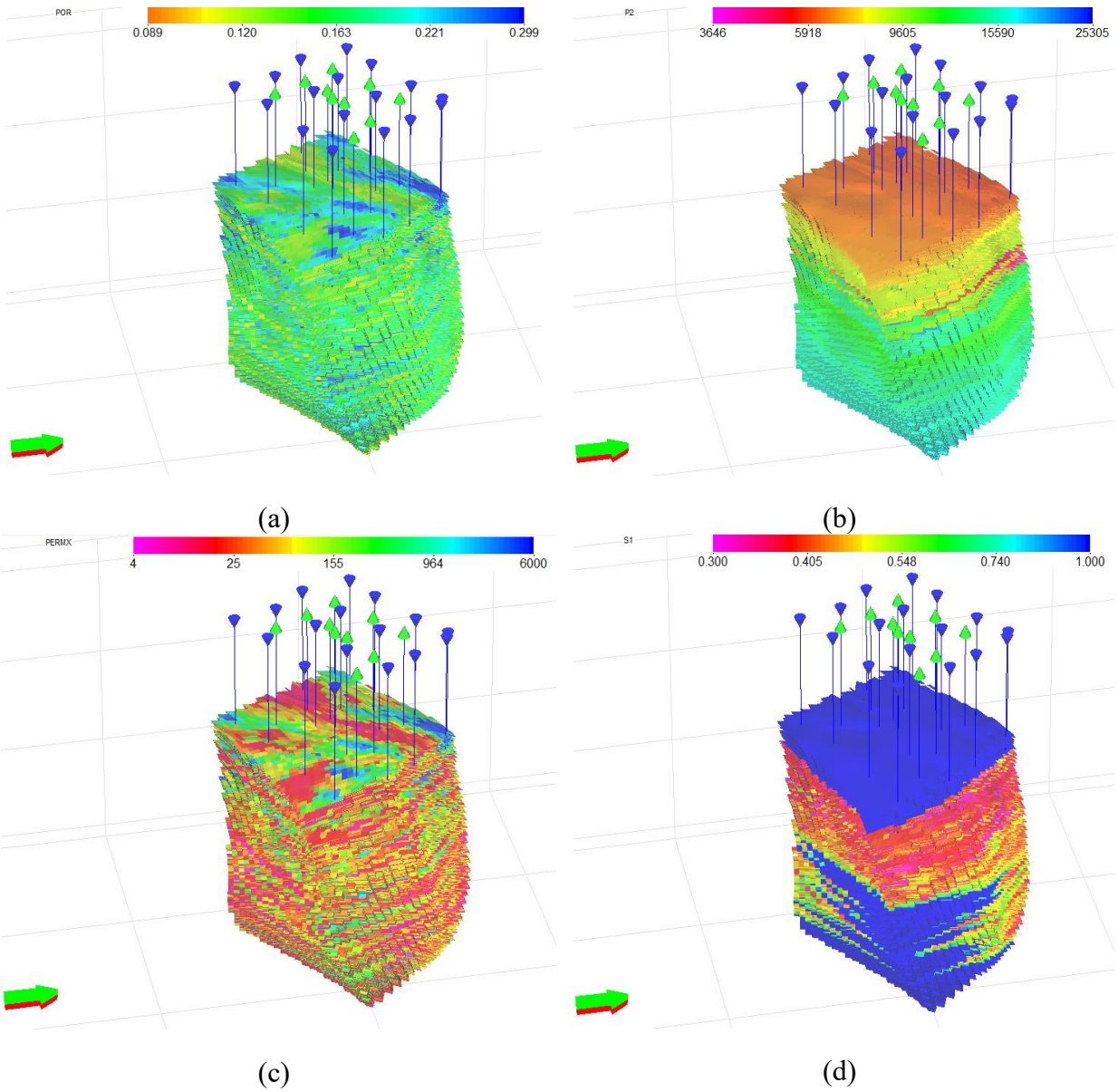

Figure 4.3. Grid properties migrated to UTCHEMRS. (a) Porosity (fraction) (b) Pressure (kPa) (c) Permeability (mD) (d) Water saturation (fraction).

The geological model uses *corner point* grid geometry, which is constructed following the complex geological features of the reservoir. Therefore, the migration of the static model is a task

particularly challenging. Such complexities include changes in dip, azimuth, and thickness of the deposit layers, and truncations caused by faults.

The geological model has five rock types defined. According to the lab core analysis, four of five rock types are considered as reservoir and the last one (RT5) is considered as non-reservoir. The relative permeability curves of those four-rock type are presented in the Figures 4.4 and 4.5. The parameters included in the UTCHEMRS model are shown as follow:

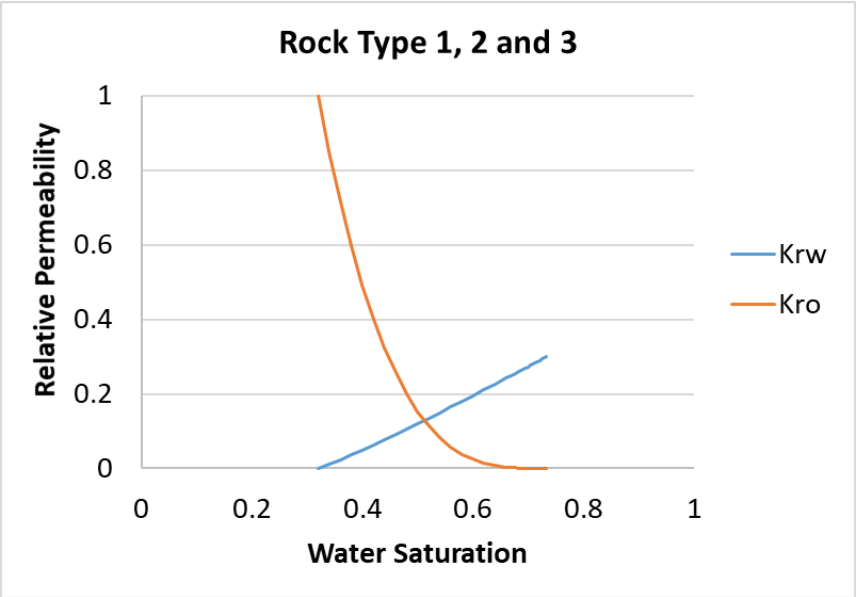

Figure 4.4. Relative permeability curves of rock type 1, 2, and 3.

The water and oil relative permeability curves are calculated using the Corey Model as

$$k_{rw} = k_{rw}^{0}\left(\frac{S_w - S_{wc}}{1 - S_{wc} - S_{orw}}\right)^{n_w} \tag{4.1}$$

$$k_{ro} = k_{ro}^{0}\left(\frac{1 - S_{orw} - S_w}{1 - S_{wc} - S_{orw}}\right)^{n_o} \tag{4.2}$$

where S_{orw} is the residual oil saturation and S_{wc} is the connate water saturation.

Relative Permeability Parameters Rock Types 1, 2 and 3.	
Residual Water Saturation - Swc	0.32
Residual Oil Saturation - Sorw	0.27
Endpoint Water Relative Permeability - krw0	0.3
Water Exponent - nw	1.1
Endpoint Oil Relative Permeability - krow0	1
Oil Exponent - no	3.18

Table 4.1. Relative permeability parameters for RT 1, 2 and 3.

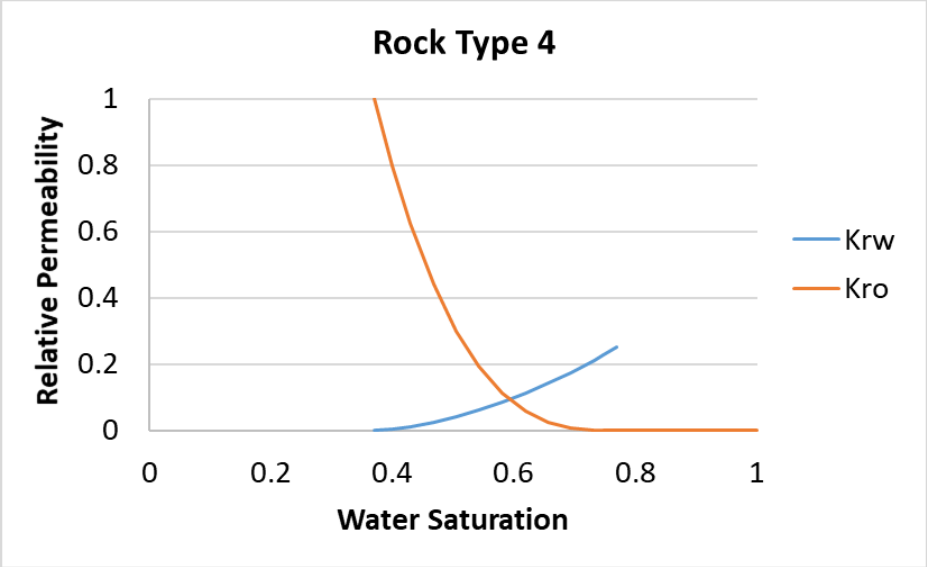

Figure 4.5. Relative permeability curves of rock type 4.

Relative Permeability Parameters Rock Type 4.	
Residual Water Saturation - Swc	0.37
Residual Oil Saturation - Sorw	0.23
Endpoint Water Relative Permeability - krw0	0.25
Water Exponent - nw	1.7
EndPpoint Oil Relative Permeability - krow0	1
Oil Exponent - no	2.88

Table 4.2. Relative permeability parameters for RT 4.

Polymer viscosity dependence at shear rate

In this conversion process, it was necessary to convert and adapt the PF parameters to UTCHEMRS model input. The model of PF in UTCHEMRS begins with the viscosity dependence on shear rate with the equation given below. The polymer viscosity (Eq. 4.3) depends on water viscosity (μ_w), the viscosity at zero shear rate (μ_p^0), the shear rate (γ), the shear rate at which viscosity is approximately 1/2 of of μ_p^0 and P_α is an input parameter corresponding to the slope of shear thinning curve (UTCHEM, 2017).

$$\mu_p = \mu_w + \frac{\mu_p^0 - \mu_w}{1 + \left(\frac{\gamma}{\gamma_{1/2}}\right)^{P_\alpha - 1}} \tag{4.3}$$

The polymer viscosity at zero shear rate as a function of concentration and effective salinity is given by:

$$\mu_p^0 = \mu_w\left(1 + \left(A_{p1}C_{41} + A_{p2}C_{41}^2 + A_{p3}C_{41}^3\right)C_{SEP}^{Sp}\right) \tag{4.4}$$

where A_{p1}, A_{p2}, A_{p3} are fitting parameters. C_{41} is the polymer concentration in water and S_p is the parameter for salinity dependence, which could be found by the slope of measured lab data of $\frac{\mu_p^0 - \mu_w}{\mu_w}$ vs C_{SEP}. The viscosity at zero shear rate μ_p^0 is from the lab results at different polymer concentrations, C_{41} , starting from 500 ppm to 2500 ppm and a fixed shear rate.

Effective Salinity C_{SEP} (Eq. 4.5) is dependent on total anion concentration (in meq/mL C_{51}, the total divalent cation concentration in meq/ml C_{61}, the water concentration C_{11} assumed to be 1 in the absence of surfactant and cosolvent, and β_p which is a parameter for calculating the effective divalent salinity. In this work, the effective salinity was calculated from the compositions of the injection water and reservoir water reports of the Colombian field.

$$C_{SEP} = \frac{C_{51} + (\beta_p - 1)C_{61}}{C_{11}} \tag{4.5}$$

From Equations 4.3 and 4.4, it is possible to find the remaining parameters, such as $\gamma_{1/2}$ and P_α. Therefore, the equation 4.4 is redefined as

$$\frac{\mu_p^0 - \mu_w}{\mu_w * C_{SEP}^{sp}} = A_{p1}C_{41} + A_{p1}{C_{41}}^2 + A_{p1}{C_{41}}^3 \tag{4.6}$$

or it can be defined as follows:

$$\mu_p^0 - \mu_w = e^{\ln\left(A_{p1}C_{41} + A_{p1}{C_{41}}^2 + A_{p1}{C_{41}}^3\right)} * (\mu_w + C_{sep}^{sp}) \tag{4.7}$$

In addition, the Equation 4.3 is expressed in a similar form as Equation 4.6.

$$ln\left(\frac{\mu_p^0 - \mu_w}{\mu_p - \mu_w} - 1\right) = (P_\alpha - 1) * \ln(\gamma) - (P_\alpha - 1) * \ln\left(\gamma_{1/2}\right) \tag{4.8}$$

Later, Equation 4.7 is replaced in Equation 4.8 as follows:

$$\underbrace{ln\left(\frac{\left(A_{p1}C_{41} + A_{p1}{C_{41}}^2 + A_{p1}{C_{41}}^3\right) * (\mu_w + C_{sep}^{sp})}{\mu_p - \mu_w} - 1\right)}_{y} = \underbrace{(P_\alpha - 1)}_{m} * \underbrace{\ln(\gamma)}_{x} - \underbrace{(P_\alpha - 1) * \ln\left(\gamma_{1/2}\right)}_{b} \tag{4.9}$$

Knowing x and y axes, it is possible to curve fit the lab data for each polymer concentration (C_{41}) in order to find the slope and the term b. Subsequently, the parameters P_α and $\gamma_{1/2}$ are computed. Polymer viscosity can then be modeled as a function of shear rate using Equation 4.3. Finally, the results of the polymer viscosity model are compared with the laboratory data. For instance, Figure 4.6(a) depicts measured data for reservoir water at 500 ppm of polymer, C_{41}, and Figure 4.6 (b) shows data for injection water at 1000 ppm of polymer. Both plots show an agreement between the model and the lab data.

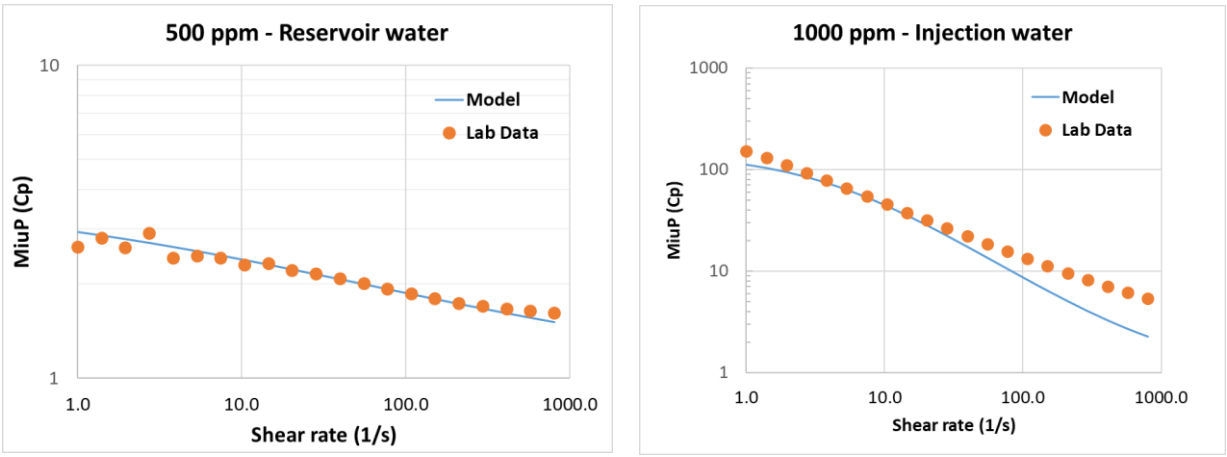

(a) (b)

Figure 4.6. Model of polymer viscosity behavior (a) Polymer concentration at 500 ppm with reservoir water (b) Polymer concentration at 1000 ppm with injection water.

Polymer adsorption

The polymer adsorption or polymer retention is due to physical trapping, in the small pores (fine grain sand), and adsorption onto solid surfaces, since the larger the surface area the greater the polymer loss (Omar, 1983). Modeling polymer adsorption is relevant in order to closely represent the physics of polymer injection. Consequences of the polymer retention are slowing down the polymer velocity and depleting of polymer slug. As a result, there is reduction of polymer effectiveness in the swept process (Omar, 1983). In this work, the results from the lab data (Figure 4.7), are used to obtain the parameters AD41, AD42, and B4D as input parameters for UTCHEMRS.

Adsorbed concentration $\hat{C}_4$ is related to the polymer concentration in water C_{41}, water volume fraction $\hat{C}_1$ and the matching parameters a_4 and b_4, which intrinsically denote the dependence of $\hat{C}_4$ on salinity and permeability.

$$\frac{\hat{C}_4}{\hat{C}_1} = min\left(\hat{C}_4, \frac{\frac{a_4(C_{41})}{\hat{C}_1}}{1 + b_4 C_{41}}\right) \tag{4.10}$$

where $a_4 = (a_{41} + a_{42} C_{SEP})$.

For this case, polymer adsorption parameter a_{42} is assumed to be zero since the effect of the salinity on the adsorption is neglected. Therefore, $a_4 = a_{41}$. On this same line, $\hat{C}_1$ is 1 because lab tests were calibrated only with water. According to the special conditions, for this model, the Equation 4.8 could be described by the following terms of a curve with the equation:

$$y = \frac{a * x}{(1 + b * x)} \tag{4.11}$$

In order to obtain the parameters $a_4 = a$ and $b_4 = b$ in Equation 4.11, y and x are known values from lab test as $\hat{C}_4$ and C_{41}, respectively. The curve fitting tool was applied to find the matching parameters AD41=7.39 and B4D=143.6.

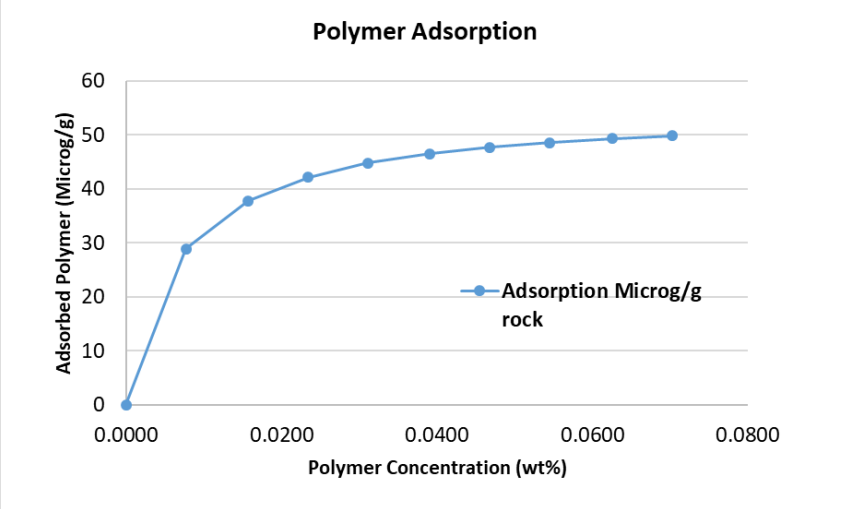

Figure 4.7. Polymer adsorption plot based on the lab results.

Step 2. History Match models

This step shows the history match (HM) results for three different simulators. where HM focuses on the polymer flooding performance. Therefore, it starts from June 2014, which is five months before the first injection of polymer, to February 2018. Since the ECLIPSE HM begins on February 1985, it was necessary to run a restart case from June 2014 in order to compare the same period of time. The figures below show the HM results of ECLIPSE, INTERSECT, and UTCHEMRS compared to the field data.

The original HM model is controlled by liquid rate. Same constraint was used for the other two simulators. This explains why the liquid rate (Figure 4.8) is fairly similar to the field data.

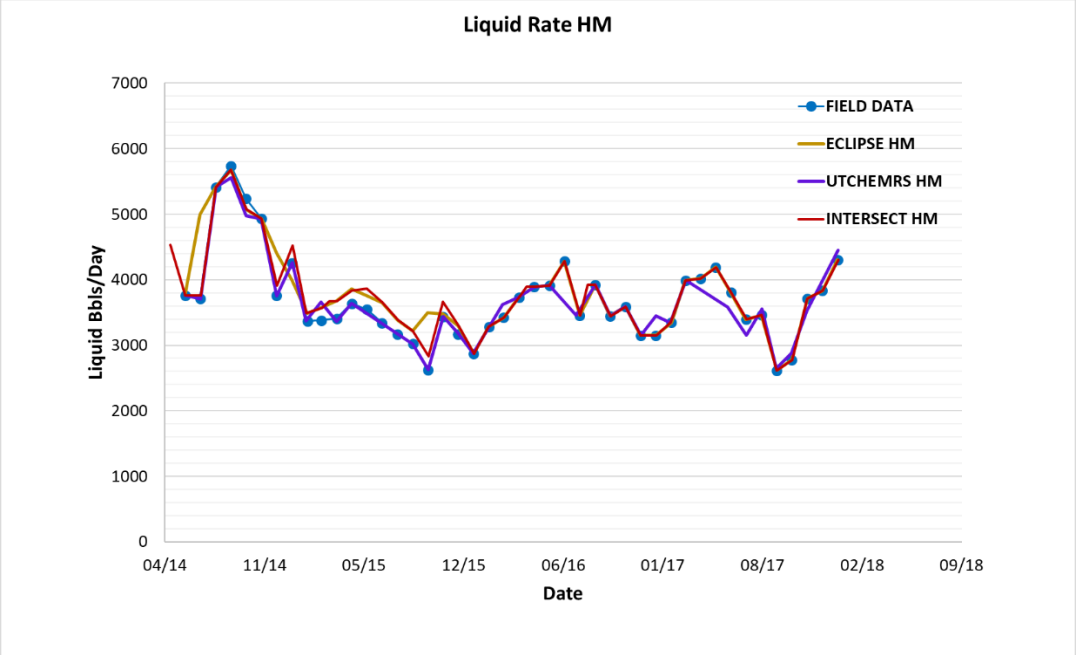

Figure 4.8. Liquid rate History Match comparison.

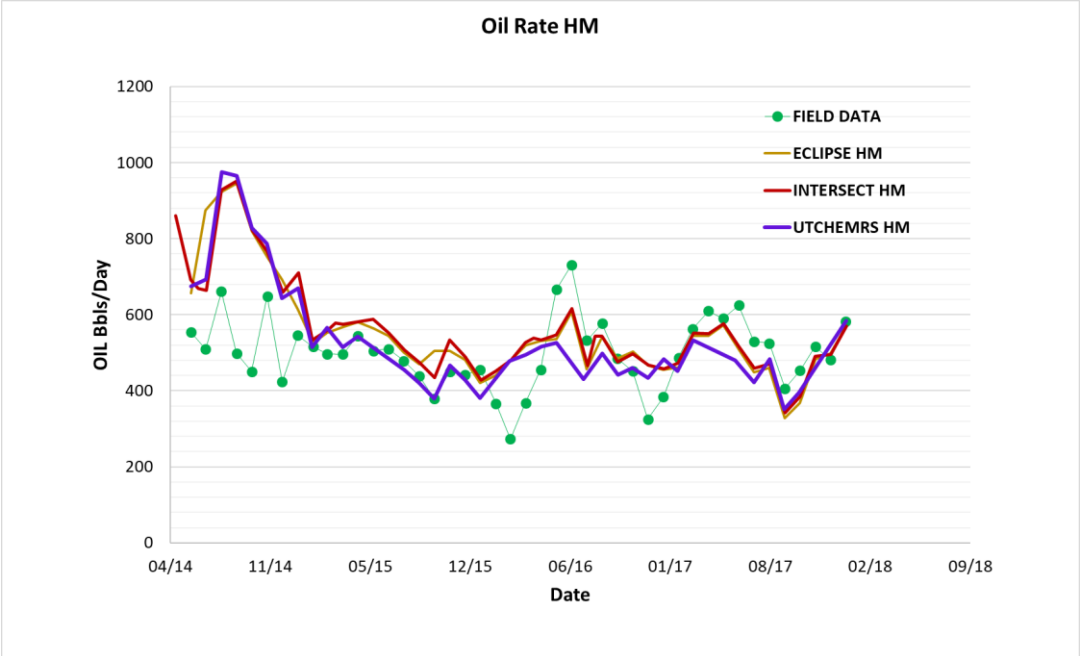

Figure 4.9. Oil rate History Match comparison.

According to the Figure 4.9, the results of oil rate HM show divergences among simulation results and the field data at the beginning of June 2014 and for the subsequent eight months. However, the similar responses of the simulators, which are created with different assumptions and models, indicated the reliable HM. One reason for the difference between the field and simulation results might be related with the uncertainty in the geological modeling. Chapter 6 will describe potential future work to address this.

On the other hand, the remaining part, which is affected by PF, shows a similar tendency of oil production rate. There are some spikes in the field data production that the simulators cannot mimic in detail. Since the UTCHEMRS and INTERSECT reservoir models were generated from the ECLIPSE model, it is expected to have comparable results for all simulators. However, the UTCHEMRS model matches the field cumulative oil recovery only slightly better as shown in Figure 4.10 and Table 4.3.

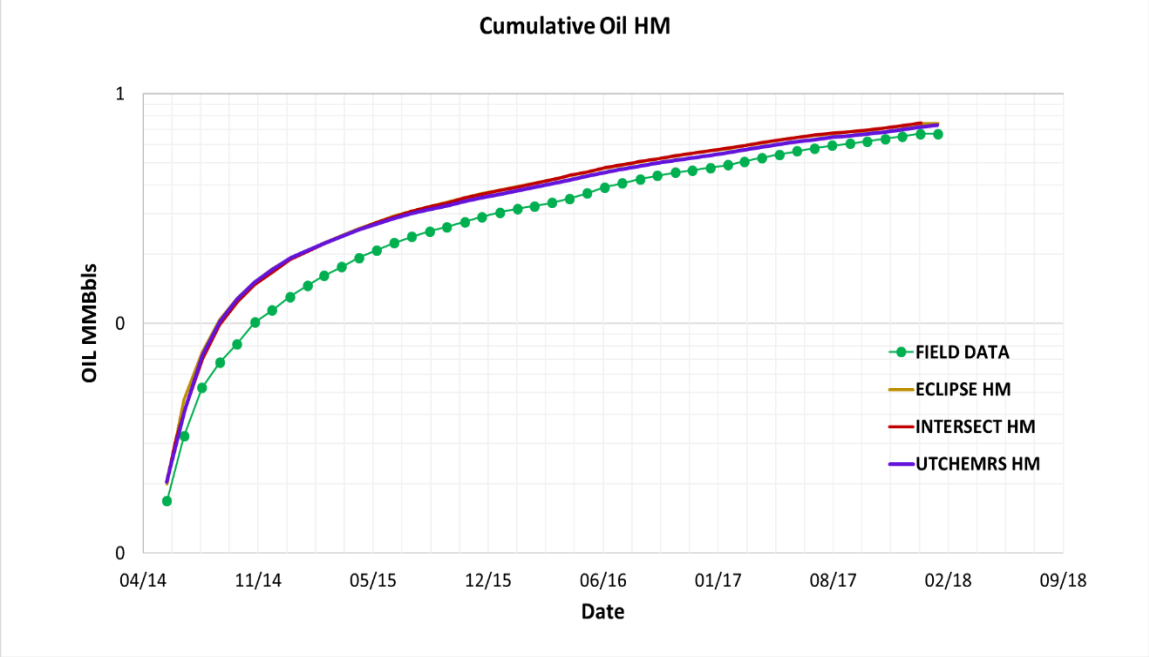

Figure 4.10. Cumulative Oil recovery during the HM.

	Cum Oil (MMBbls)	Volume difference (MMBbls)	Difference from the reference (%)
FIELD DATA	0.669		
ECLIPSE	0.739	0.071	9.5%
INTERSECT	0.745	0.076	10.2%
UTCHEMRS	0.731	0.062	8.5%

Table 4.3. Comparative oil volumes at January 2018 what time.

The HM performance in UTCHEMRS will be used as a foundation for the future simulation cases defined in the next steps of the workflow.

Step 3. Water Flooding HM and Base Case Forecast

In order to determine the oil recovery by the PF process in A2 and A2i, we simulated a hypothetical case without polymer injection during the HM. The WF simulation is a base for the next cases of PF and SPF.

The Base Case is the scenario forecast without additional activity as the drilling of new wells or the injection of a new EOR process. This case is keeping the activity before finishing the HM. In this work the forecast is extended for almost six years or 2129 days starting from February 2018 and finalizing on December 2023. The WF HM and forecast results are presented in the following sections.

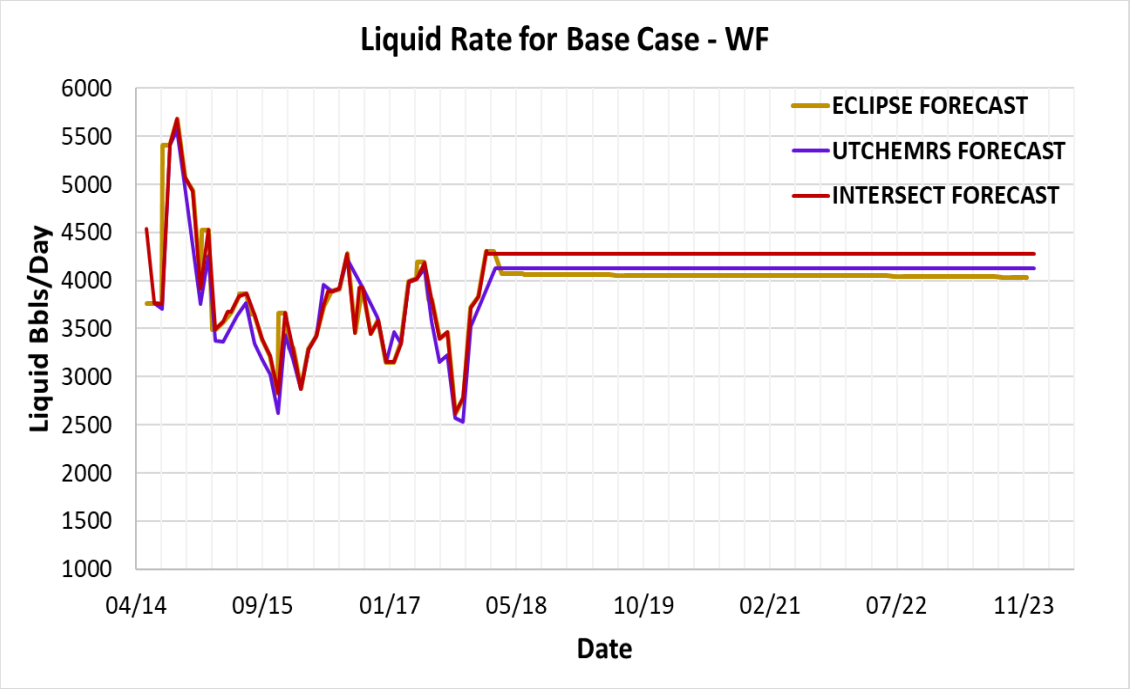

Figure 4.11. Liquid rate for base case WF.

The original HM and forecast model in ECLIPSE are controlled by liquid rate for injectors and producers as well. Same constraint was applied in the other two simulators and the results are shown in Figure 4.11.

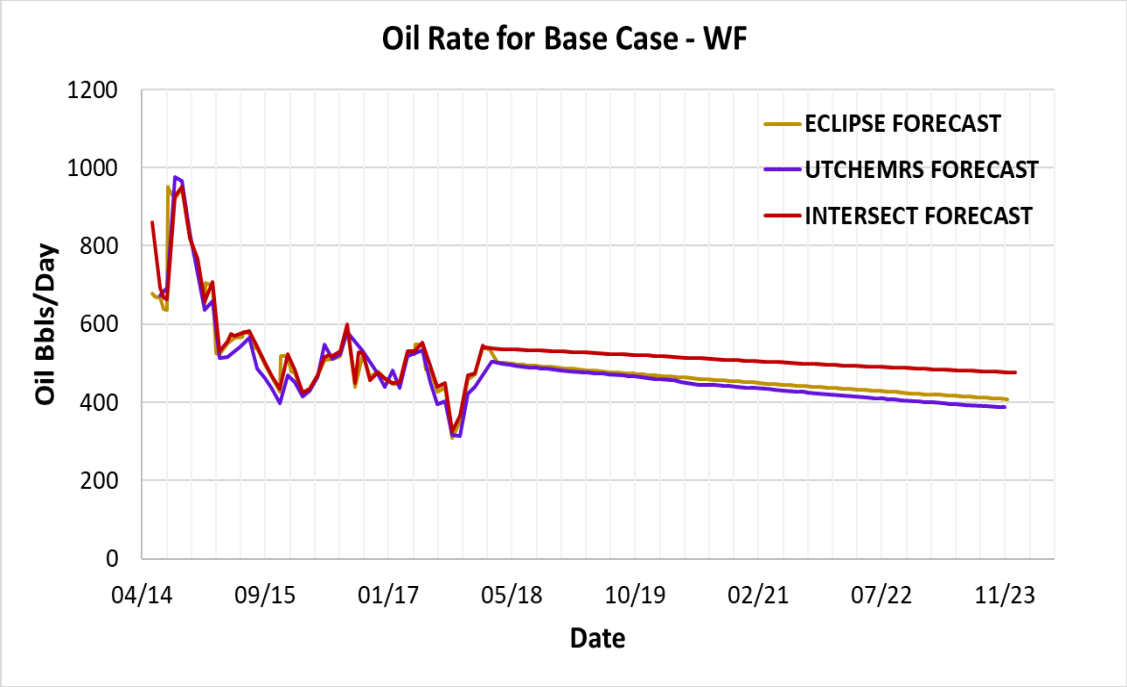

Figure 4.12. Oil rate for base case WF.

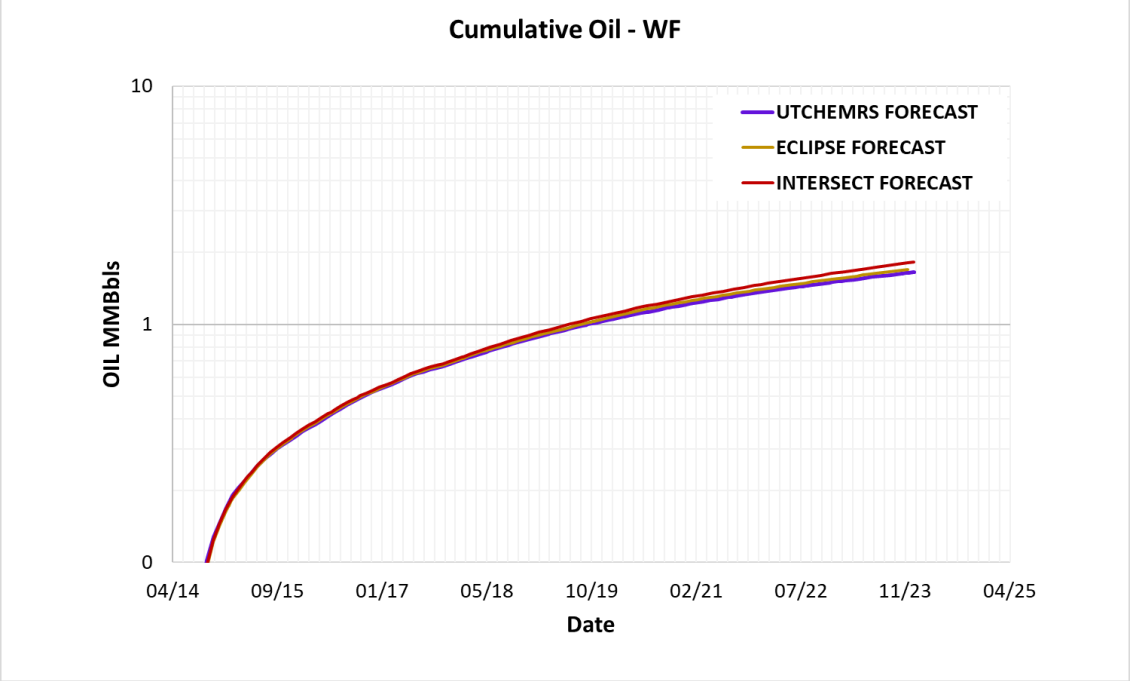

Figure 4.13. Cumulative oil recovery for base case WF.

In general, the results of three simulators are similar in oil production rate (Figure 4.12) and cumulative oil recovered (Figure 4.13). These simulations show good agreement in both HM

and forecast modes with confidence in these results. As we mentioned in the last step, the field data is the reference for the HM evaluation. In the case of forecast, ECLIPSE is the reference point for the evaluation results considering that it is the original simulator of the sector model and it is the widely used commercial simulator. Table 4.4 shows the quantitative differences between the results of the simulators. The results reveal a difference of less than 7% among them. In Chapter 5 the performance of PF versus WF during HM and forecast will be shown.

	Cum Oil (MMBbls)	Volume difference (MMBbls)	Difference (%)
ECLIPSE	1.694		
INTERSECT	1.821	0.127	7.0%
UTCHEMRS	1.655	-0.039	-2.4%

Table 4.4. Comparative oil volumes HM and forecast simulations for WF as of December 2023.

Step 4. Polymer Flooding Base Case Forecast in A2 and A2i

Starting with the Step 3 results, the PF base case is performed. The conditions for this scenario are defined as the same specifications at the end of the HM. The polymer is injected through the four injectors - with equal polymer concentration. The simulation results for the three simulators will be presented in the next chapter of results and discussions.

Step 5. Perform scenario for polymer injection in A2, A2i, B2c, and B2d.

The positive results of PF in A2 and A2i brings the possibility of testing the same technology in a reservoir structurally lower than A sands, called B sands. This step considers injecting polymer in A2, A2i, B2c, and B2d at same time. The purpose of this scenario is to evaluate the possibility of injecting polymer in both sands. The results will be appraised with the oil recovery comparison between this case and the case of the previous step.

In this case, according to the previous analyses of productivity done by the Colombian Company, the sands B2c and B2d are the most prospective layers at B reservoir. The rock properties of those sub sands are shown in the Table 4.5. In addition, the operator performed a

polymer injectivity evaluation and selection study where a total of 8 polymers were tested. This fluid-fluid study (ICP, 2019) includes test of viscosity performance, thermal/ mechanical stability and filterability. As a conclusion, one of the most complete polymers that met the minimum conditions for be injected in "B" Sands is the conventional polyacrylamide Flopaam 5115 used for "A" Sands. The fluid-rock study is still in process. Meanwhile, the reference of polymer concentration used for the simulations in UTCHEMRS will be the same as for "A" sands. However, this brings the possibility of variate the concentration in order to see the affectation to the producer wells.

Sands	Gross h (ft)	Net h (ft)	Net to Gross	Avg Porosity of Net sand (%)	Permeability Range of Net sand (mD)
A	1100	220	0.20	22	100-1000
B	1300	350	0.27	20	50-500
→ B2c	168	101	0.60	20	80-500
→ B2d	77	30	0.39	20	70-500
C	200	60	0.30	20	50-600

Table 4.5. Rock properties of A, B and C sands and sub sands of B in Colombian Field

The well configuration for B sands changes respect to A sands. Most of the wells open in the upper layers are shut-in or they are not completed at the depth of B2c and B2d reservoir sands. Figure 4.11 is presenting a schematic comparison of the wells activate in each sand. For this schematic the Figure 3.4 has been recalled. Regarding to the polymer injectors the only well that is completed in the B sands depth is Well 1222. Therefore, Well 520 is injecting in those B2c and B2d sands as a replacement. This condition applies for the cases where the polymer is injected in the lower sands.

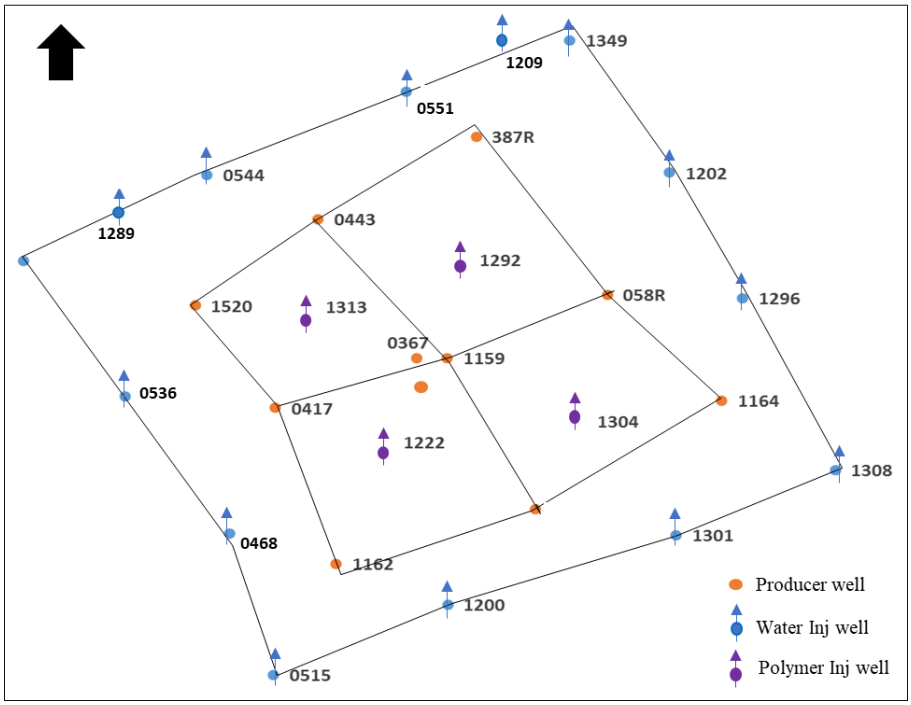

(a)

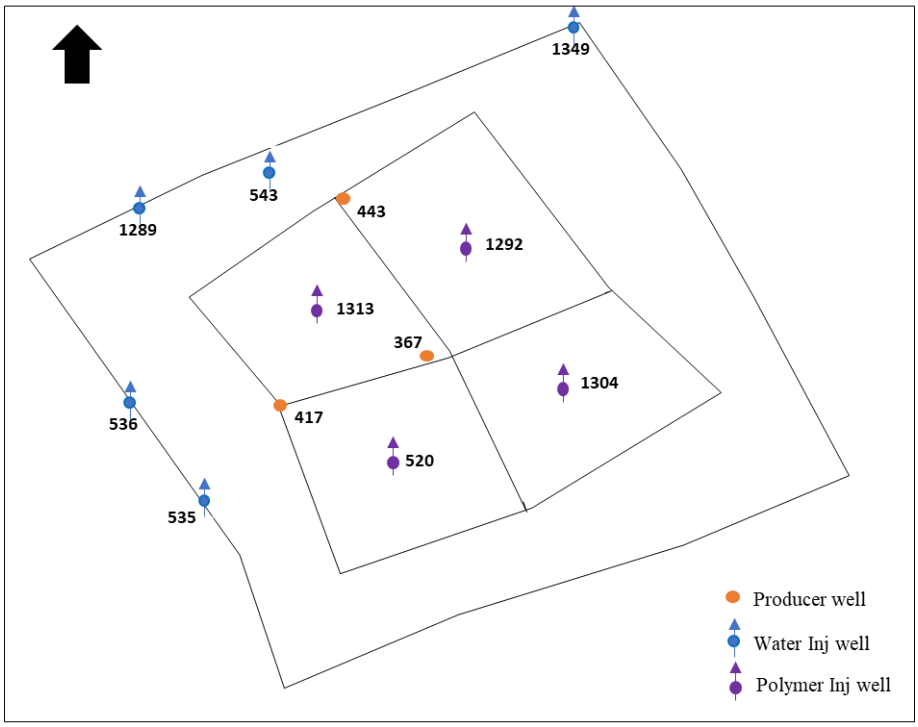

(b)

Figure 4.14. Schematic comparison of the activate at different depths (a) Active wells at A sands (b) Active wells at B sands.

The flow rate in the four injectors was updated according to the new completions open in B2c and B2d layers. As reported by Colombian Company the barrels injected per foot, which comes from injection logging test (ILT) and the rate of other wells, was the reference taken in order to increase the injection rate associated to adding "B" sands which is about 3 bbls/ft.

Step 6. Comparison of oil recovery performance of PF for A and B sands

The preceding step simulated the cases with A and B sands at the same time. However, the polymer injection process in each formation is likely different because the diverse conditions of rock and fluid properties. Table 4.6 presents the major properties comparison between A and B reservoirs.

	A Sands	**B Sands**
Porosity of Net Sand (%)	22	20
Permeability Range of Net Sand (mD)	100-1000	50-500
Oil viscosity (cP)	40	12
°API of Oil	21.5	23.7
Datum (SS) (ft)	3035	4015
Reservoir Temp (°F)	116	125
Reservoir Pressure (psi)	1510	1963
Bubble Pressure (psi)	1228	1756

Table 4.6. Reservoir and fluid data for A and B reservoirs.

With the aim of knowing the real performance of PF in B sands, this step focuses on the comparison in terms of oil recovery factor. The recovery evaluation will be through the drilling of three new oil producers at the north area of the current polymer pilot. Figure 4.15 illustrates the location of the proposed producer wells. Those wells are strategically located at the first line of the polymer injectors 1313 and 1292. From the existing wells, the Well 443 and Well 417 are the only two producers completed in both reservoirs (A and B). In this case the new wells NW01,

NW02 and NW04 are neighboring the Well 443. The location of those wells is for the purpose of surveillance of the polymer flood through the two injectors mentioned above.

With the final goal of identifying the consequence of injecting polymer in those layers, this step includes the simulation of two cases per sand. One case is injecting exclusively water (WF) and the other case is injecting polymer (PF). In total we will perform four cases. The comparison of oil recovery associated with WF versus the oil recovery associated with PF will give the quantitative reference about the effectiveness of PF in each one reservoir.

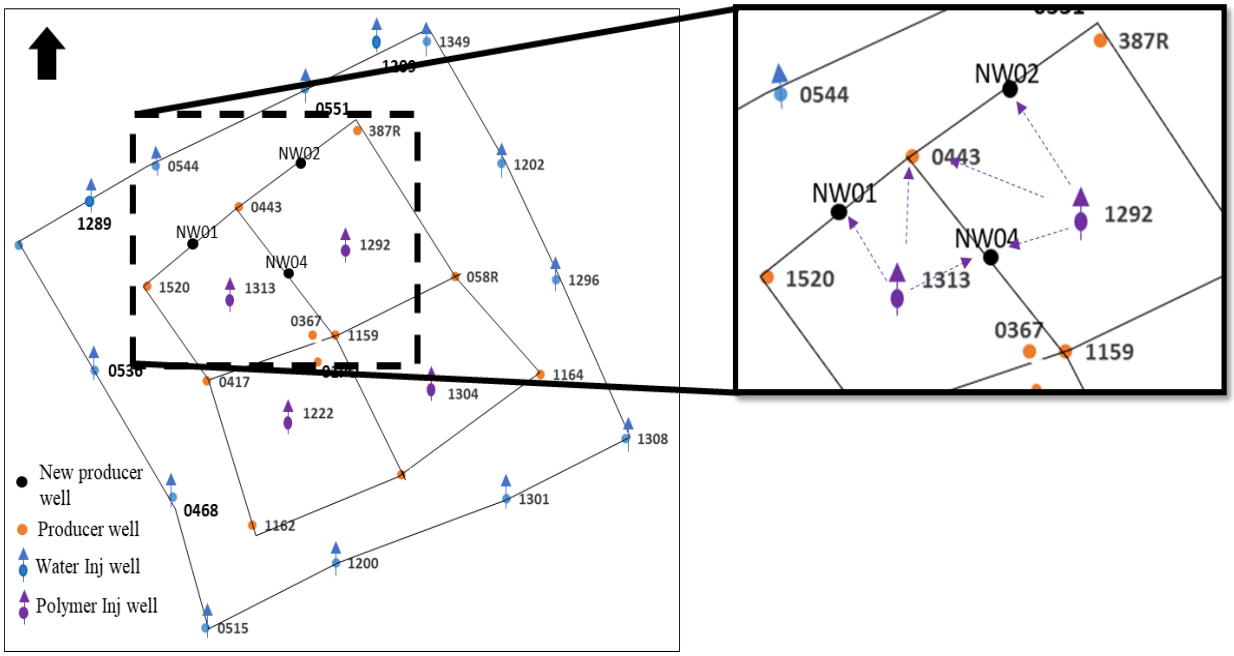

Figure 4.15. Schematic of the new wells for the selective polymer injection in A or B sands. Map at A sands depth.

Injecting and Producing only in A Sands.

Colombian field has a challenge associated to the uncertainty of the production potential by each reservoir as the oil production is not reliably allocated. The vast majority of the oil wells produce in commingled of up to three formations (A, B and C). Therefore, these cases consider the squeeze of all completions unlike to A2 and A2i sands in the wells 443, NW01, NW02 and

NW03 in order to ensure the selective affectation of PF to A sands. In addition, the polymer injectors 1292 and 1313 keep the injection through A2 and A2i.

Injecting and Producing only in B Sands.

These cases contemplate the squeeze of all completions unlike to B2 and B2i sands in the wells 443, NW01, NW02 and NW04 to ensure the selective injection of PF to B sands. In addition, the completions of A2 and A2i will be closed and the B2c and B2d sands will be open in the polymer injectors 1292 and 1313. As was mentioned before the injection rates were updated according to the thickness open in B, in Table 4.7, there are the rates per sand injected.

Injector Name	Barrels injected per day in A2 and A2i	Barrels injected per day in B2c and B2d
1292	403	149
1313	388	233

Table 4.7. Injection rates for A and B sands.

The completion of the new wells and the interventions for the current wells will be performed in March 2018.

Step 7. Base case Simulation for surfactant polymer injection

The purpose of this step is to evaluate the feasibility of surfactant polymer flooding (SPF) in A2 and A2i sands. After the results with the Steps 3 and 4, the SPF is a scenario with the goal of reaching the oil that the previous mechanisms cannot recover. The result of this scenario for A2 and A2i is a valuable reference of production optimization through a new EOR implementation in the Colombian Field. This surfactant polymer injection will take advantage of the previous polymer pilot facilities and polymer injectors. Thus, the SP injection for this scenario is through the same four injectors mentioned above.

The SPF formulation uses the UTCHEMRS parameters described below together with the values used as simulation input.

Surfactant retention

The surfactant retention model uses a Langmuir adsorption isotherm model as:

$$\hat{c}_3 = \frac{(a_{31} + a_{32} c_{se}) c_{31}}{1 + b_3 c_{31}} \tag{4.12}$$

where the parameters a_{31}, a_{32} and b_3 are obtained by matching laboratory data from coreflood surfactant retention results and UTCHEMRS considers both reversible and irreversible adsorption. Table 4.8 shows the surfactant retention parameters used for this simulation.

UTCHEMRS Parameters	Values
Surfactant Retention	
Surfactant Adsorption parameter a31 (AD31)	1.57
Surfactant Adsorption parameter a32 (AD32)	0.50
Surfactant Adsorption parameter b3d (B3D)	1000

Table 4.8. Surfactant retention parameters.

Microemulsion Viscosity Model

The original viscosity model considered in UTCHEMRS (2017) uses five parameters correlation (α_1 *to* α_5) in order to calculate the microemulsion viscosity as follows:

$$\mu_3 = C_{13}\,\mu_{pw} e^{\alpha_1 (C_{23} + C_{33})} + C_{23}\,\mu_o e^{\alpha_2 (C_{13} + C_{33})} + C_{33}\,\alpha_3 e^{(\alpha_4 C_{13} + \alpha_5 C_{23})} \tag{4.13}$$

where μ_o is the viscosity of pure oil and μ_{wp} is calculated from the modified Equation 4.3 (Meter and Bird, 1964)

$$\mu_{pw} = \mu_w + \frac{\mu_p^0 - \mu_w}{1 + \left(\frac{\dot{\gamma}_{eq,j}}{\dot{\gamma}_{1/2}} \right)^{P_\alpha - 1}}, \tag{4.14}$$

where μ_w is the brine viscosity, $\dot{\gamma}_{1/2}$ is a parameter, $\dot{\gamma}_{eq,j}$ is the equivalent shear rate of phase j, P_α is the power law exponent, μ_p^0 is the polymer solution viscosity at zero shear rate that is computed as a modified Equation 4.4 as

$$\mu_p^0 = \mu_w \left[1 + \left(A_{p1} \frac{c_{4j}}{c_{1j}} + A_{p2} \left(\frac{c_{4j}}{c_{1j}} \right)^2 + A_{p3} \left(\frac{c_{4j}}{c_{1j}} \right)^3 \right) C_{SEP}^{S_P} \right], \tag{4.15}$$

where A_{p1}, A_{p2}, A_{p3}, and S_P are model parameters, C_{SEP} is the effective salinity.

From Equation 4.14, the equivalent shear rate ($\dot{\gamma}_{eq,j}$) is calculated as

$$\dot{\gamma}_{eq,j} = \frac{3.97C\left|\vec{u}_j\right|}{\sqrt{\bar{k}k_{rj}\phi S_j}}, \tag{4.16}$$

where C is the shear rate correction factor, $\vec{u}_j$ is the phase j velocity, S_j is the phase j saturation, and $\bar{k}$ is an average absolute permeability. Table 4.9 displays the microemulsion viscosity parameters used for this simulation.

UTCHEMRS Parameters	Values
Microemulsion viscosity parameters (default model)	
Alpha1	0.8
Alpha2	1.5
Alpha3	0.1
Alpha4	0.1
Alpha5	0.1

Table 4.9. Microemulsion viscosity parameters

Capillary Desaturation Model

Delshad et al. (1996) in their work presented a capillary desaturation model (CDM), which the residual saturation of each phase is affected by the trapping number as.

$$S_{rj} = \min\left[S_j, \left(S_{rj}^{high} + \frac{S_{rj}^{low} - S_{rj}^{high}}{1 + T_j N_{Tj}} \right) \right], \tag{4.17}$$

where the superscript *high* means a property at high trapping number while the superscript *low* means a property evaluated at low trapping number and N_{Tj} is given by:

$$N_{Tj} = \frac{\left|\bar{\bar{K}} \cdot \left(\vec{\nabla} P_{j'} - \rho_j g \vec{\nabla} D\right)\right|}{\sigma_{jj'}}, \tag{4.18}$$

where *j'* denotes the displacing fluid phase.

The interfacial tension for computing the trapping number of the microemulsion phase in the three-phase environment (O/W/ME) is computed as

$$\sigma_{33} = \begin{cases} \sigma_{23}, & for \;\; S_1 \le S_{r1} \;\; and \;\; S_2 > S_{r2} \\ \sigma_{13}, & for \;\; S_1 > S_{r1} \;\; and \;\; S_2 \le S_{r2} \end{cases}, \tag{4.19}$$

The relative permeability endpoints and exponents are a function of the residual saturations as

$$k_{rj}^0 = k_{rj}^{0,low} + \left(\frac{S_{rj'}^{low} - S_{rj'}}{S_{rj'}^{low} - S_{rj'}^{high}} \right) \left(k_{rj}^{0,high} - k_{rj}^{0,low} \right), \tag{4.20}$$

and

$$n_j = n_j^{low} + \left(\frac{S_{rj'}^{low} - S_{rj'}}{S_{rj'}^{low} - S_{rj'}^{high}} \right) \left(n_j^{high} - n_j^{low} \right), \tag{4.21}$$

where low and high superscripts refer to low and high trapping numbers.

New Capillary Desaturation Model

According to Fernandes (2019), the new model proposed here assumes the effect of all other phases. This CDM is the model used in this work. Fernandes assumes that the displacing phase is a combination of all phases except for the displaced phase.

$$k_{rj}^0 = k_{rj}^{0,low} + \left(k_{rj}^{0,high} - k_{rj}^{0,low} \right) \prod_{l=1; l \neq j}^{n_p} \left(\frac{S_{rl}^{low} - S_{rl}}{S_{rl}^{low} - S_{rl}^{high}} \right) \tag{4.22}$$

and

$$n_j = n_j^{low} + \left(n_j^{high} - n_j^{low} \right) \prod_{l=1; l \neq j}^{n_p} \left(\frac{S_{rl}^{low} - S_{rl}}{S_{rl}^{low} - S_{rl}^{high}} \right), \tag{4.23}$$

The interfacial tension used for the microemulsion phase when three phases are present is also obtained through a continuous interpolation written as

$$\sigma_{33} = \frac{S_1\sigma_{13} + S_2\sigma_{23}}{S_1 + S_2}, \tag{4.24}$$

Table 4.10 presents the capillary desaturation parameters used for this simulation.

UTCHEMRS Parameters	Values
Capillary Desaturation Parameters for Phase 1, 2 and 3	
Trapping parameter for water, T11	2000
Trapping parameter for oil, T22	40000
Trapping parameter for microemulsion, T33	2000
Residual Saturation at high trapping number for water	0.37
Residual Saturation at high trapping number for oil	0.23
Residual Saturation at high trapping number for water	0.2

Table 4.10. Capillary desaturation parameters for phases 1, 2 and 3.

Relative Permeabilities

The relative permeabilities are computed using the Corey type model

$$k_{rj} = k_{rj}^0 \bar{S}_j^{n_j}, \tag{4.25}$$

with

$$\bar{S}_j = \frac{S_j - S_{rj}}{1 - \sum_{l=1}^{n_p} S_{rl}}, \tag{4.26}$$

There is a challenge with this approach because some discontinuities rise when any of the endpoints, exponents, or residual saturations are not the same for all phases. According to Lashgari et al. (2018) such issue was resolved assuming that the microemulsion parameters are computed

as an interpolation between the pure oil and water parameters based on the oil volume fraction in the microemulsion phase. Therefore, the relative permeabilities model is used in this work:

$$\Psi_3 = (1 - c_{23})\Psi_1 + c_{23}\Psi_2, \tag{4.27}$$

where the parameter Ψ is any of the following: $k_{r3}^{0,high}$, $k_{r3}^{0,low}$, n_3^{high}, n_3^{low}, S_{r3}^{high}, S_{r3}^{low}, and T_3, where $k_{r3}^{0,high}$ is the microemulsion relative permeability endpoint at high trapping number, $k_{r3}^{0,low}$ is the microemulsion relative permeability endpoint at low trapping number, n_3^{high} is the microemulsion relative permeability exponent at high trapping number, n_3^{low} is the microemulsion relative permeability exponent at low trapping number, S_{r3}^{high} is the microemulsion relative permeability residual saturation at high trapping number, and S_{r3}^{low} is the microemulsion relative permeability residual saturation at high trapping number.

Phase Behavior Model

Effective Salinity

The effective salinity model mentioned in UTCHEMRS (2017) is represented by the next equation:

$$C_{SE} = C_{51}(1 - \beta_6 f_6^s)^{-1}\left(1 + \beta_T(T - T_{ref})\right)^{-1} \tag{4.28}$$

where $C_{51}$is the aqueous phase anion concentration; β_6 is a positive constant; $f_6^S = \frac{C_6^s}{C_3^m}$ is the fraction of the divalent cations bound to surfactant micelles; and β_T is the temperature coefficient.

Binodal Curve

The phase behavior for microemulsion systems can be modelled using the extended Hand's rule (Pope and Nelson, 1978). The extended Hand's rule considers the following relationship for the binodal curves:

$$\frac{C_{3l}}{C_{2l}} = A\left(\frac{C_{3l}}{C_{1l}}\right)^B \; for\; l = 1,2\; or\; 3 \tag{4.29}$$

the constraints for the phase compositions are

$$c_{1\ell} + c_{2\ell} + c_{3\ell} = 1, \qquad \ell = 1,\ldots,n_p \tag{4.30}$$

and *B=-1* for symmetric binodal curves, C_{3l} is denotes as

$$C_{3l} = \frac{1}{2}\left[-AC_{2l} + \sqrt{(AC_{2l})^2 + 4AC_{2l}(1 - C_{2l})}\right] \; for\; l = 1,2\; or\; 3 \tag{4.31}$$

and A controls the height of the binodal curve as follows:

$$A_m = \left(\frac{2C_{3max,m}}{1 - C_{3max,m}}\right)^2 \quad for\ m = 0, 1\ and\ 2 \tag{4.32}$$

where m = 0 denotes low salinity, m = 1 denotes optimal salinity, and m = 2 denotes high salinity. In addition, $C_{3max,m}$ is equals to

$$C_{3max,m} = H_{BNC,m} + H_{BNT,m}\left(T - T_{ref}\right) \quad for\ m = 0, 1\ and\ 2 \tag{4.33}$$

where $H_{BNC,m}$ and $H_{BNT,m}$ are input parameters.

The parameter A is computed from a linear interpolation between its values at zero salinity (0), optimum salinity (1), and twice the optimum salinity (2), as

$$\begin{aligned} A &= (A_0 - A_1)\left(1 - \frac{C_{SE}}{C_{SEOP}}\right) + A_1 \quad for\ C_{SE} \le C_{SEOP} \\ A &= (A_2 - A_1)\left(\frac{C_{SE}}{C_{SEOP}} - 1\right) + A_1 \quad for\ C_{SE} > C_{SEOP} \end{aligned} \tag{4.34}$$

where $C_{SEOP} = \frac{C_{SEL} + C_{SEU}}{2}$ and the parameters A_i are computed from the height of binodal curves at the same salinity as

$$A_i = \left(\frac{2c_{3,i}^{\max}}{1 - c_{3,i}^{\max}}\right)^2 \tag{4.35}$$

For the SPF simulation, a synthetic phase behavior model was created using laboratory data (R13 and R23) with 50% oil at 47 C (temperature of "A" reservoir). Figure 4.16 shows the phase behavior with an optimum salinity of 9500 ppm TDS based on equal solubilization ratios. The formulation is aqueous stable up to 14,000 ppm TDS. The Type III window ranges from 6,000 ppm to 13,000 ppm TDS. Table 4.11 indicates the phase behavior parameters used for this simulation.

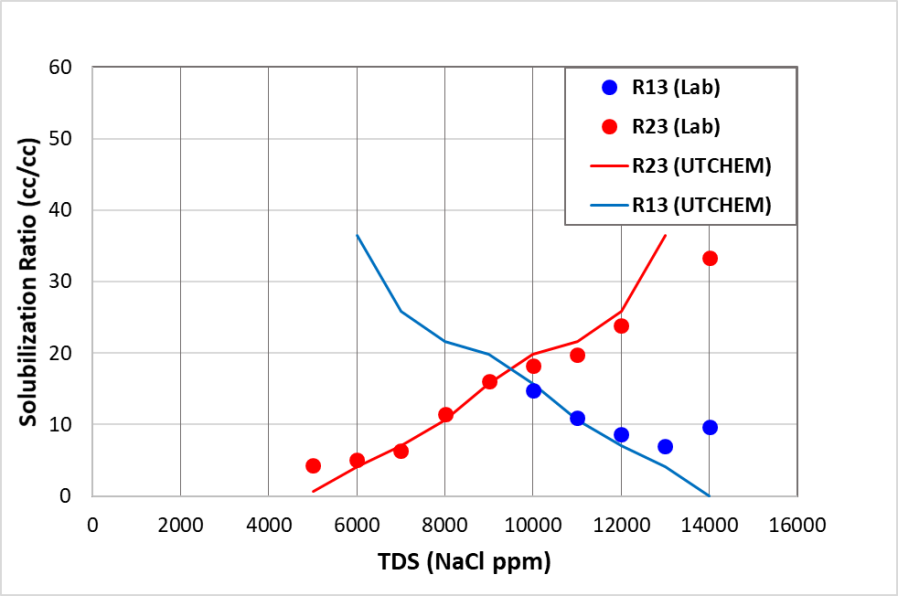

Figure 4.16. Solubilization ratio vs. salinity with 50% oil volume.

UTCHEMRS Parameters	Values
Effective Salinity	
Lower limit of effective salinity - CSEL (meq/ml)	0.0855
Upper limit of effective salinity - CSEU (meq/ml)	0.2393
Height of binodal curve at zero effective salinity - HBNC70	0.0550
Height of binodal curve at optimum effective salinity - HNBC71	0.0250
Height of binodal curve at twice optimum effective salinity - HBNC72	0.0550

Table 4.11. Surfactant phase behavior parameters.

Interfacial Tension

According to Huh (1979) the interfacial tension (IFT) is a function of solubilization ratio and its represented in Huh's equation as

$$\sigma_{l3} = \frac{c}{R_{l3}^2} \quad \text{for } l = 1 \text{ or } 2 \tag{4.36}$$

where the value of c is about 0.3. The equation was modified to reduce the water-oil IFT (σ_{ow}) as the surfactant concentration approaches zero.

$$\sigma_{l3} = \sigma_{ow} e^{-aR_{l3}} + \frac{cF_l}{R_{l3}^2}\left(1 - e^{-aR_{l3}^2}\right) \quad \text{for } l = 1 \; or \; 2 \tag{4.37}$$

where $R_{l3} = \frac{C_{l3}}{C_{33}}$ (solubilization ratio) and F_l as

$$F_l = \frac{1 - e^{-\sqrt{con_l}}}{1 - e^{-\sqrt{2}}} \quad \text{for } l = 1 \; or \; 2 \tag{4.38}$$

where $con_l = \sum_{k=1}^{3}(C_{kl} - C_{k3})^2$. The Table 4.12 displays the Chun Huh IFT Parameters used for this simulation.

UTCHEMRS Parameters	Values
Chun Huh IFT Parameters	
Huh Constant, c	0.35
Huh Constant, a	10

Table 4.12. Chun Huh IFT parameters.

SPF sequence

Table 4.13 gives the sequence of injection for a SPF. The design ensures the optimal conditions for surfactant effectiveness in the reservoir. The initial condition is the PF during the HM, then the SP slug to be injected starting March 2018. The parameters are defined by the solubilization curves presented above in the Figure 4.17. The optimum salinity for the highest solubilization ratio is around 9500 – 10,000 ppm. At that salinity, the SP slug should contain adequate polymer concentration to maintain mobility control and stability of the SP slug, and prevent fingering into the previous PF. The 0.3 pore volumes (PV) SP slug injected assure that enough surfactant will be injected because some of it is retained by adsorption on the permeable-media surfaces and also phase trapping (Lake, 2014).

Figure 4.17. SPF sequence.

The polymer drive or mobility buffer is injected after the SP slug (see Figure 4.16) with the objective of protecting the SP slug acting as a shield. The polymer drive viscosity should guarantee less or same mobility of the SP slug to prevent viscous fingering from the mobility buffer to the SP slug or even from the following phase to the polymer drive. Generally, the mobility buffer size is 50 to 100% of the floodable pore volume (Lake, 2014). In addition, the polymer drive is injected in water with salinity corresponding to Type I phase behavior to minimize the chance of surfactant being trapped (called salinity gradient design).

Parameters	Values
SP Slug	
Slug size (PV)	0.3
Surfactant (Vol fraction)	0.01
Salinity (ppm)	10,000
Polymer viscosity (cP)	23 - 35
Polymer Drive after SP	
Slug size (PV)	1
Salinity (ppm)	8000
Polymer viscosity (cP)	23

Table 4.13. Parameters of the SP injection sequence.

Step 8. Evaluate and compare the results

Step 8 has a critical role in the final recommendations for the production optimization of Colombian field through the EOR scenarios. The results generated from different cases mentioned in Steps 4 and 7 are compared by the oil recovery and economic viability to be implemented. The Steps 5 and 6 will define the feasibility and performance comparison of PF in “B” sand against “A” sand.

Chapter 5. Results and Discussions

This chapter describes the simulation results for the EOR scenarios proposed for A and B reservoir sands with PF and SPF. The results obtained will be presented in the same order as the methodology of Chapter 4. In addition, the discussion and analysis of each case will be presented. The economic evaluation will be a helpful tool to rank the most convenient scenario between the base case scenario for PF and SPF.

5.1 Polymer Flooding in A Sands

5.1.1 Base case forecast in A2 and A2i sands.

Figure 5.1 displays the results of all three reservoir simulators for the original case of the original activity of PF through the four injectors mentioned in Chapter 3. The well control for this scenario is the constant liquid rate during HM and forecast.

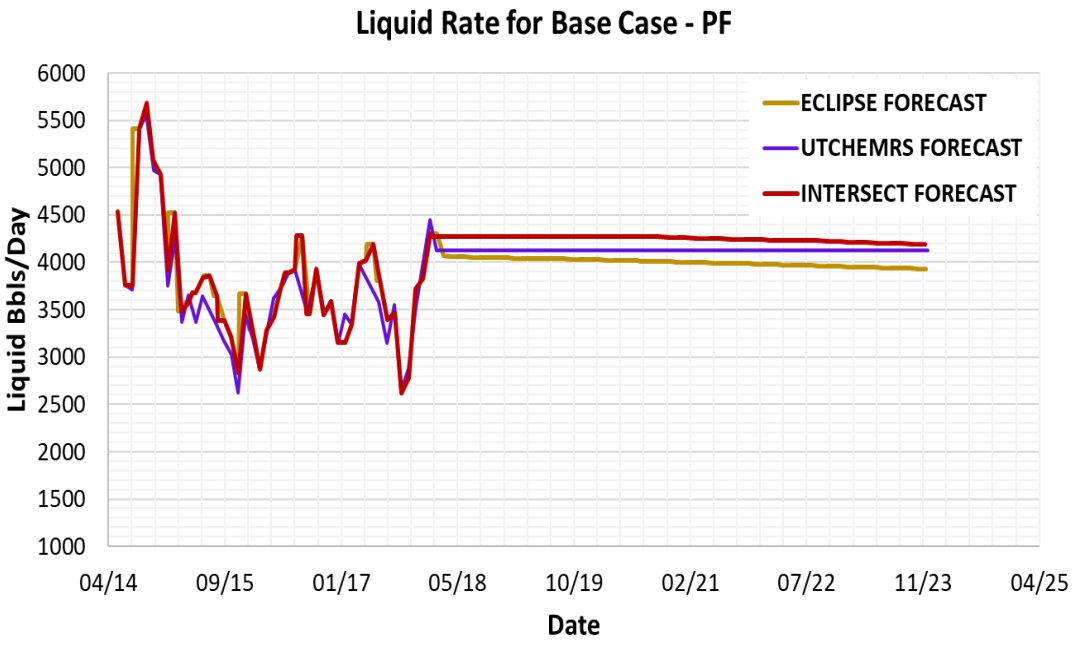

Figure 5.1. Liquid rate for base case PF.

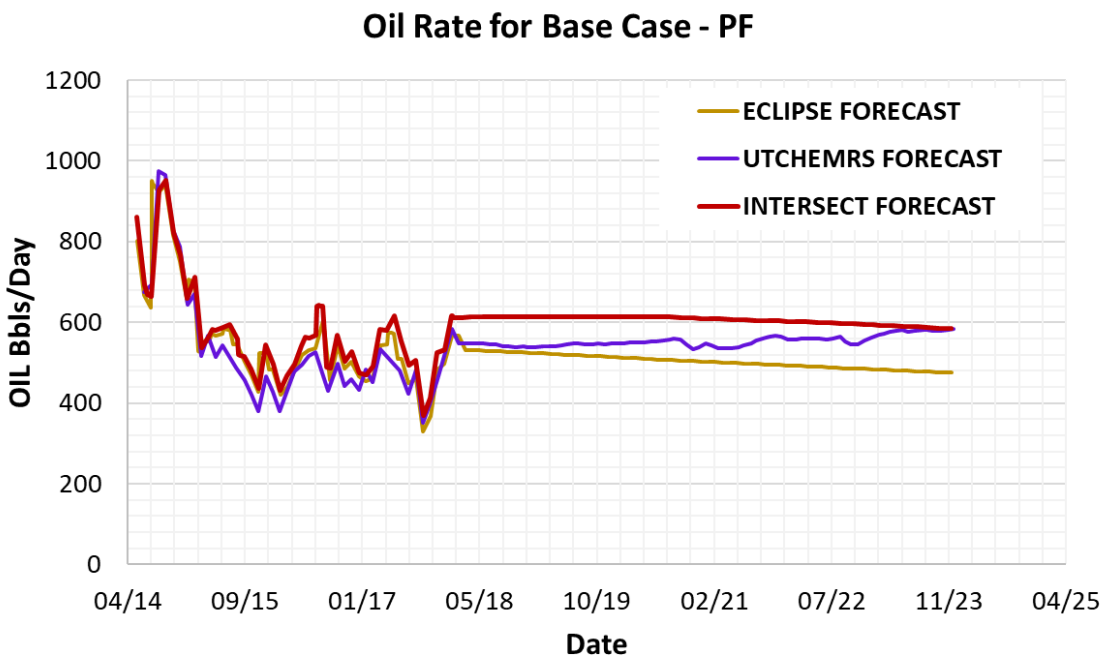

Figure 5.2. Oil rate for base case PF.

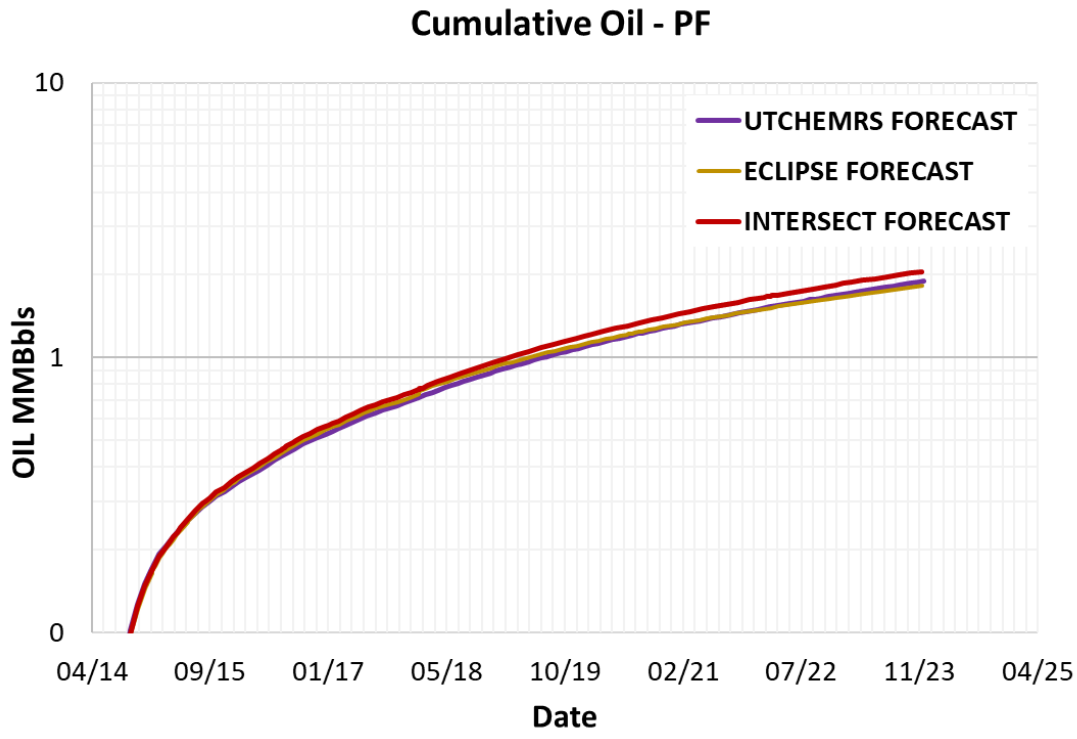

Figure 5.3. Cumulative oil recovery for base case PF.

According to Figure 5.2 the oil rate forecast is different for different simulators. The most optimistic results are obtained from the INTERSECT simulation but very similar trend to ECLIPSE results b. On the other hand, UTCHEMRS simulation has slightly different trend but the production data are between ECLIPSE and intersect results. The cumulative oil production from UTCHEMRS increases with time with a closer agreement to ECLIPSE results. Figure 5.3 and Table 5.1 are revealing that the cumulative oil of UTCHEMRS forecast is closer to the simulation results of ECLIPSE.

	Cum Oil (MMBbls)	Volume difference (MMBbls)	Difference (%)
ECLIPSE	1.827		
INTERSECT	2.140	0.313	14.6%
UTCHEMRS	1.897	0.070	3.7%

Table 5.1. Comparative PF oil volumes forecast for each simulator as of December 2023.

After comparing the PF forecast among the three simulators, the next step is to evaluate the PF performance in terms of oil recovery, taking the WF results as a reference shown in Chapter 4. The comparison is for each simulator. Figures 5.4, 5.5, and 5.6 display the results obtained with the ECLIPSE, INTERSECT and UTCHEMRS simulators respectively. Despite the differences shown in Tables 5.2, 5.3 and 5.4, we can observe similar polymer flood effectiveness in A reservoir. One noticeable effect is the reduction in water cut which indicates the delay in water breakthrough as reported by Figures 5.4 to 5.6 part (d). Additionally, the adverse mobility ratio due to the high oil viscosity is improved as evidenced in oil recovery increase in a range of 7.3% to 12.8% of the remaining oil in place (ROIP). This additional oil produced could be related to a more homogeneous swept front and access to the unreached oil spots by the previous WF.

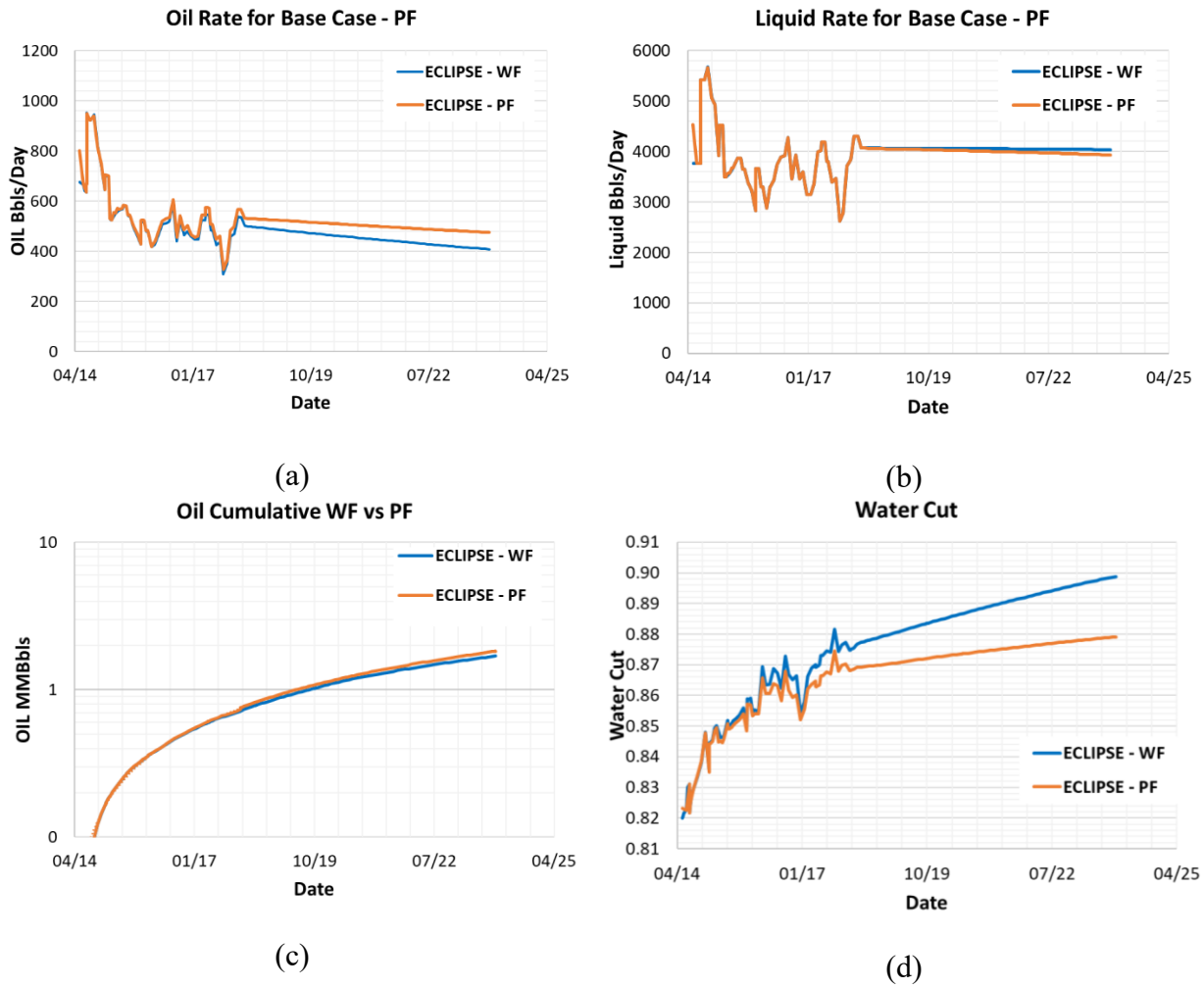

Figure 5.4. Comparative results of WF vs PF simulation of ECLIPSE. (a) Oil rate (b) Liquid rate (c) Oil cumulative (d) Water cut

	Cum Oil (MMBbls)	Volume difference (MMBbls)	Oil recovery (%)
ECLIPSE - WF	1.694		
ECLIPSE - PF	1.827	0.133	7.3%

Table 5.2. Comparative PF oil volumes forecast for ECLIPSE as of December 2023.

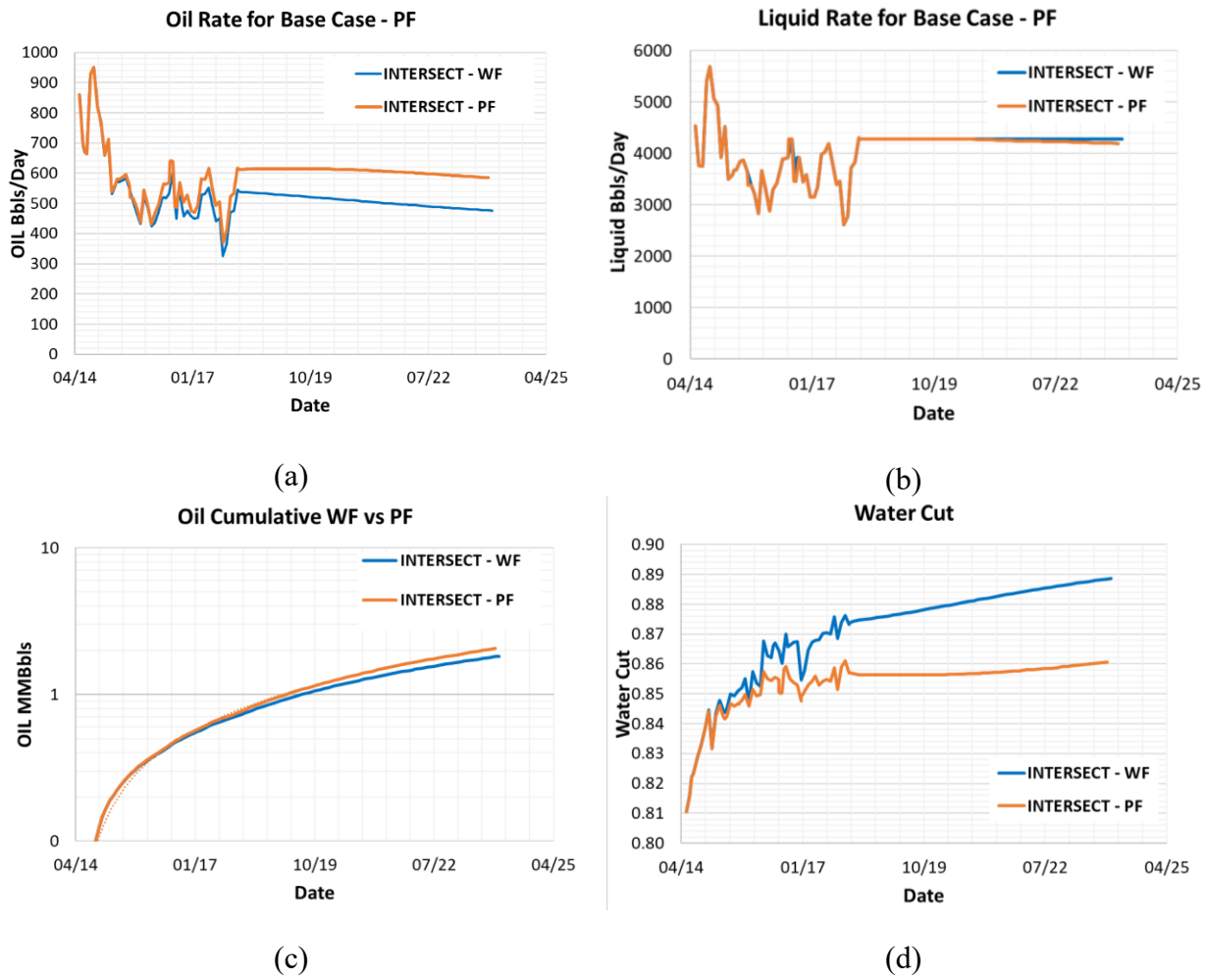

Figure 5.5. Comparative results of WF vs PF simulation of INTERSECT. (a) Oil rate (b) Liquid rate (c) Oil cumulative (d) Water cut

	Cum Oil (MMBbls)	Volume difference (MMBbls)	Oil recovery (%)
INTERSECT - WF	1.821		
INTERSECT - PF	2.054	0.233	11.3%

Table 5.3. Comparative PF oil volumes forecast for INTERSECT as of December 2023.

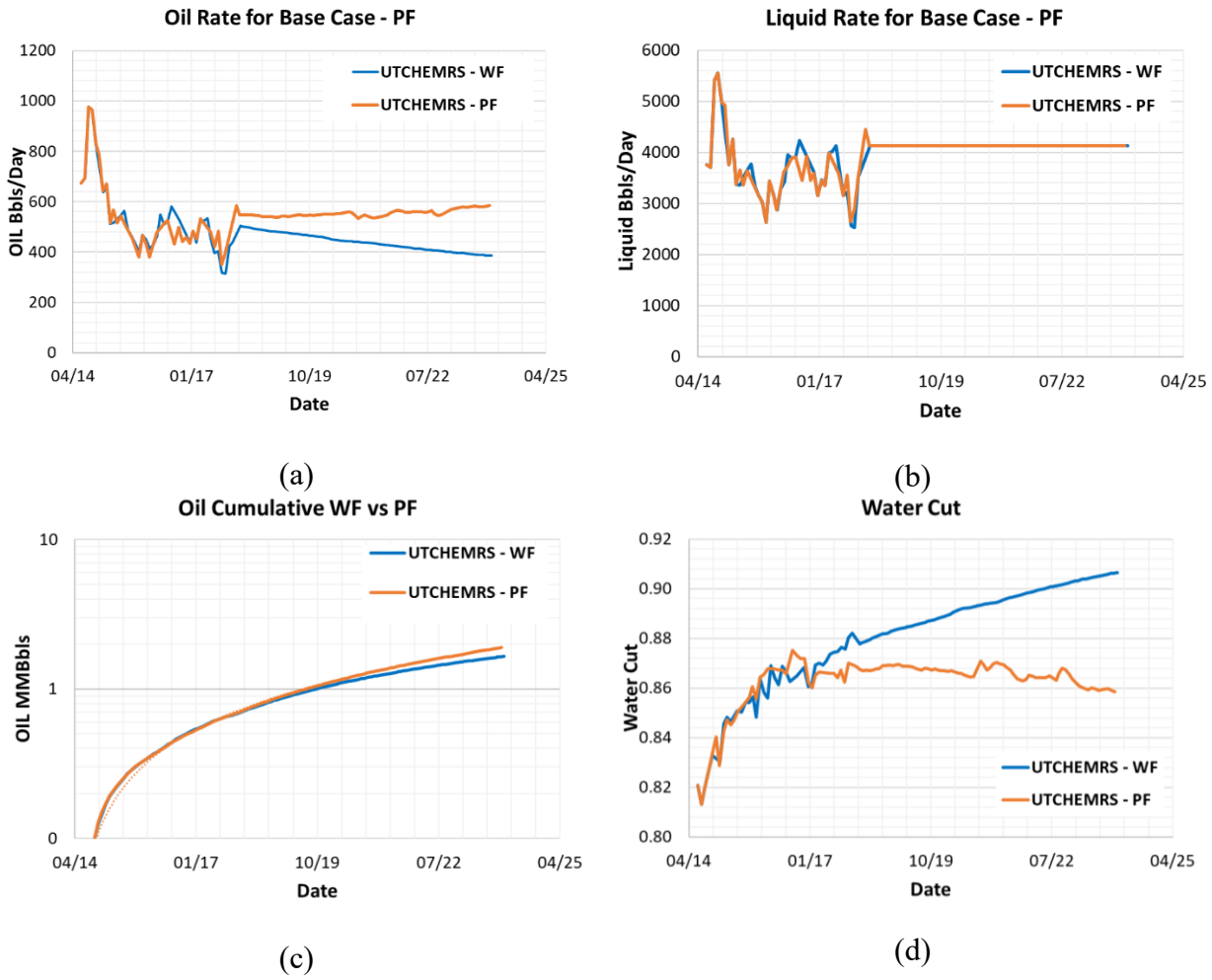

Figure 5.6. Comparative results of WF vs PF simulation of UTCHEMRS. (a) Oil rate (b) Liquid rate (c) Oil cumulative (d) Water cut

	Cum Oil (MMBbls)	Volume difference (MMBbls)	Oil recovery (%)
UTCHEMRS - WF	1.655		
UTCHEMRS - PF	1.897	0.242	12.8%

Table 5.4. Comparative PF oil volumes forecast for UTCHEMRS as of December 2023.

5.2 Polymer Flooding in A and B Sands

The above mentioned comparison was for the original base cases in "A sands". The purpose of these comparisons was to ensure reliable correspondence of UTCHEMRS with the results of other simulators in favor to forecasting new hypothetical cases. All subsequent simulations discussed below use The University of Texas at Austin simulator, UTCHEMRS version 19.2.

5.2.1 Base case forecast in A2, A2i, B2c and B2d sands.

The Colombian company is looking for new opportunities in this Colombian Field to increase the oil reserves and improve the company profitability. The B2c and B2d sands are part of the development plan in the near future because both sands are the most prospective layers after the A sands. Therefore, the evaluation of the PF application in B2c and B2d sands are the scope of this study.

The objective of this task is to evaluate the polymer injection in the four layers A2, A2i, B2c and B2d simultaneously through the original four injectors shown in Figure 4.11.

The case of commingled production is the most likely scenario in Colombian field due to the current production configuration. In Figure 5.7 there is the plot of polymer concentration injected with reservoir depth at two different dates. Part (a) is the case at the beginning of the forecast of February 2018 and part (b) is the case at the end of the simulation in December 2023 with 0.034 pore volumes injected (PVI). The ellipsoid diameter explains how far the polymer propagated and the color shade shows the variation in polymer concentration. This plot helps to understand qualitatively how the formations are admitting the polymer. One particular observation is that the injector 1304 is not injecting in B sands although the B2c layer is open. According to the petrophysical evaluation done by the Colombian company, this sand of 19 feet completed in B2c has an average permeability of 30 mD and porosity of 0.18. The low flow capacity could be a likely argument for excluding PF in this sand.

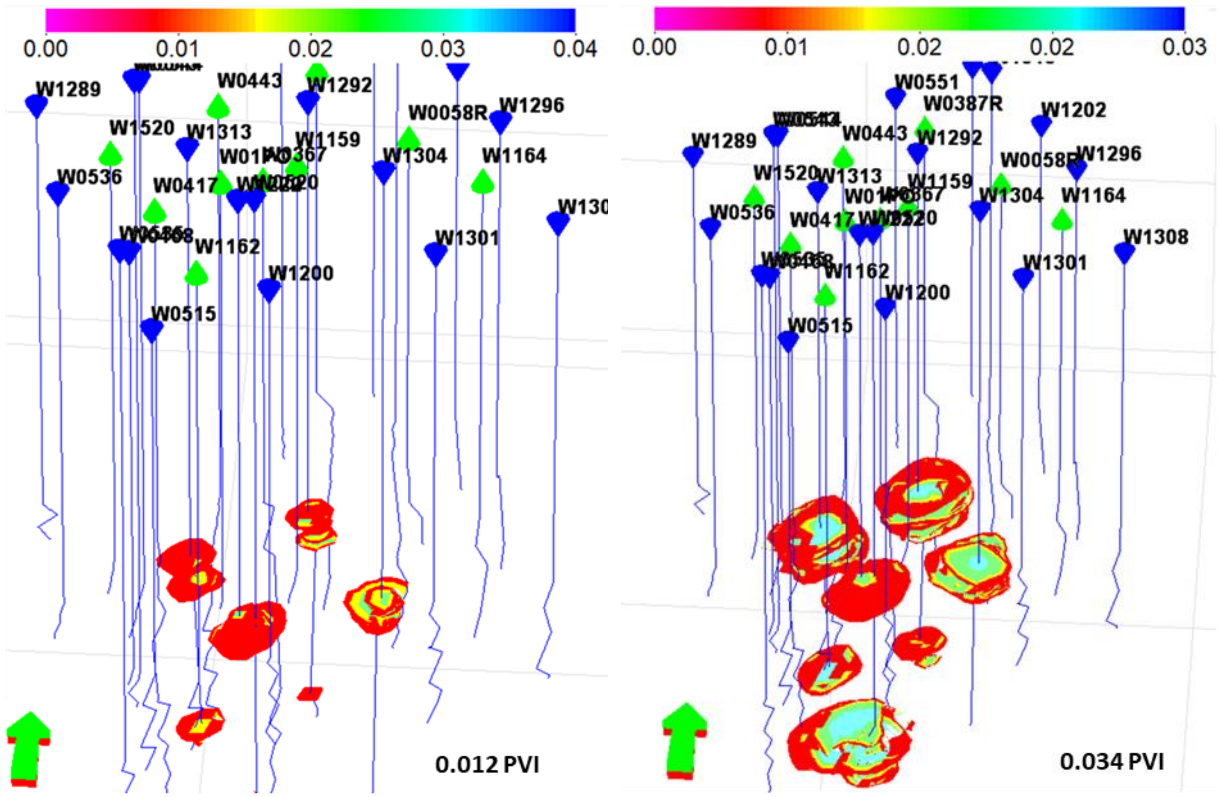

(a) (b)

Figure 5.7. Polymer concentration injected in A and B sands (a) Polymer concentration at March 2018 (b) Polymer concentration as of December 2023.

Figure 5.8 and Table 5.5 displays an evident loss of PF effectiveness in both A and B sands because the oil production is 3% lower with the PF in two formations compared to A sand alone. It seems that is a counterproductive option injecting polymer in both sands simultaneously.

	Cum Oil (MMBbls)	Volume difference (MMBbls)	Oil recovery (%)
PF A Sands	1.166		
PF A&B Sands	1.136	-0.030	-3%

Table 5.5. Comparative oil volumes for to PF in A vs. both A and B sands as of December 2023.

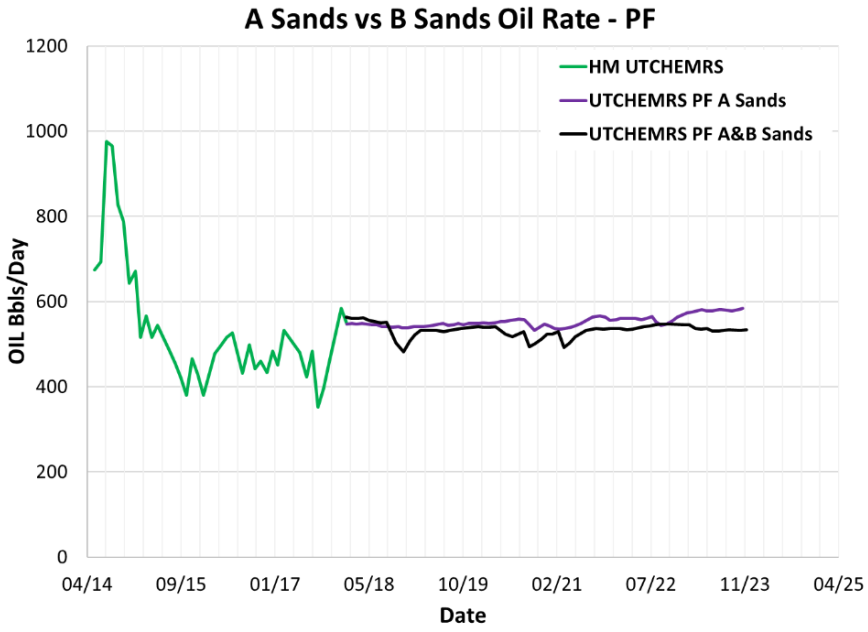

Figure 5.8. Oil rate comparison between PF in A sands and PF in both A and B sands.

Figure 5.9 reveals the possible reason of this loss of oil production. In part (b) the water cut is increasing for the "A and B" case while keeping the same liquid production (a). Therefore, we inspect the water saturation at B sands and compare with that in A sands. The water saturation maps after 1673 days (Sept. 2022) are presented below in Figure 5.10. It is clear that water saturation in A sands around most producer wells is lower indicating higher oil saturation (note, this model is not considering the gas phase). B sands map, has higher water saturations close to oil producers (note: only 3 producers completed at this depth). In addition, the injector 1304 is located at the edge of an aquifer.

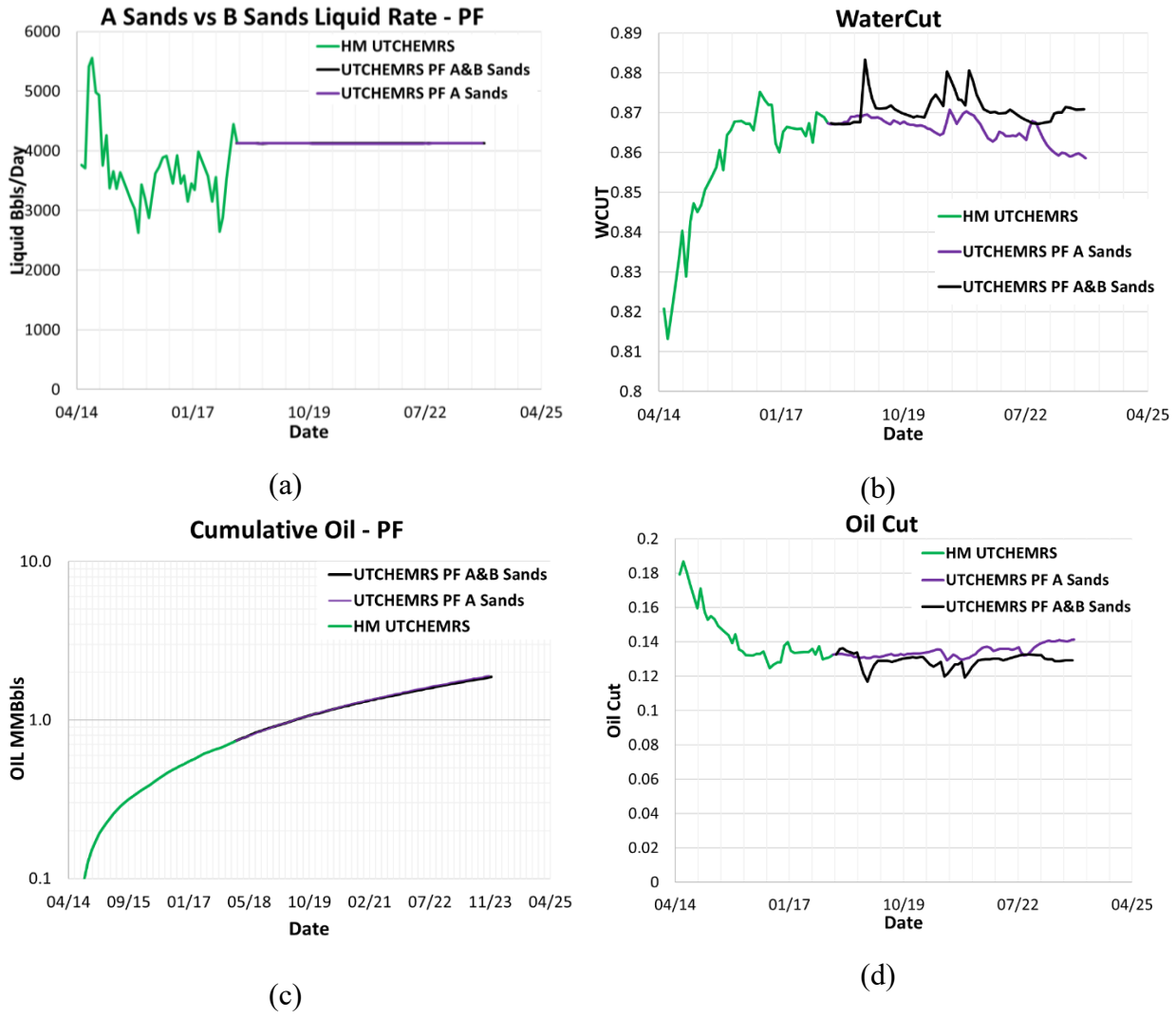

Figure 5.9. Comparative results of WF vs PF simulation of UTCHEMRS. (a) Oil rate (b) Water cut (c) cumulative Oil (d) Oil cut

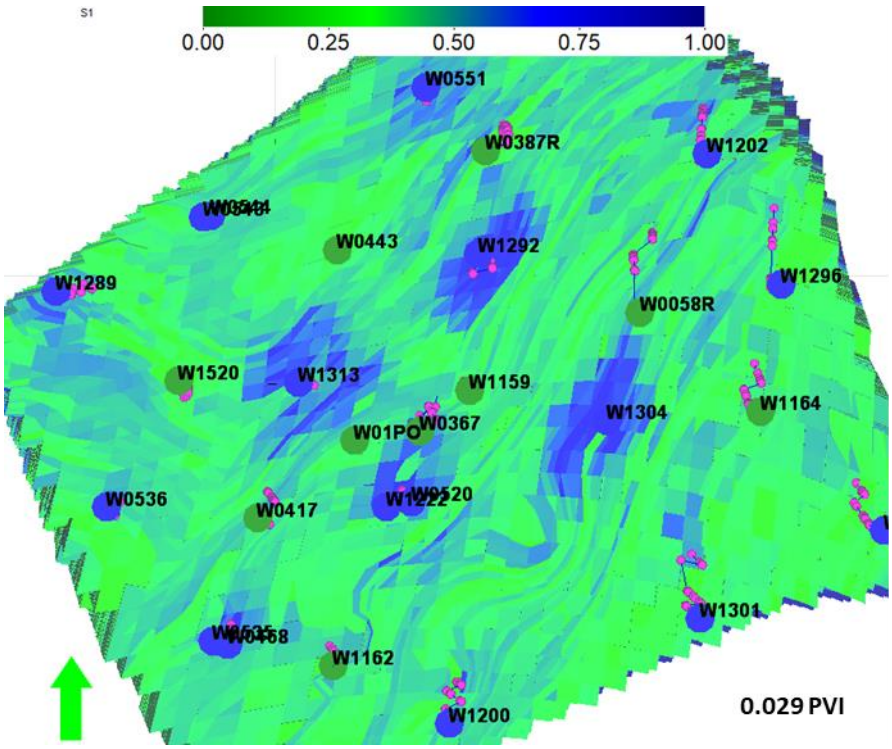

(a)

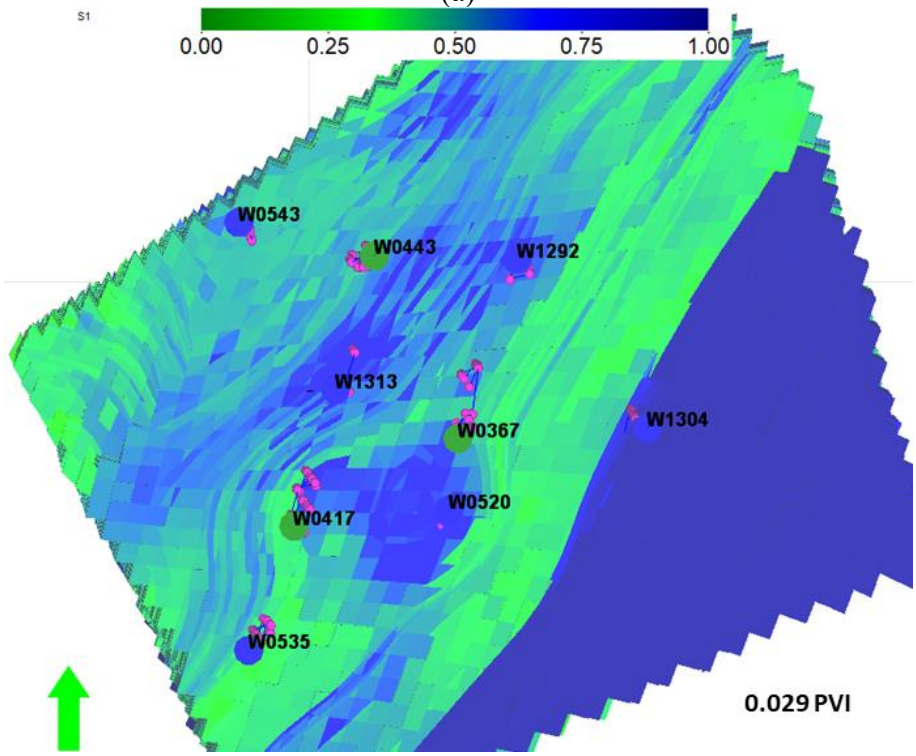

(b)

Figure 5.10. Comparative results at Sept. 2022. (a) Water saturation map for A sands (b) Water saturation map for B sands.

On the other hand, it is pertinent to compare the pressure profiles for these formations. As was mentioned in Chapter 2, an additional effect associated to the PF besides the improving of mobility ratio is the reservoir pressurization. Figure 5.12 shows the pressure behavior after the 0.03 PVI in both layers. For part (a), the pressure near all four injector is slightly higher than the rest of the regions. The PF is pressurizing near the injectors compared to the WF. However, in Figure 5.12 (b) in B sands there is no evidence of pressure change in the neighborhood of injector wells.

Figure 5.11 shows the example of the production well 417. The plot presented below corroborates the increasing of water production due to the opening of B sands for PF.

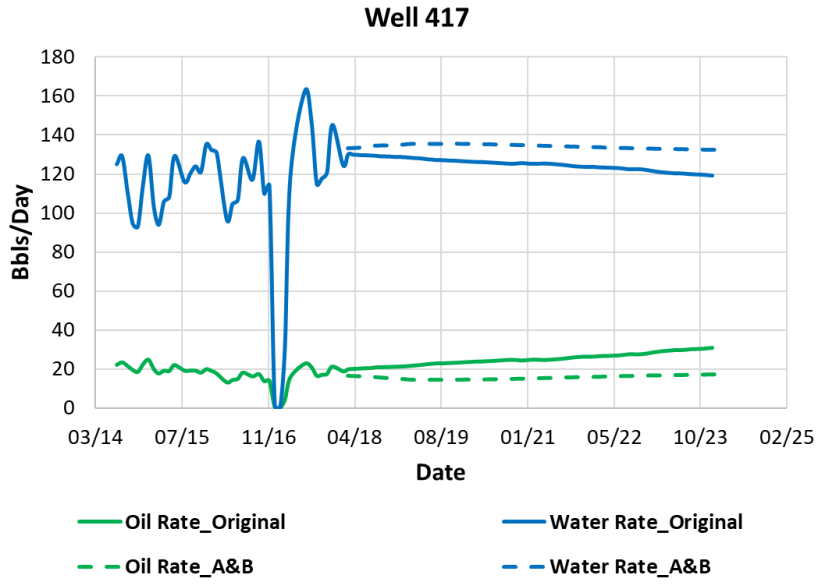

Figure 5.11. Comparison of liquid production of Well 417.

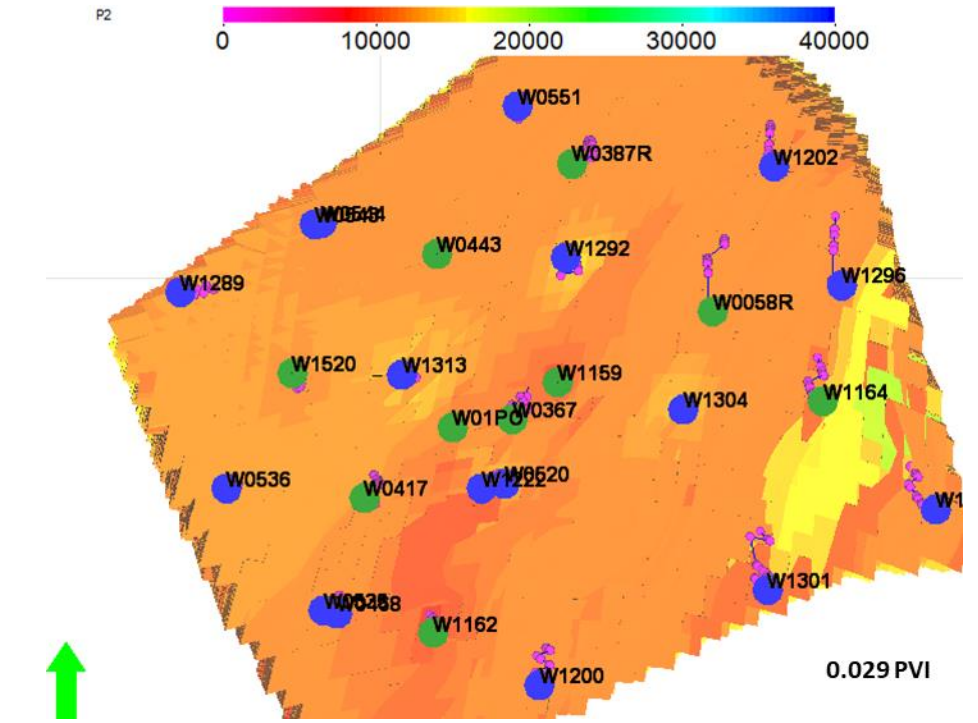

(a)

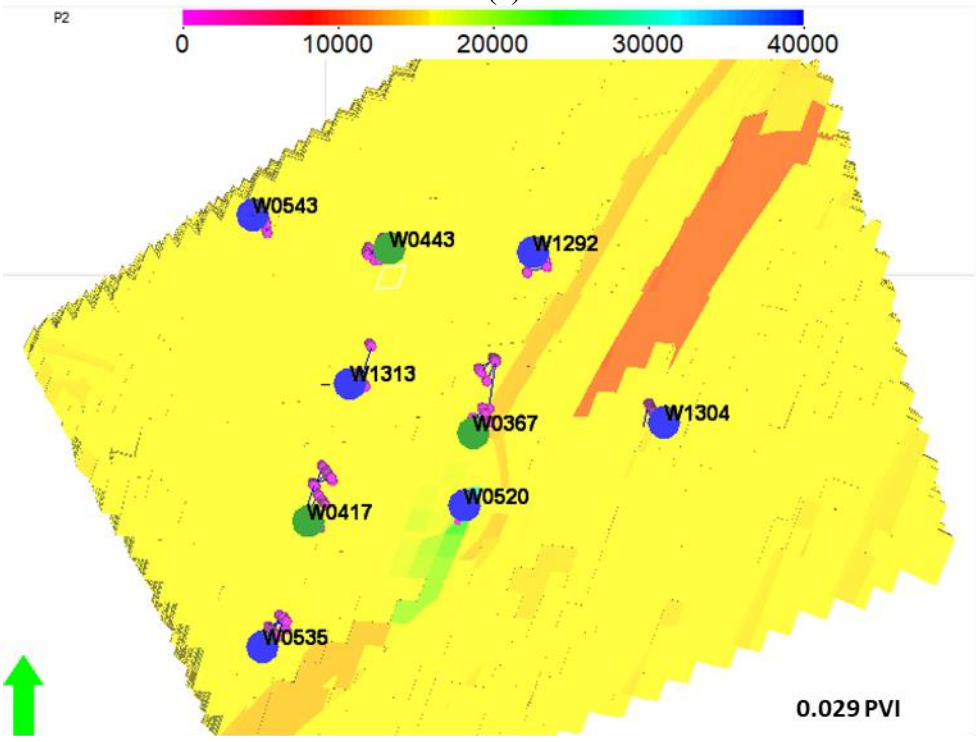

(b)

Figure 5.12. Comparative results at Sept 2022. (a) Pressure (kPa) map at A sands (b) Pressure (kPa) map at B sands.

The results given by this case are considered non-conclusive due to the few wells currently operating in B sands in the pilot area and their locations in areas with likely high water saturations. Therefore, a new scenario is required to evaluate the real potential of B sands. Consequently, the next step proposes cases with the addition of new infill wells and production from a single formation.

5.3 Polymer Flooding Performance in A sands versus B sands

The results that will be shown in this step are a comparison of the PF oil recovery in four oil wells at two specific conditions of production and injection mentioned in Chapter 4. NW01, NW02, and NW04 are new infill wells proposed for this step with the purpose to evaluate the PF effect in closer well spacing and located in areas likely not drained of oil. The well spacing reduction is at least half, changing from 200 to 100 meters approximately. Figure 5.13 displays the area limited by red color dashed lines which is the sector that will be analyzed in the scenarios discussed below. It is important to mention that this surface is plane with constant z. The grid lines observed in the figure look like contour lines but they are in fact a result of the intersections of the grid lines with the plane.

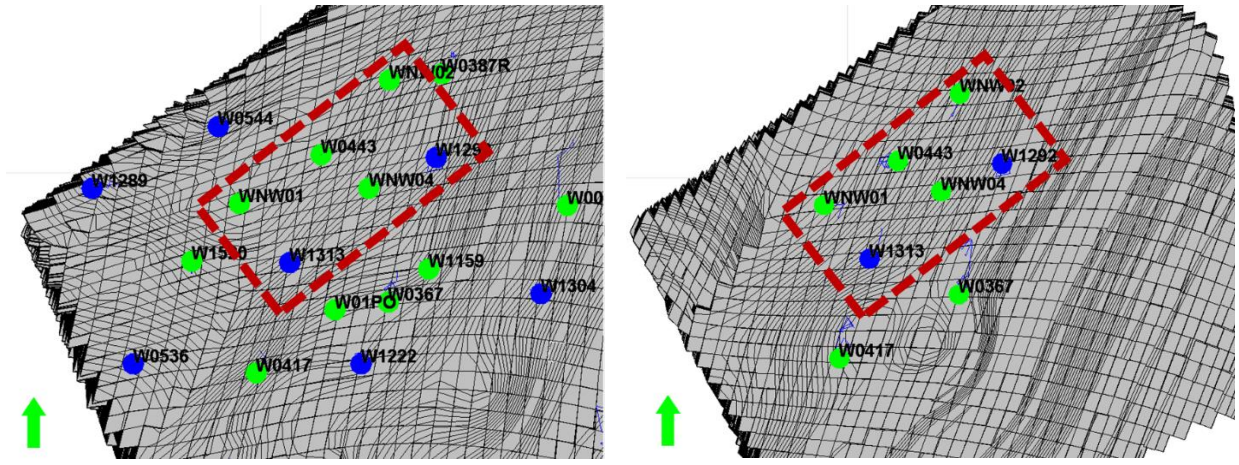

(a) (b)

Figure 5.13. Location map of evaluation case for comparing performance A vs. B (a) Area location at A sands (b) Area location at B sands.

5.3.1 Results

For the four producers mentioned above, Figures 5.14 to Figure 5.17 show the simulation results and Table 5.6 to Table 5.9 display the oil recovery of PF for each case: the case of injecting and producing only in A sands (only A) versus the case of injecting and producing only in B sands (only B). The selective injection is through the wells 1292 and 1313.

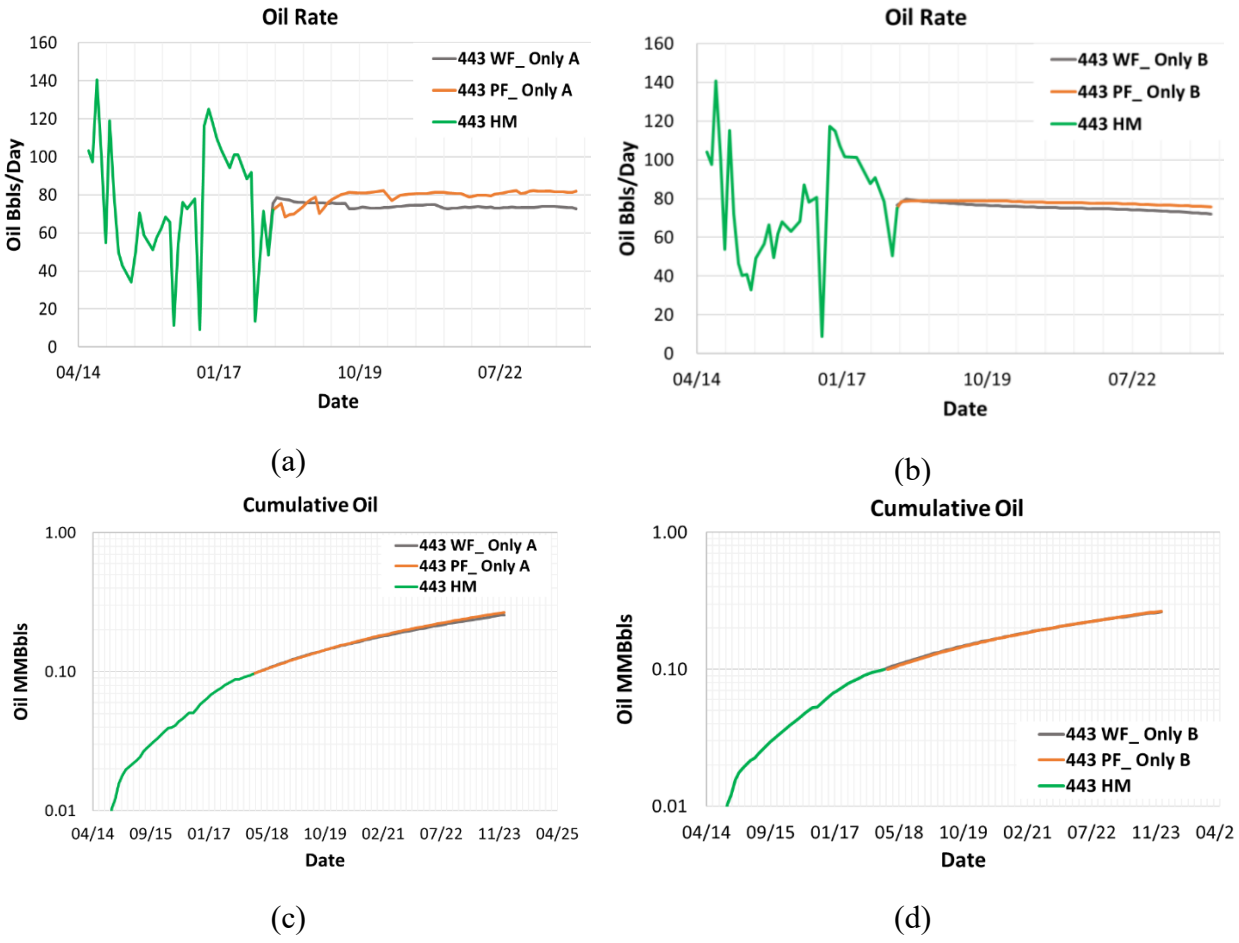

Figure 5.14. Performance comparison of WF vs PF in Well 443. (a) Oil rate only in A sands (b) Oil rate only in B sands (c) Cumulative oil only in A sands (d) Cumulative oil only in B sands

	Only A case	Only B case
Oil recovery (%)	6.7%	1.7%

Table 5.6. Oil recovery by Well 443 associated to PF in cases Only A sands versus Only B sands as of December 2023.

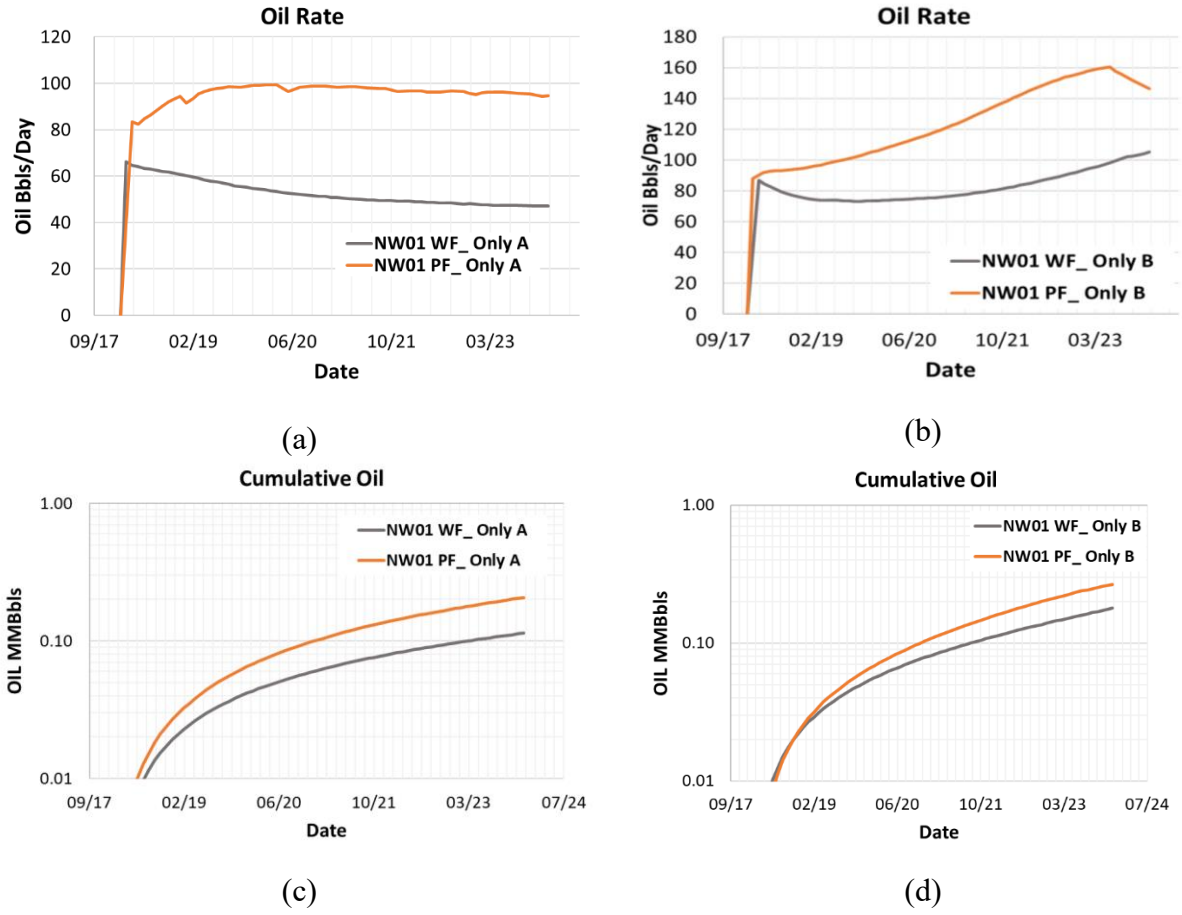

Figure 5.15. Performance comparison of WF vs PF for Well NW01. (a) Oil rate only in A sands (b) Oil rate only in B sands (c) Cumulative oil only in A sands (d) Cumulative oil only in B sands

	Only A case	Only B case
Oil recovery (%)	44.5%	32.9%

Table 5.7. Oil recovery by Well NW01 associated to PF in cases Only A sands versus Only B sands as of December 2023.

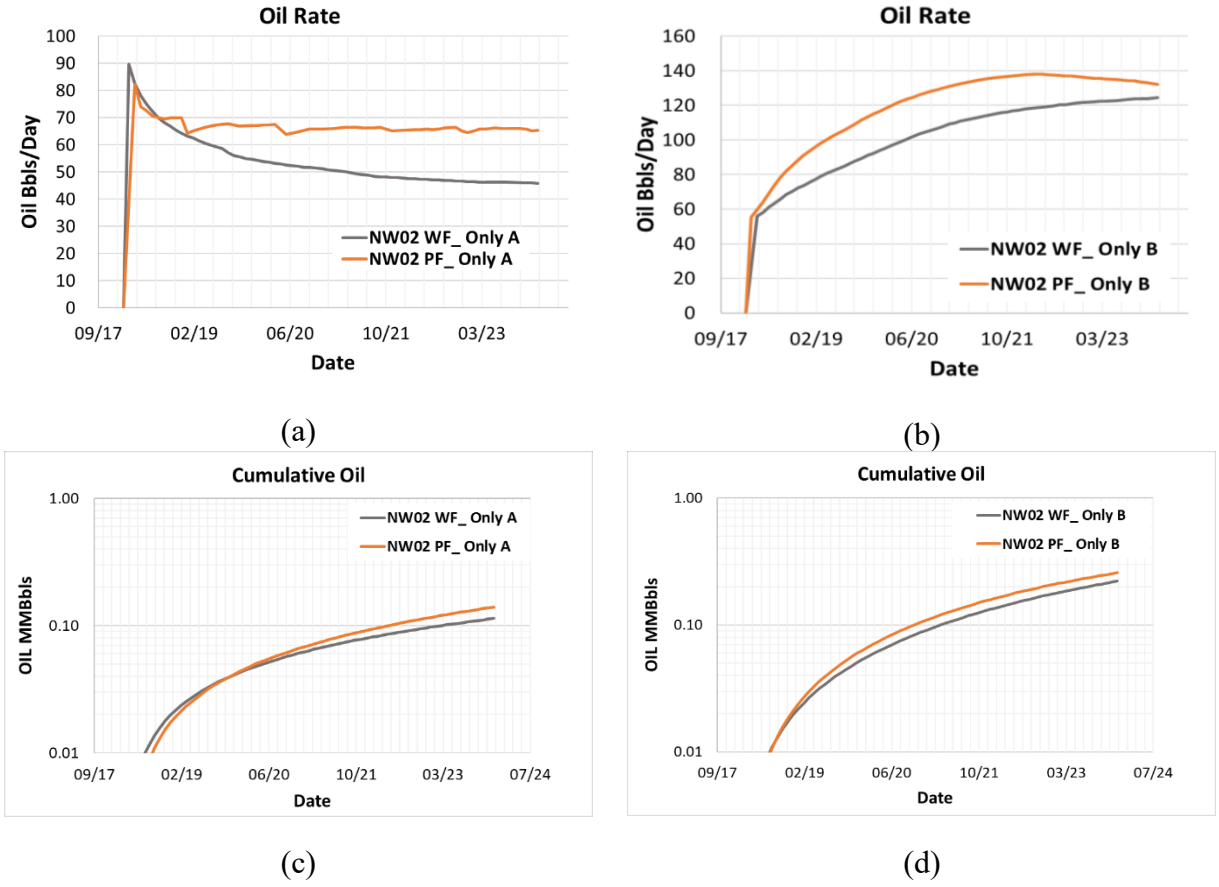

Figure 5.16. Performance comparison of WF vs PF in Well NW02. (a) Oil rate only in A sands (b) Oil rate only in B sands (c) Cumulative oil only in A sands (d) Cumulative oil only in B sands

	Only A case	Only B case
Oil recovery (%)	18.6%	14.0%

Table 5.8. Oil recovery by Well NW02 associated to PF in cases Only A sands versus Only B sands as of December 2023.

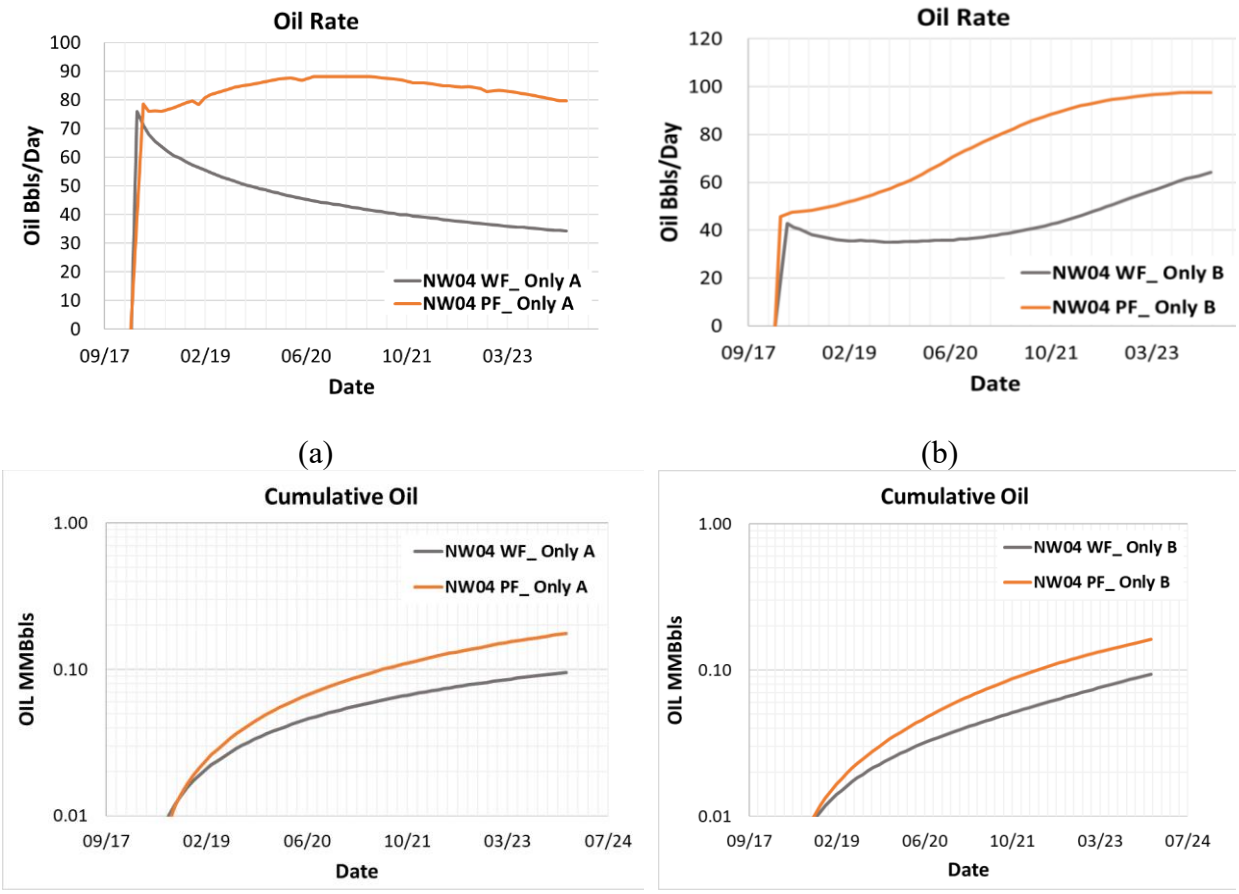

Figure 5.17. Performance comparison of WF vs PF in Well NW04. (a) Oil rate only in A sands (b) Oil rate only in B sands (c) Cumulative oil only in A sands (d) Cumulative oil only in B sands

	Only A case	Only B case
Oil recovery (%)	45.8%	42.1%

Table 5.9. Oil recovery by Well NW04 associated to PF in cases Only A sands versus Only B sands as of December 2023.

5.3.2 Discussion

In this section the previous results will be analyzed starting from the existing Well 443 and then new infill wells.

5.3.2.1 Well 443

Well 443 is a producer operating exclusively in B sands from year 1958 to 2011 with a cumulative oil recovery of 0.65 MMBbls. From March 2011 until Feb 2018, the well has been producing from both A and B sands with an additional cumulative oil of 0.18 MMBbls. Therefore, the area surrounding the well has undergone prior drainage where the vast majority comes from B reservoir. According to the results, this well has receiving the effect of oil recovery associated to PF more noticeable in A sands. Figure 5.18 reveals in two stages of time the forecast that describes the polymer concentration and its influence on the water saturation and reservoir pressure in A sands. The right side of the figure is at March 2018 which is at the beginning of the forecast and the left side is as of December 2023 which is at the end of the forecast.

In part (a) and (b) the advanced front of polymer is evident after 0.017 pore volume (PV) that is the PV injected in this lapse of time of forecast. That injection is flowing preferentially to the west of the injector wells affecting directly the four wells of investigation in this case. Then, parts (c) and (d) are comparing the water saturation (S_w) and implicitly the oil saturation (S_o). The polymer injection is creating a sweeping front that is moving forward over time as reported by the S_w maps. For the case of Well 443, this producer is benefiting from the injection because the frontal effect is moving to the Wells NW04, NW01, NW02, 387R, and 1520. This benefit is represented by additional 7% oil recovery. Finally, parts (e) and (f) correlate positively with the injection due to the expected pressurization near injectors and depressurization close to producers. This associated to the extraction of liquid volume from the reservoir.

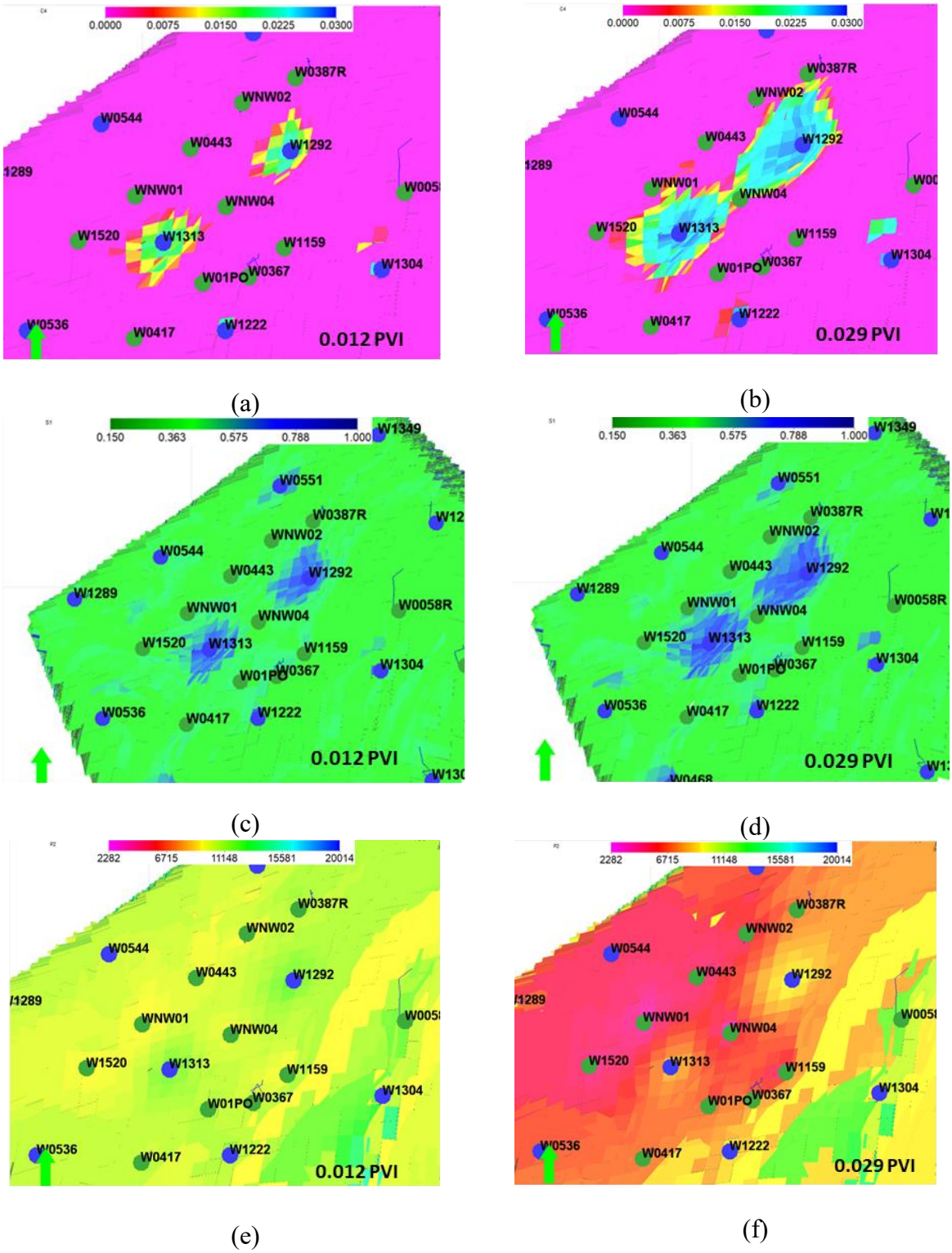

Figure 5.18. Simulation maps for case "Only A sands" (a) Polymer concentration at 03-2018 (wt%) (b) Polymer concentration at 12-2023 (wt%) (c) S_w at 03-2018 (d) S_w at 12-2023 (c) Pressure at 03-2018 (kPa) (d) Pressure at 12-2023 (kPa)

From Figure 5.20 the analysis of the low oil recovery in B sands is described. According to part (a) and (b), the advance of polymer concentration is similar to the behavior in A sands, which denotes a clear connectivity between polymer injectors and west side producers. However, the S_w maps are showing the Well 443 located in a medium to high water saturations from the beginning of the forecast. A possible explanation for this result is the previous effect of the WF process on B sands before the injectors 1313 and 1292 were closed in the lower sands to being exclusively open for A sands for PF in 2014. Figure 5.19 shows a water cut comparison between the simulation only A and the simulation only B. This case has similar results with the scenario explained in 5.2 where the PF in A and B together lowered the oil production and increases the water production.

The effect of PF over this production well after 0.014 pore volume injected is almost negligible because the saturation around the well did not change with time. That explains the 1.7% of additional recovery by the PF only in B sans.

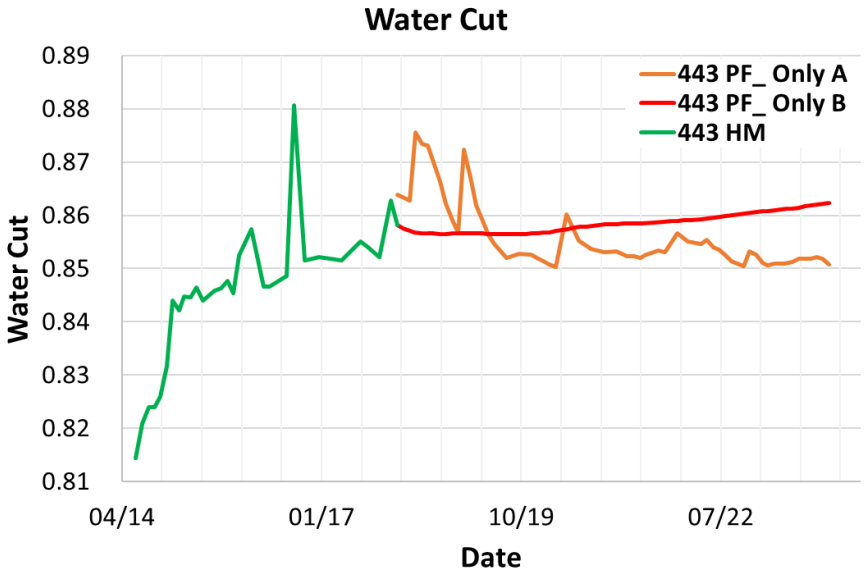

Figure 5.19. Comparison of water cut of the Well 443.

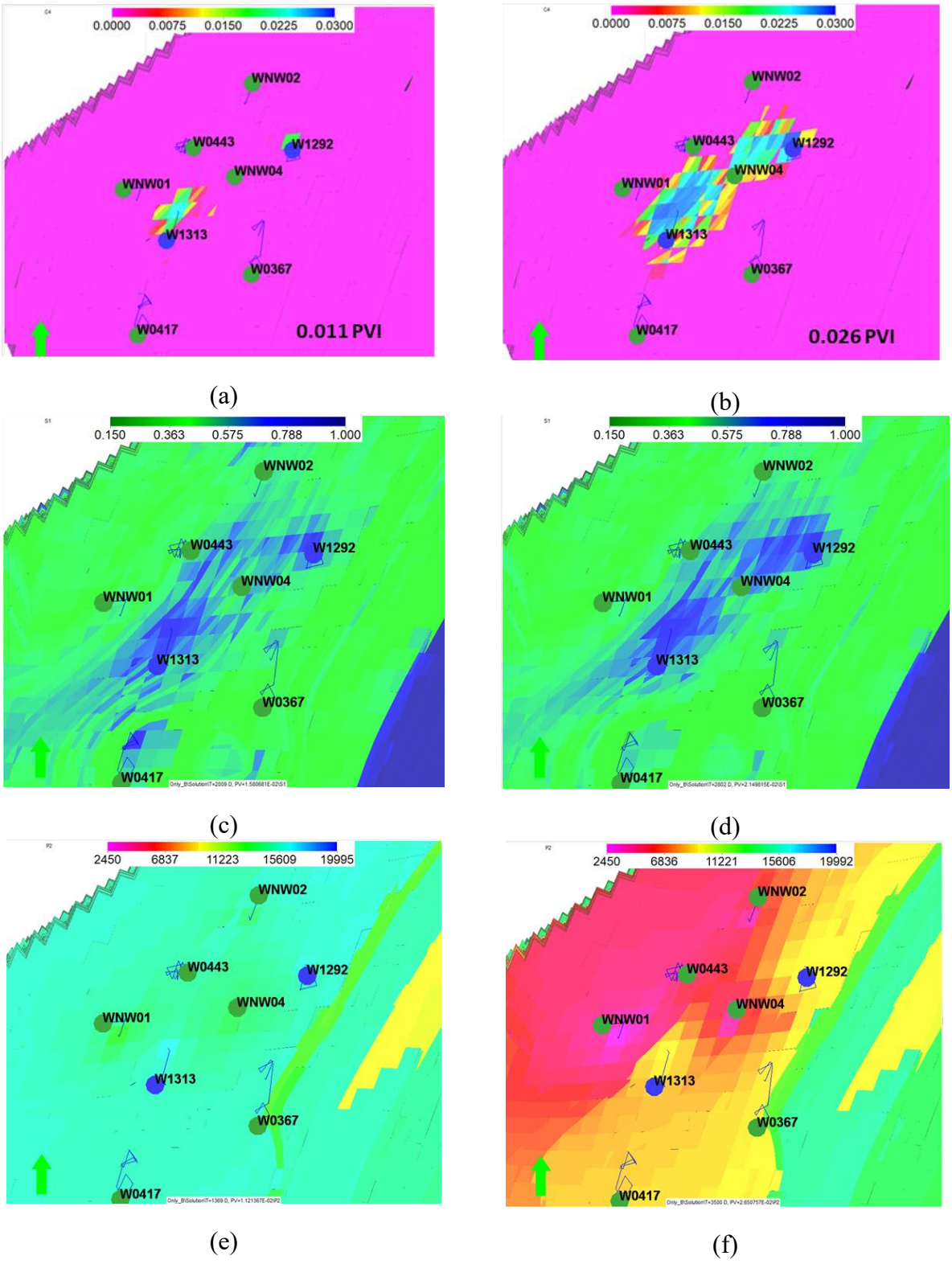

Figure 5.20. Simulation maps for case "Only B sands" (a) Polymer concentration at 03-2018 (wt%) (b) Polymer concentration at 12-2023 (wt%) (c) S_w at 03-2018 (d) S_w at 12-2023 (c) Pressure at 03-2018(kPa) (d) Pressure at 12-2023 (kPa)

5.3.2.2 New infill wells

The positive results of the three wells perforated close to Well 443 bring the need of reviewing the possible argument that explain this considerable additional oil recovery.

- **PF on A sands**

According to the comparison between the WF and PF in two different stages of the simulation is evident with the effect of polymer injection in A sands. The Figure 5.21 (a) depicts the consequence of WF at the beginning of the forecast. As was mentioned before this scenario is the hypothetical case without polymer injection during the entire history of the field; with the objective to see clearly the benefits of the PF. The parts (c) and (d) of Figures 5.21, 5.22, 5.26 and 5.27 are the cross-section SE-NW at deliberated region of the plane surface given in the (a) and (b) parts.

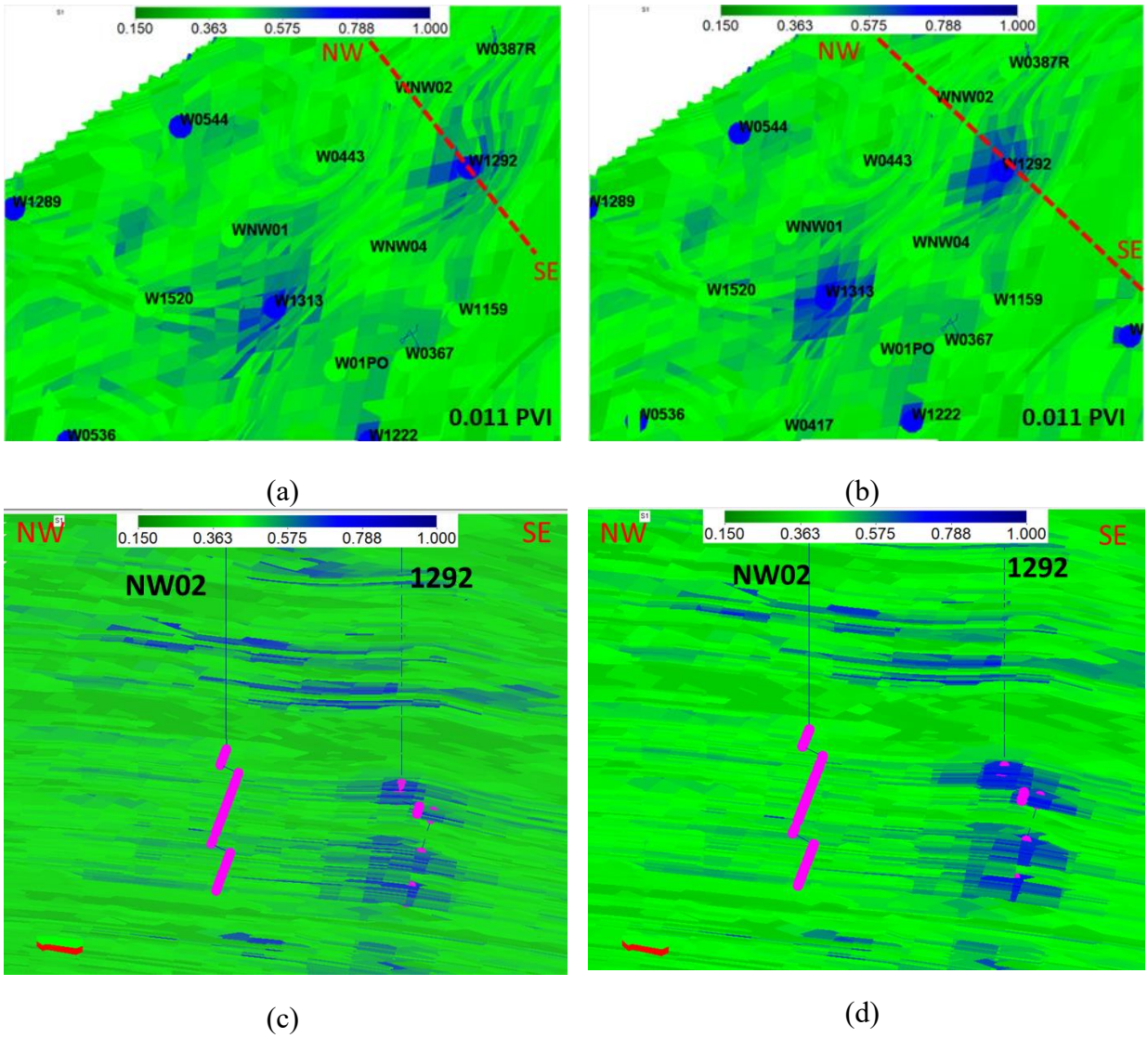

Figure 5.21. Water saturation maps for Only A at 03-2018 (a) Surface view at A sands for WF (b) Surface view at A sands for PF (c) Cross-section SE-NW for WF (d) Cross-section SE-NW for PF

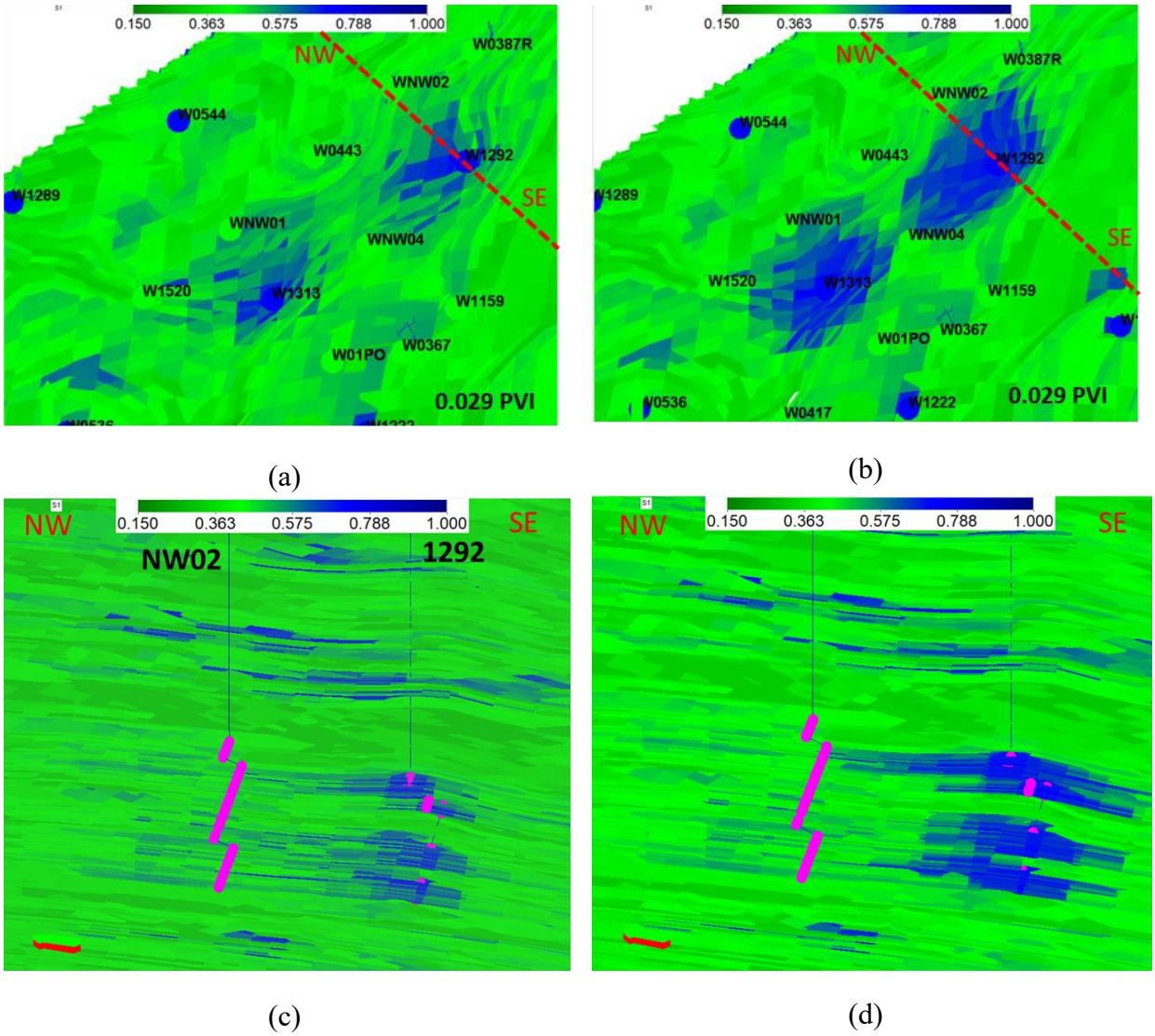

Figure 5.22. Water saturation maps for Only A at 12-2023 (a) Surface view at A sands for WF (b) Surface view at A sands for PF (c) Cross-section SE-NW for WF (d) Cross-section SE-NW view for PF.

Figures 5.22 (c) and (d) represent the connection between the Injector 1292 and the Producer NW02 and the pink dots are the well completions. This figure gives the vertical permeability variations. For instance, the upper and one of the lowest injection completions i are considered as thieves' layers. The profile of advance with WF shows the early arrivals of water to the producers due to those layers with high flow capacity. The early water breakthrough is a frequent event which have been proved in the oil wells in this Colombian field. As a consequence

of this early arrival the WF turns to an inefficient process where the water goes for the layer with the lower pressure and already channelized sand, leaving behind important regions with significant remaining oil. In Figure 5.23 the water cut of the producers is showing that most of the injected water is almost immediately produced, creating the typical channeling in this widely heterogeneous reservoir.

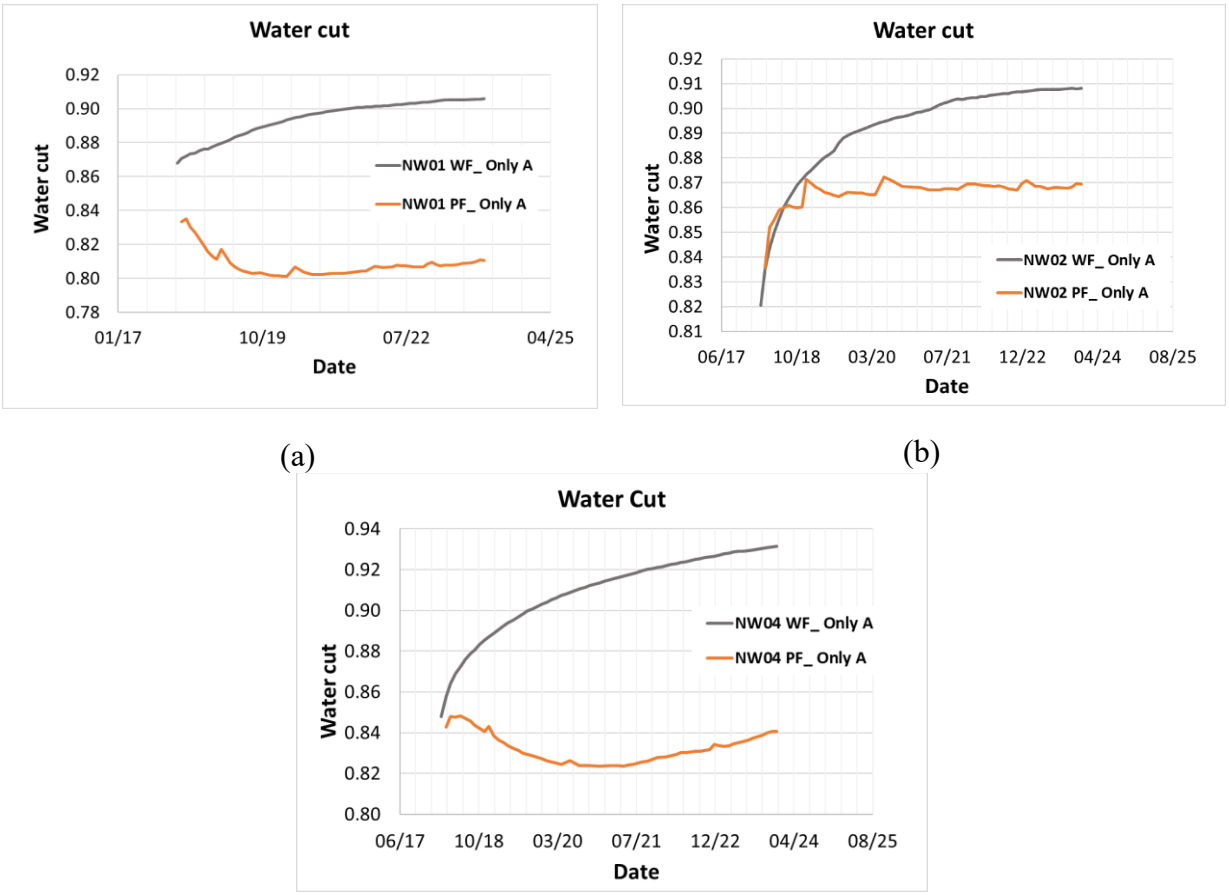

Figure 5.23. Water cut plots for WF vs PF only A sands (a) Well NW01, (b) Well NW02F, (c) Well NW04

The previous results demonstrate the improvement of the E_A and E_I due to the reduction of mobility ratio and subsequently the vertical crossflow. Causing a delay in the early arrival of water and raising oil production from layers with lower permeability. In Figure 5.22 (a) and (b) is seen

how the polymer causes a more homogenized advanced front sweeping a larger region than the WF. Additionally, Figure 5.22 (c) and (d) shows that with 0.017 PVI during the forecast, the neighbor area to the injector is having lower oil saturation. Thus, PF is mobilizing the remaining oil bypassed by the WF.

Figure 5.24 is an illustration that describes the direct relation between the polymer concentration and the effect on the water/oil saturation on A sands.

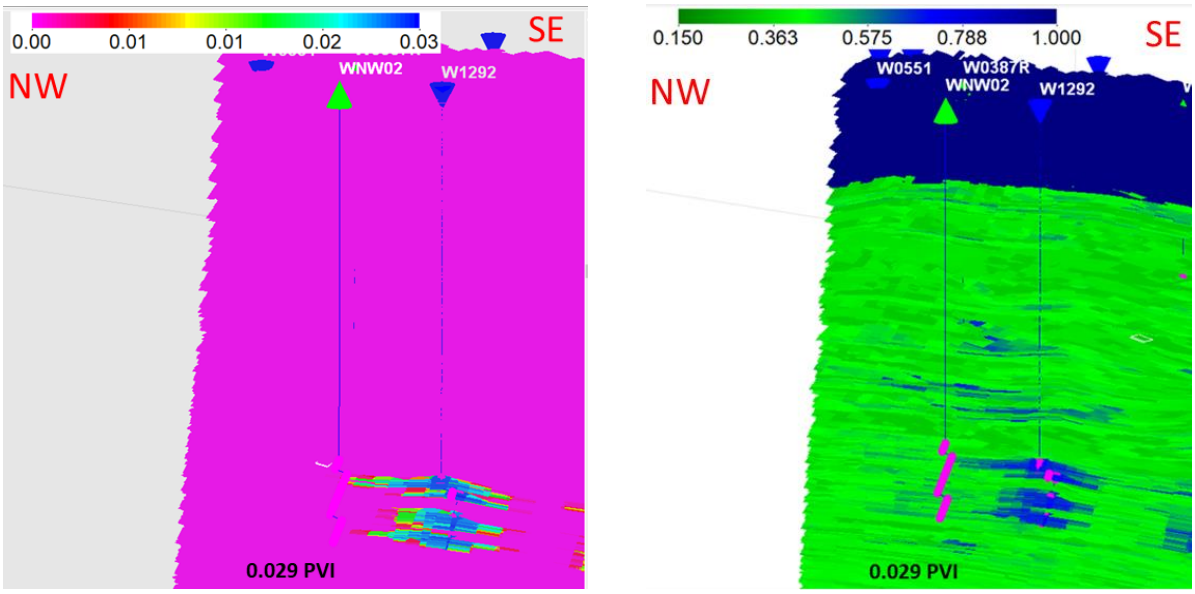

(a) (b)

Figure 5.24. Vertical view maps for Only A at 12-2023 (a) Polymer concentration (b) Water saturation for PF.

- **PF on B sands**

Previous simulations have shown in Sections 5.2 and 5.3.2.1 the unsuccessful results for the application of PF in B sands. Nevertheless, the conditions of those evaluations were on existing wells and/or commingled production. That is why this scenario of testing PF in new wells and exclusively in B sands becomes relevant because it evidences how B2c and B2d sands respond to this EOR process.

According to the positive response of B2c and B2d sands with the new infill drills for polymer injection are opening the possibility to extend the polymer pilot to those lower sands. However, it will require more evaluation and the inclusion in the sector model the rock-fluid lab tests for those sands.

Figures 5.26 and 5.27 show the surface view at B sands and also the vertical view (cross-section SW-NE) which includes the injectors 1313 and 1292 with the new infill producer NW04. The purpose of this cross section is to review the vertical advancement of the polymer slug with time. In addition, Well NW04 is strategically located in the middle of two PF injectors. Therefore, the response to this polymer slug is remarkably positive because the geological connection between both injectors and the Well NW04 is evident in the surface water saturation maps at the end of the forecast simulation.

Figures 5.26 (a) and (b) indicate that these layers have higher water saturation than A sands from the beginning of the forecast. Therefore, the early arrival of water in the producers is also evident in the production data. Figure 5.25 confirms the high water rate of those three wells since the beginning of the production with water cut from 82 to 92%.

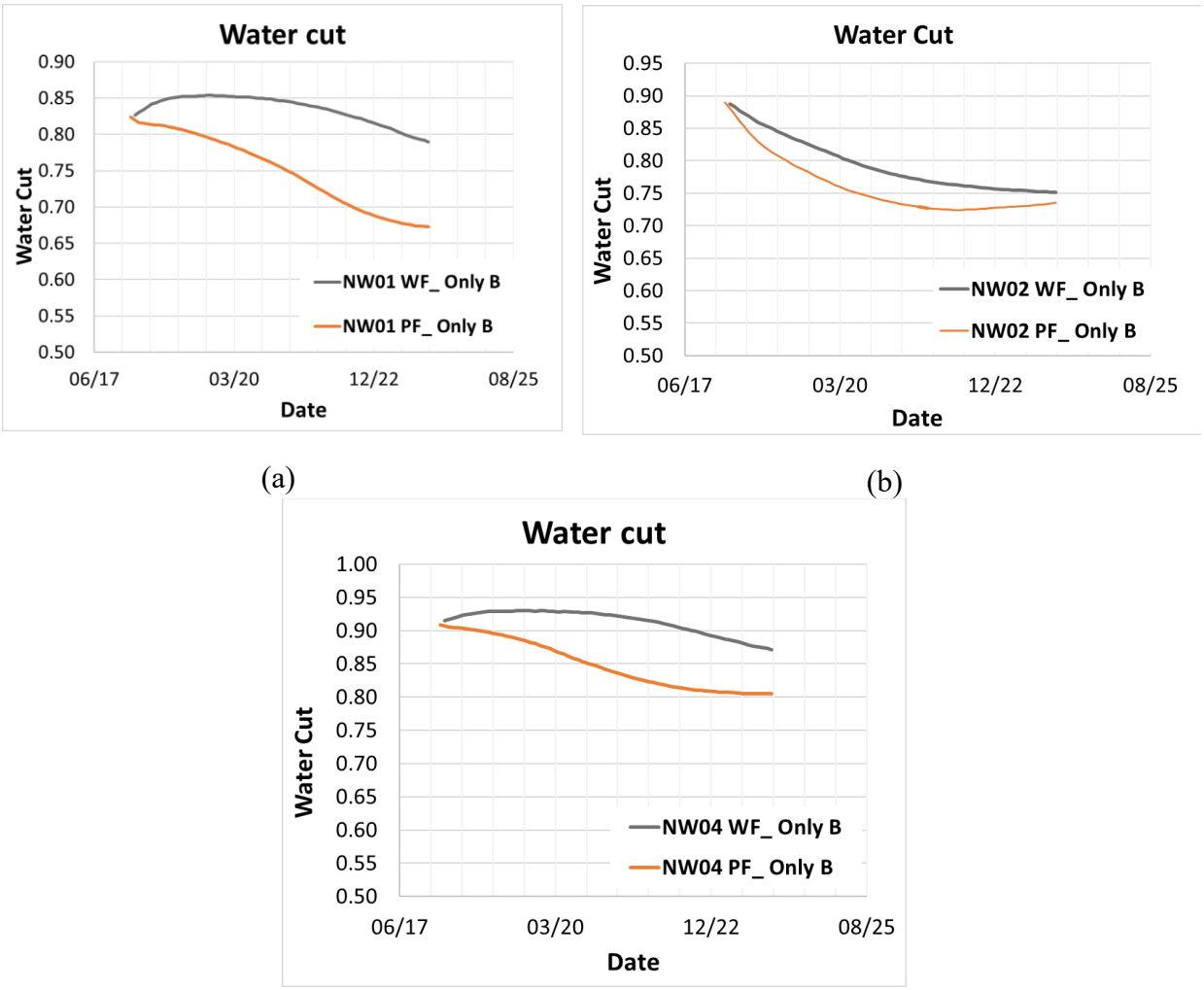

Figure 5.25. Water cut plots WF vs PF only B sands (a) Well NW01 (b) Well NW02F (c) Well NW04

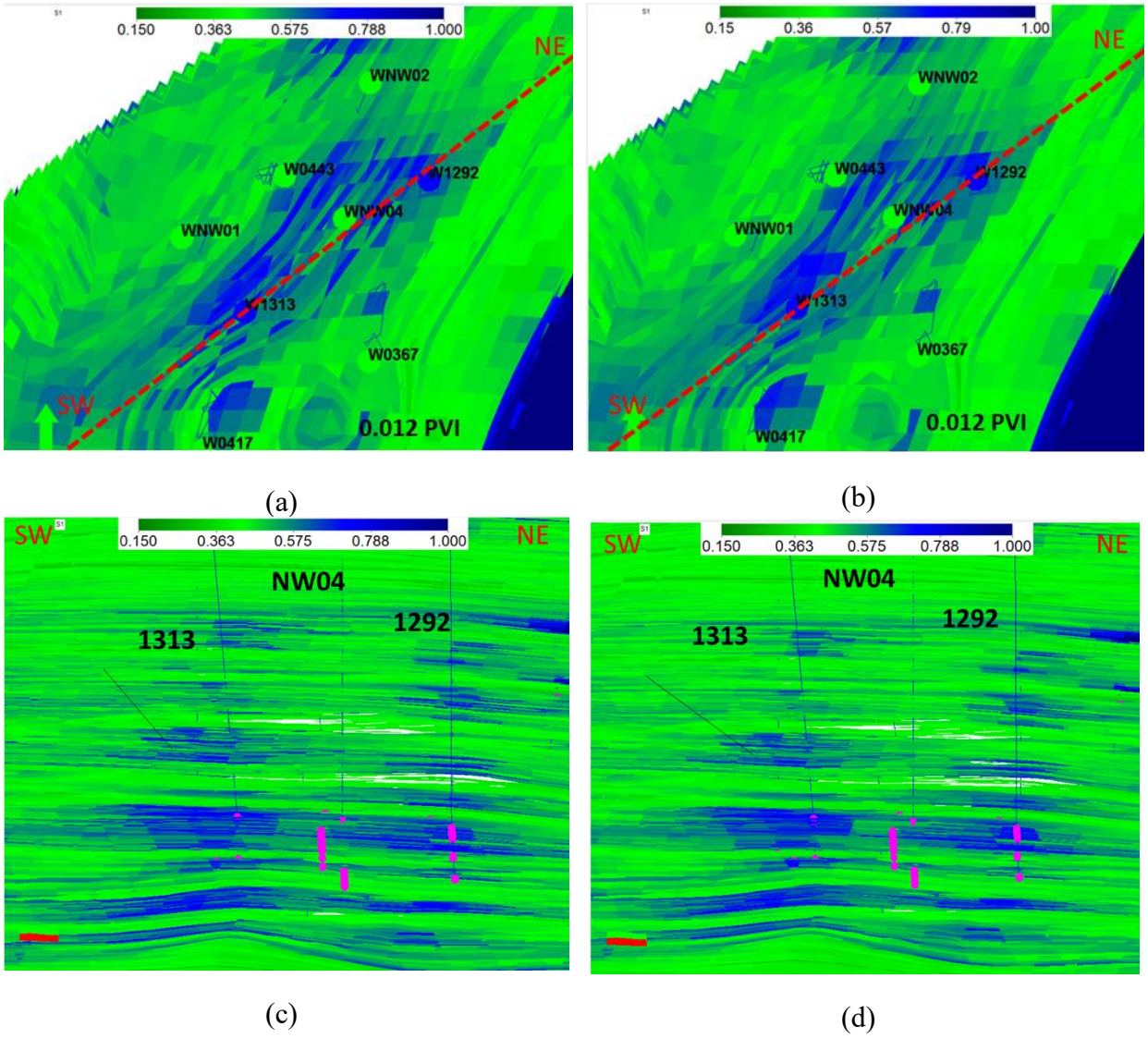

Figure 5.26. Water saturation maps for Only B at 05-2018 (a) Surface view at B sands for WF (b) Surface view at B sands for PF (c) Cross section SW-NE for WF (d) Cross section SW-NE for PF.

Figures 5.27 (a) and (b) indicate that despite the high S_w the PF homogenizes the displacement front which causes the formation of oil bank and delays the breakthrough of water and reducing the water cut by 3% to 10% (Figure 5.25). The WFunswept area is shown in Figure 5.27(c) in comparison with part (d) which reveals that polymer affects positively the same region.

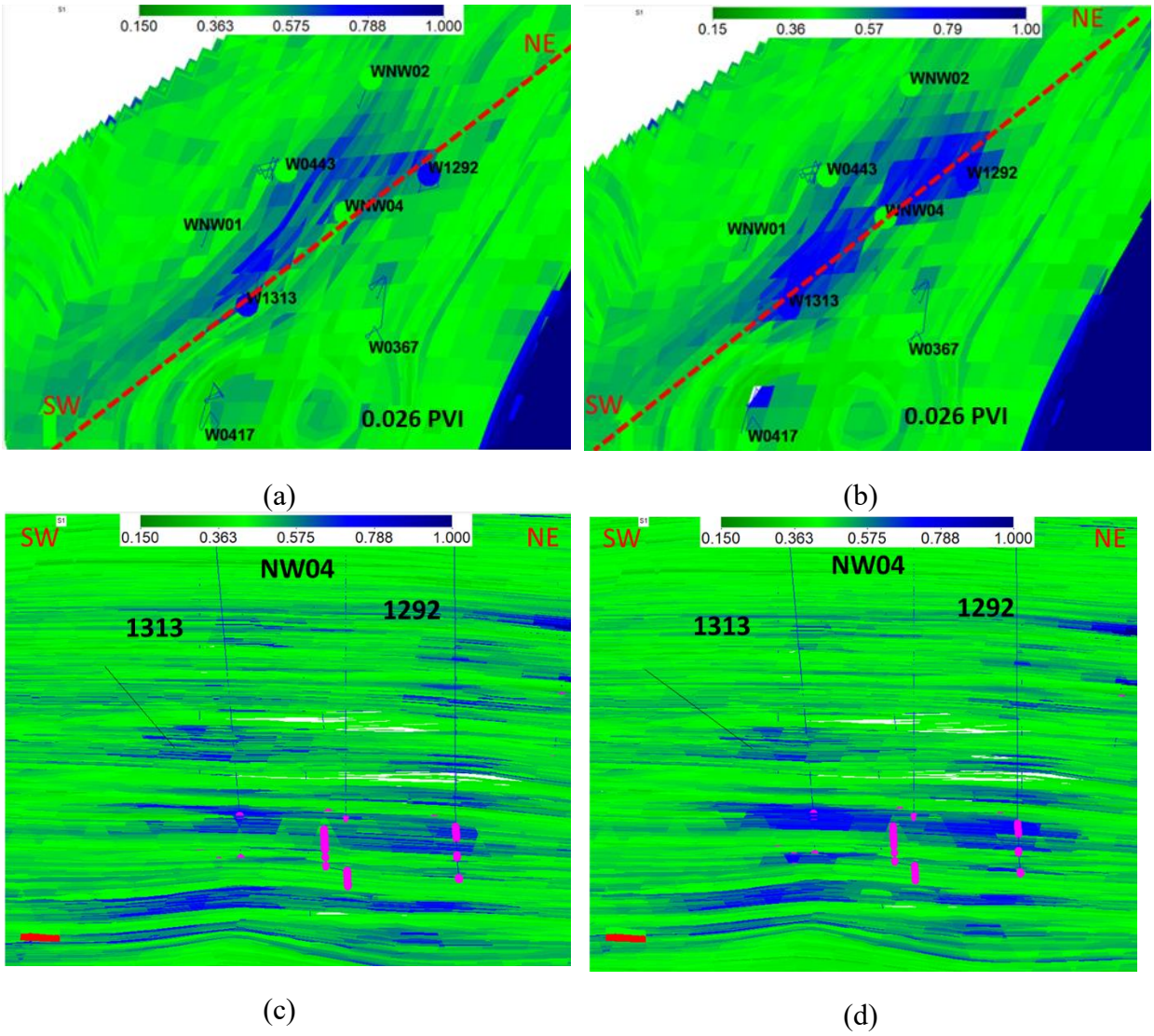

Figure 5.27. Water saturation maps for Only B at 12-2023 (a) Surface view at B sands for WF (b) Surface view at B sands for PF (c) Cross section SW-NE for WF (d) Cross section SW-NE for PF.

Figure 5.28 is an illustration that describes the direct relation between the polymer concentration and the effect on the water/oil saturation on B sands. It is important to mention that polymer injected in A sands (Figure 5.28) was during the HM. Currently, for this case the completions in A2 and A2i are shutin.

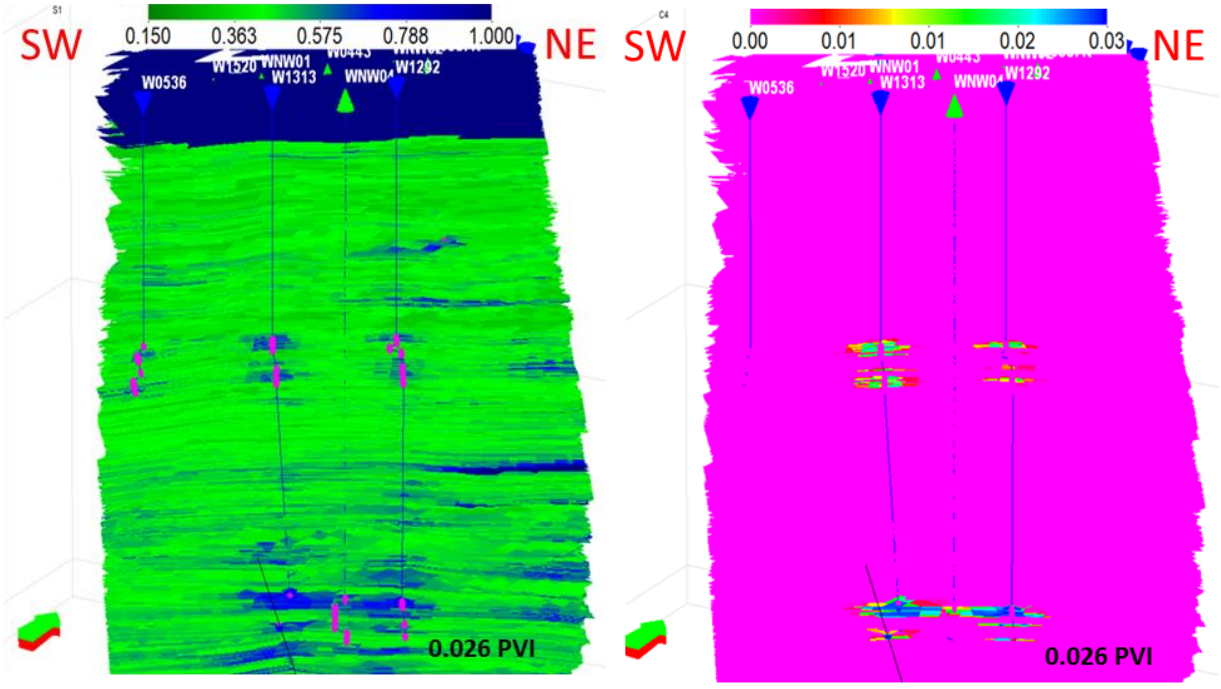

(a) (b)

Figure 5.28. Vertical view maps for Only A at 12-2023 (a) Water saturation for PF (b) Polymer concentration.

After the analysis of UTCHEMRS results for the selective injection and single production in oil wells. The polymer effect in A and B sands is appreciable both areally and vertically. The new producers were close to the oil bank created from the previous polymer injected (apply for A sands) plus the polymer injected during the forecast. The significant oil production is likely associated to an oil bank breakthrough. Well locations in the non-drained area plus their locations with respect to the polymer front could be the key to formation of the oil bank. However, additional simulations are needed to strengthen this interpretation.

5.4 Surfactant Polymer Flooding in A Sands

5.4.1 Base case forecast in A2 and A2i sands.

Figure 5.29 displays the comparison between the PF and SPF UTCHEMRS simulation results. For this case the reference scenario is the PF results shown in section 5.2. The well control for this scenario is the constant liquid rate.

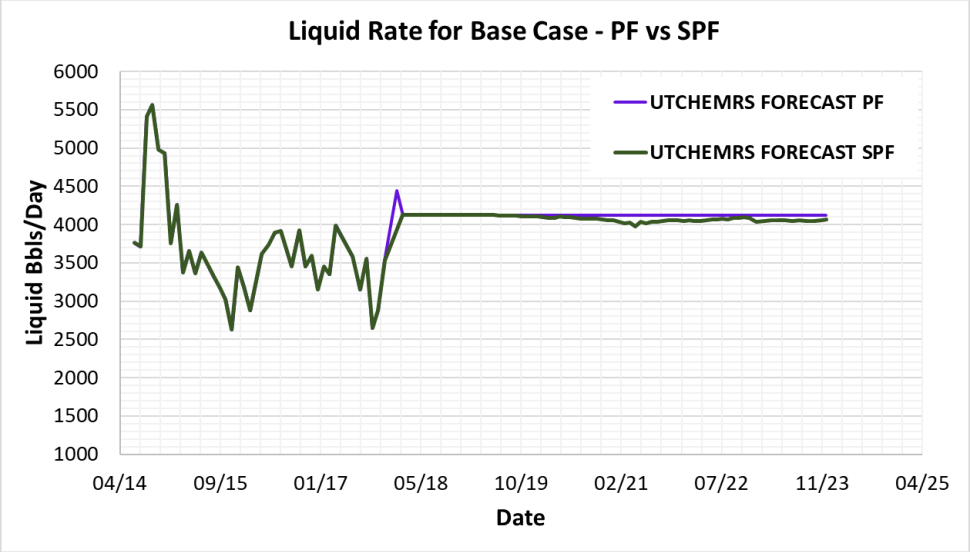

Figure 5.29. Liquid rate for base case PF vs SPF.

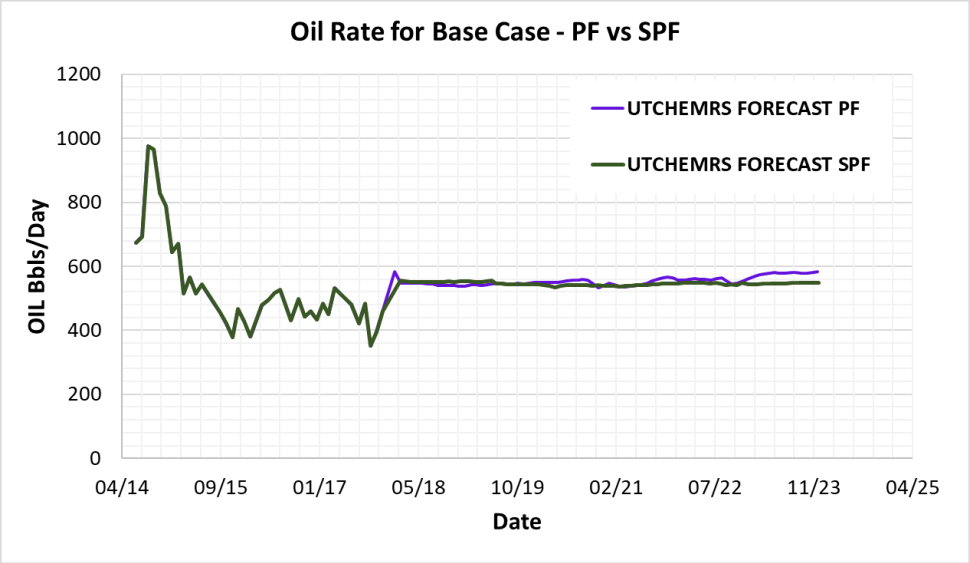

Figure 5.30. Oil rate for base case PF vs SPF.

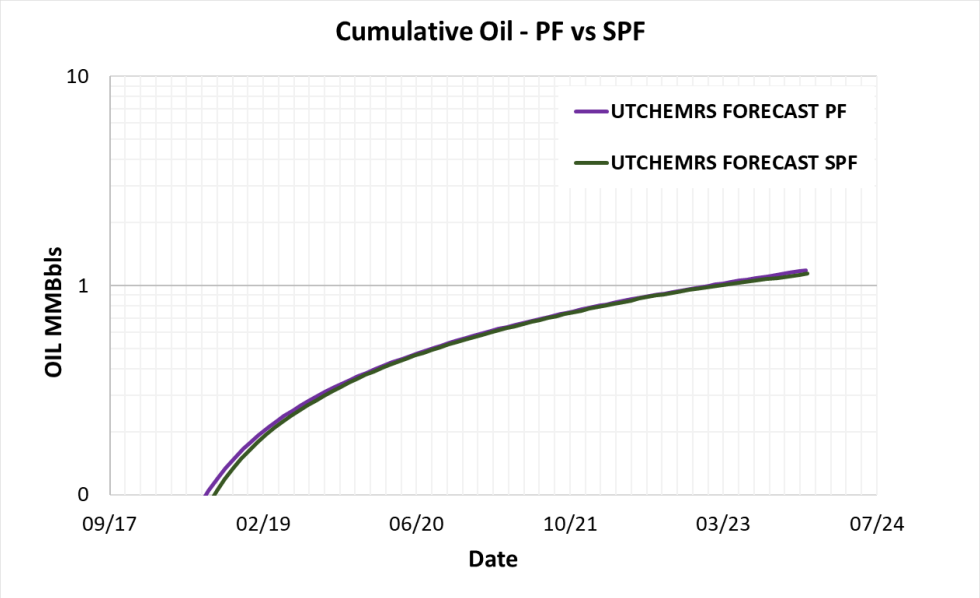

Figure 5.31. Cumulative oil recovery for base case PF vs SPF.

The results shown in the previous figures revealed that SPF is not performing effectively based on the hypothetical surfactant parameters and the injection design. Table 5.10 displays the comparison of volumes to recover with both EOR processes applied in A sands.

	Cum Oil (MMBbls)	Volume difference (MMBbls)	Oil recovery (%)
UTCHEMRS FORECAST PF	1.897		
UTCHEMRS FORECAST SPF	1.875	0.022	-1.2%

Table 5.10. Comparative oil volumes for PF vs. SPF base case in A sands as of December 2023.

The negative results are suggesting that the SPF formulation should be revised. The analysis of this case should be done going specifically with a local perspective. Therefore, this work will focuse in the results of two producer wells that are strategically located surrounded by the SP injectors. Well 1159 and Well 01PO. Through the performance and simulation information of those wells we could identify the possible causes of this ineffectiveness of the SPF results.

5.4.1.1 Well 1159 analysis

Figures 5.32 (a) shows the oil rate production comparison of the two simulations PF and SPF. This well is having a particular response to the SPF, the reduction of oil production is noticeable since the first month of production. In addition, Figure 5.32 (b) is revealing the water cut behavior of that well. It seems that an eruption of water affected the well performance.

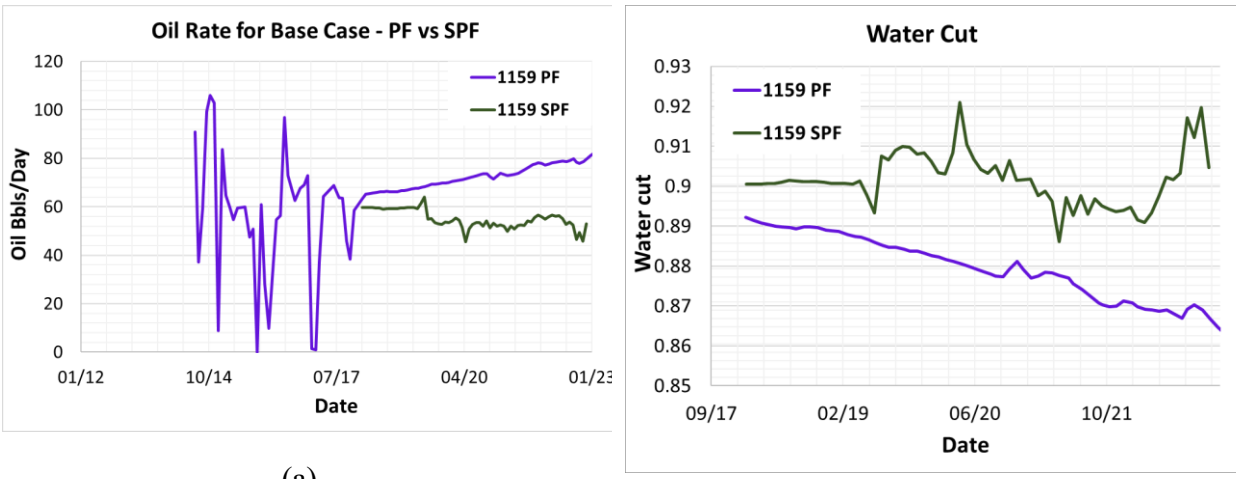

(a)

(b)

Figure 5.32. Well 1159 comparison PF vs SPF (a) Oil rate (b) Water cut.

The previous results led us to investigate the source of this breakthrough. Figure 5.33 evidences that the microemulsion (ME) reaches the well rapidly and causing a channeling from an injector to the producer.

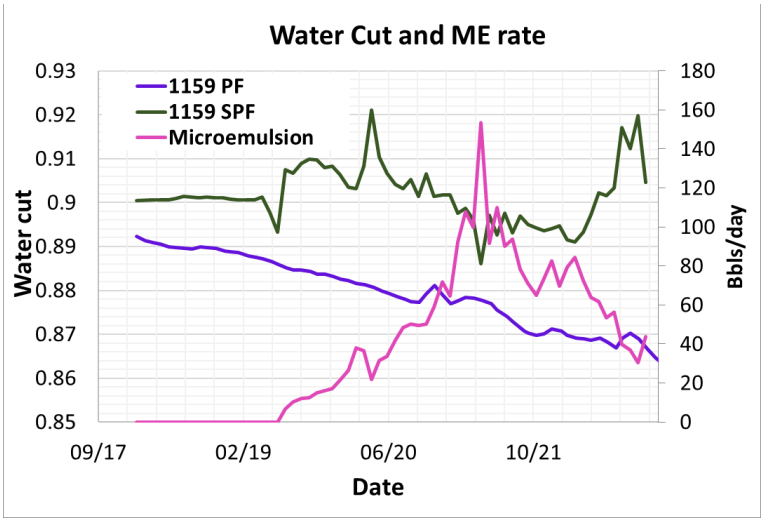

Figure 5.33. Water cut comparison and ME rate

The suspect of a channeling to the 1159 led to create a cross section to check the source of this ME. Figure 5.34 shows a ME saturation at A sands with 0.025 PVI. This map is indicating a SW-NE cross section in order to observe the influence of injector 1222 on this producer.

Figure 5.34 (b) reveals the channeling caused by the layer with permeability of 500 to 1500 mD o as is denotes in Figure 5.35.

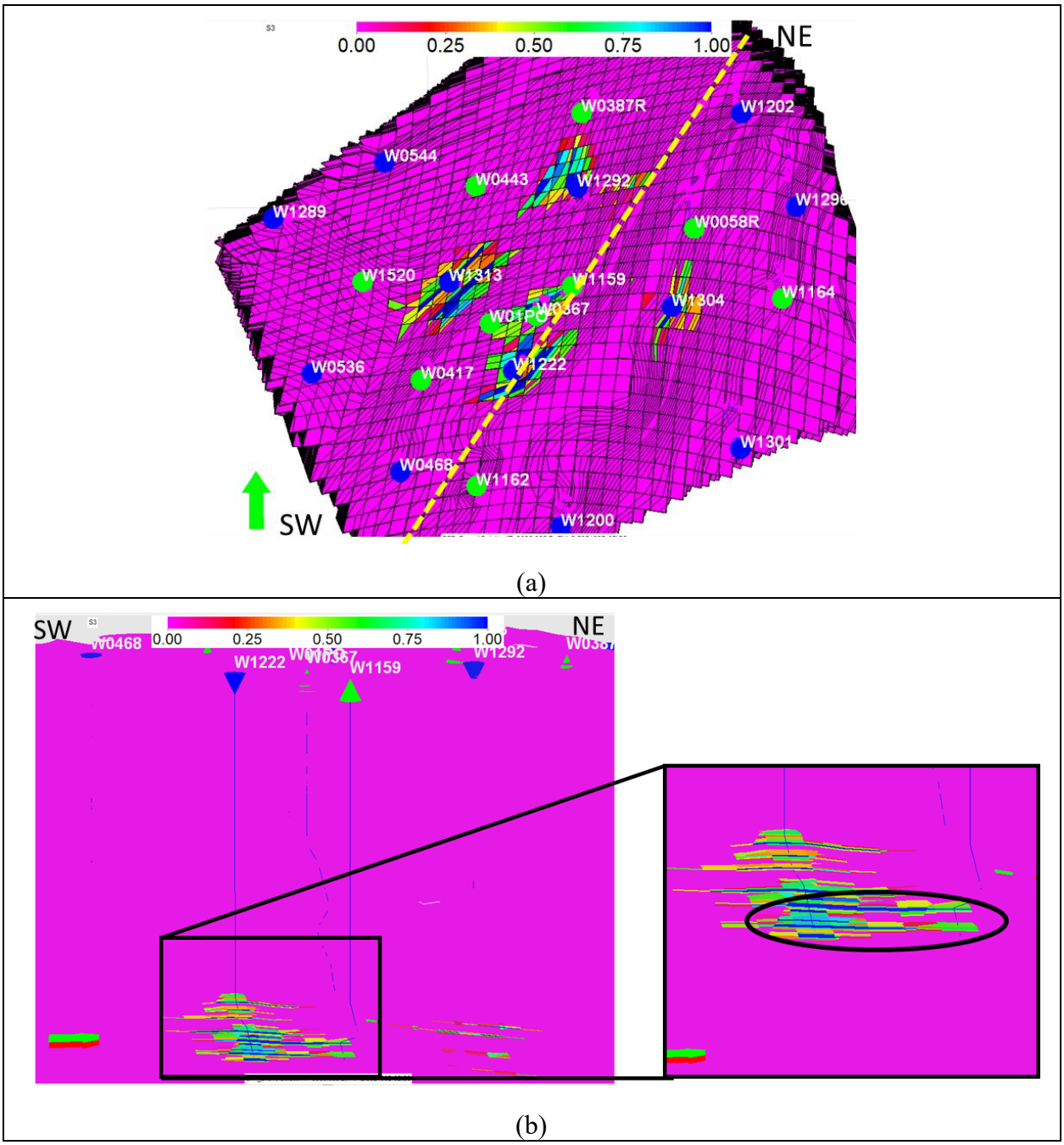

(a)

(b)

Figure 5.34. (a) ME saturation at Nov 2022 (b) Cross-section SW-NE with ME saturation between wells 1222 and 1159.

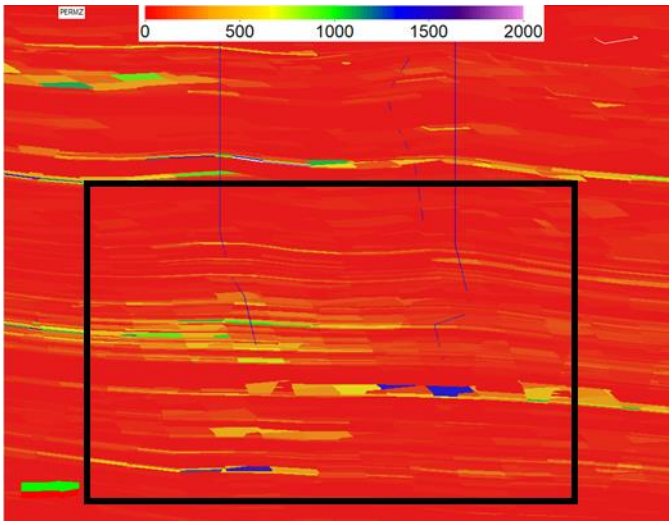

Figure 5.35. Vertical view of permeability in z direction.

The high variation of vertical permeability in Colombian field is a challenge for any process of waterflooding or EOR. In this particular case, the producer was contacted by the ME almost immediately after the SP slug begun injection. This effect could be prevented by increasing the polymer concentration for improving the mobility control, SP slug stability and avoiding the fingering from the slug.

On the other hand, despite this particular channeling, the effect of SP in the reservoir is almost negligible. Therefore, its necessary to review the water salinity variations with time. This parameter is fundamental to reach the desire Type III where the lowest IFT can be achieved. Figure 5.36 depicts the optimum salinity window limited by CSEL and CSEU and the water salinity for the Well 1159. As is illustrated, the salinity of the produced water is not low enough to achieve the Type III low interfacial tension. The fresh water injection is not sufficient for lowering water salinity of the reservoir.

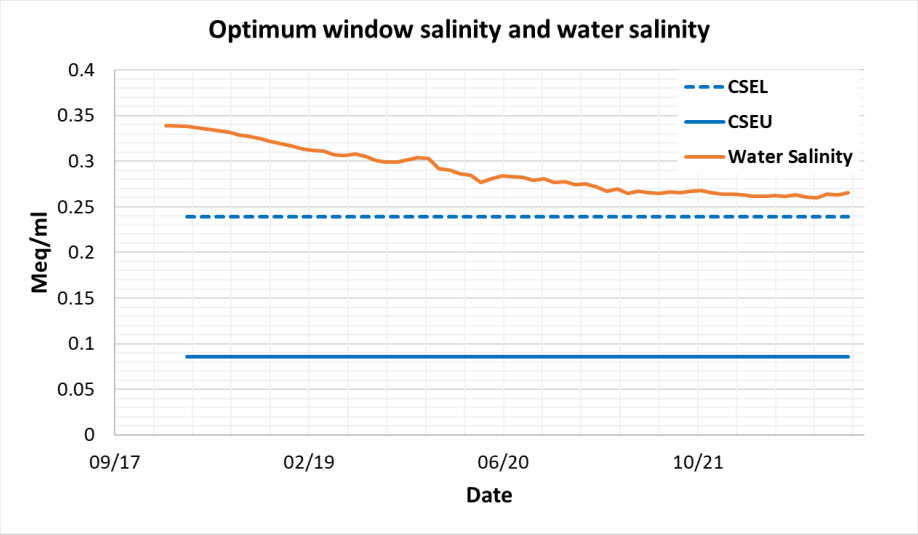

Figure 5.36. Optimum water salinity and water salinity of Well 1159.

5.4.1.1 Well 01PO analysis

Figures 5.37 shows the oil production rate comparison of the PF and SPF simulations. The production plot shows that the Well 01PO is having an oil bank breakthrough after 2 years after the start of the SP injection.

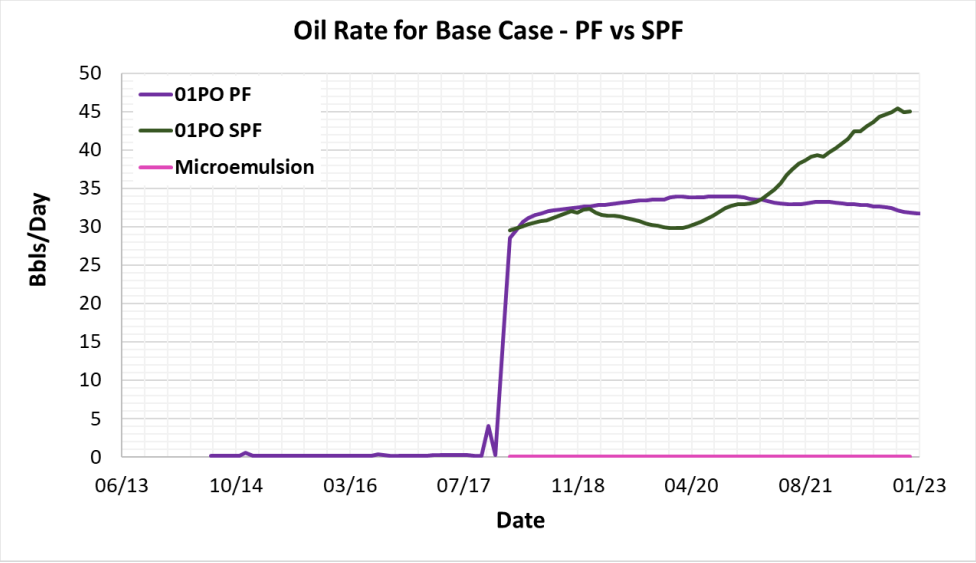

Figure 5.37. Oil rate comparison of PF vs SPF and ME rate for Well 01PO.

Unlike the Well 1159, Well 01PO shows no ME production. This could be explained because after the oil bank the ME is seen in the producer.

Figure 5.38 shows the Type III salinity window versus time for Well 01PO. According to the results of Well 1159, it was expected that the salinity concentration of water does not met the salinity required to reach the ME Type III. The possible clues for the oil breakthrough in the producer will be explained below.

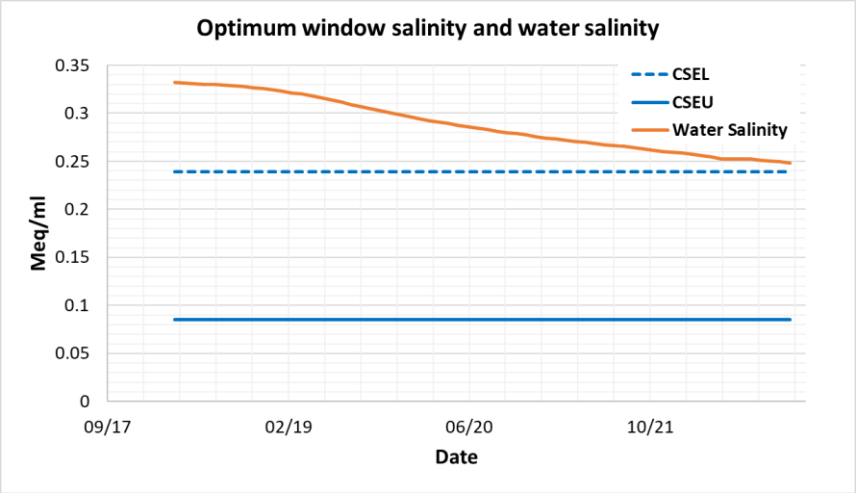

Figure 5.38. Oil rate comparison of PF vs SPF and ME rate for Well 01PO.

Figure 5.39 represents a series of oil saturation maps at different pore volumes injected. The maps are showing how the well 01PO is been affected by two well injectors 1313 and 1222. The producer well is strategically located at half distance of each injector. An evident oil bank is moving from the injector Well 1313 to the oil producer as the plots at the beginning of the injection as Figures 5.39 (a), (b) and (c) are showing. The color magenta represents zero percent of oil saturation. This means that the remaining oil saturation (ROS) is mobilized by the surfactant injection. The SP slug has replaced the oil i with a Type II(+)microemulsion phase.

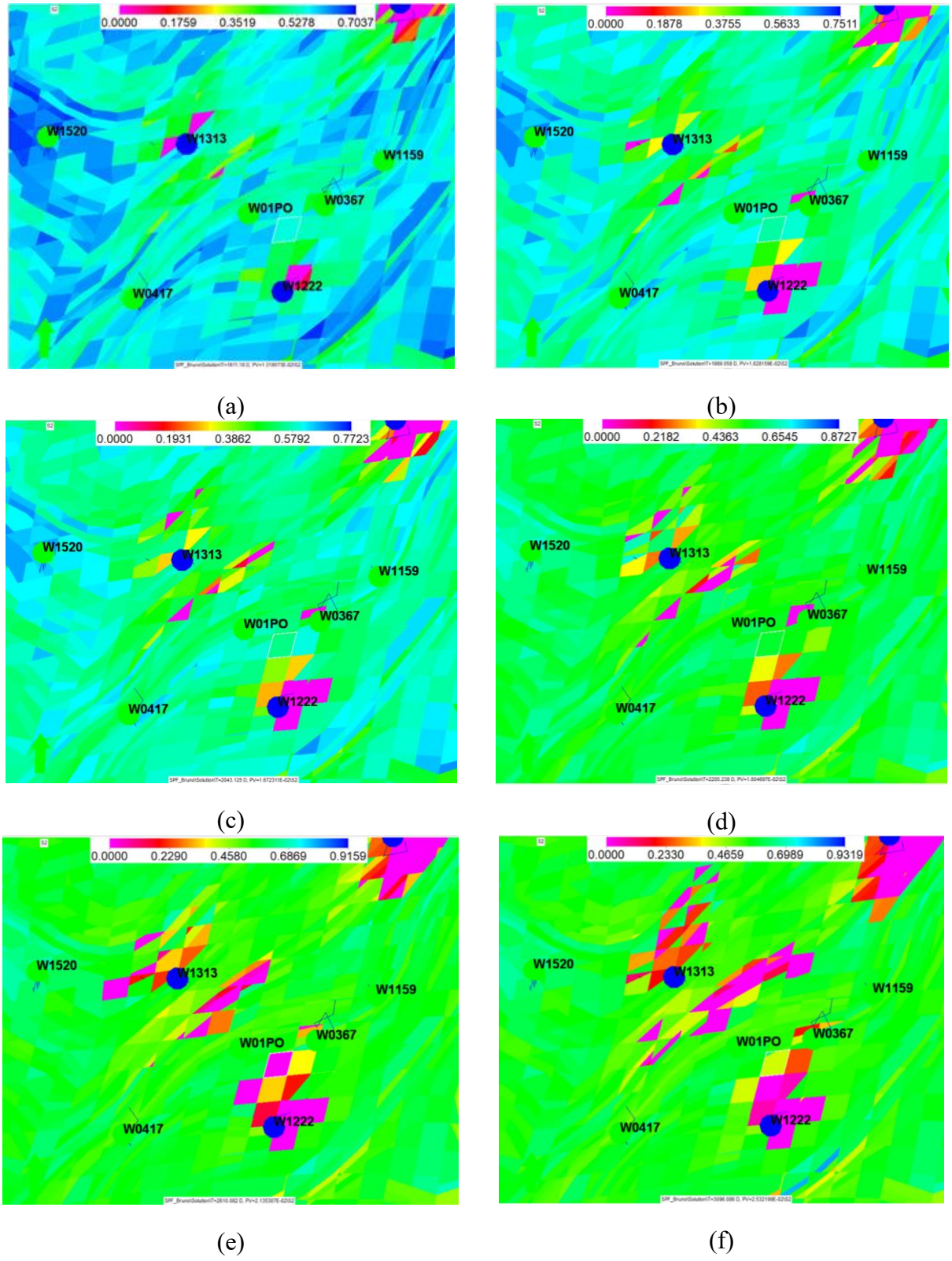

Figure 5.39. Oil saturation maps at A sands (a) 0.013 PVI (b) 0.016 PVI (c) 0.017 PVI (d) 0.018 PVI (e) 0.021 PVI (f) 0.025 PVI.

The case of SPF injection did not fulfill the expectations of an additional oil recovery for the reduction of the ROS in A reservoir sands. The reservoir water salinity does not match the optimum salinity defined in Figure 4.16. As a result, the region of highest solubility ratio (ultralow IFT) was not reached and possibly the mobility requirement was not achieved.

A channeling of ME phase is seen in the Well 1159 demonstrated that A sands has a drastic permeability variation layer by layer. Additionally, the fingering of the ME could be avoided by increasing the polymer drive viscosity and injection time in order to ensure the stability and mobility control of the slug.

5.5 Economical Evaluation For Base Cases with PF and SPF.

The oil industry is intrinsically focused on the revenues associated to the company's projects. The economic feasibility of a project is critical at the time of feasibility assessment of the proposed projects in the development plans. The total CAPEX and OPEX cost of a project should be evaluated carefully because the dynamic oil market is a relevant variable that could stop whole exploration or production project. Figure 5.40 is an example of the West Texas Intermediate (WTI) crude oil price variability from the last six years. The average price for the end of 2019 is around 55 USD/Bbl and the U.S EIA November Short-Term Energy Outlook (2019) foresees lower crude oil prices in 2020 than in 2019 as a result of the rising global oil inventories, mostly in the first half of next year.

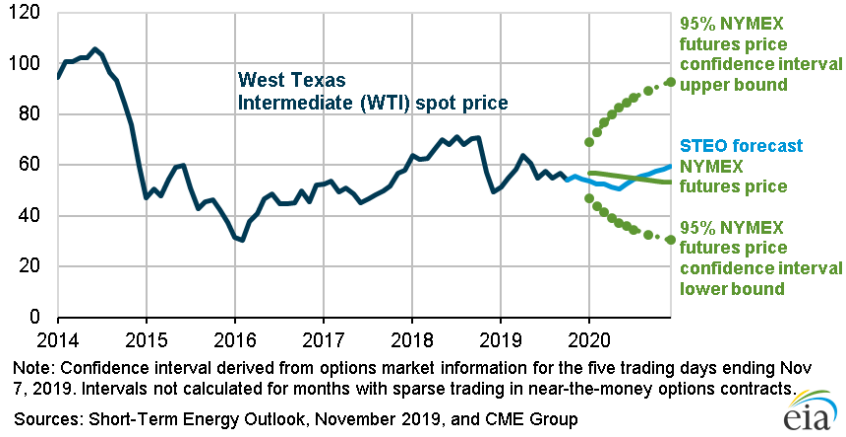

Figure 5.40. West Texas Intermediate (WTI) crude oil price and NYMEX confidence intervals (U.S. EIA, 2019)

A widely used parameter for calculating an estimate of project profitability is the net present value (NPV) which is the value of cash flow at specified discount rate. (Alusta et al., 2012). This estimation implies the existent risk in the future when the project calculation is extended to a long term. This parameter is having into account all the project investments made in the field.

$$NPV = \sum_{t=0}^{n} \frac{R_t}{(1+i)^t}$$

where $R_t$is the net cash inflows – outflows during a single period t. i is the discount rate and the t is the number of months.

Additionally, the NPV could be used for the comparison of different probabilities according to the variation of determined parameters such the volatile oil price or the material cost.

The incremental oil associated to the PF in the base case from the UTCHEMRS results will be economically evaluated. Table 5.10 shows the parameters used for this exercise which were provided by the Colombian company. The discount rate is assumed as 8% yearly. The crude oil price is assumed as a variable according to the price range shown in Figure 5.40. Therefore, the results below will show the NPV calculations with sensitivities of the crude oil price per barrel.

5.5.1 Polymer flooding base case evaluation

The economic evaluation for the PF is made during the simulation time i.e. from February 2018 to December 2023.

Parameter	Value	Units
Crude oil price per barrel	30-70	USD/Barrel
Operational plant cost	320	MMUSD/month
Polymer cost	3.79	USD/Kg
Polymer concentration	533	ppm
Discount rate	8%	per year
	0.64%	per month

Table 5.11. Parameters for the NPV calculation for the base case of PF.

Figure 5.41 shows the investment versus the cash flow of the incremental oil for PF. The black line, which is the net cash flow, is the difference between the cost and the cash flow per the incremental oil produced. For this plot the calculation is with the average oil price of 55 USD/Bbl. Figure 5.42 presents the net cash flow at different crude oil prices of 30, 50, and 70 USD/Bbl. Since the polymer and operational investment are not variables in this exercise; the cost of chemical and operations per barrel is 12.3 USD.

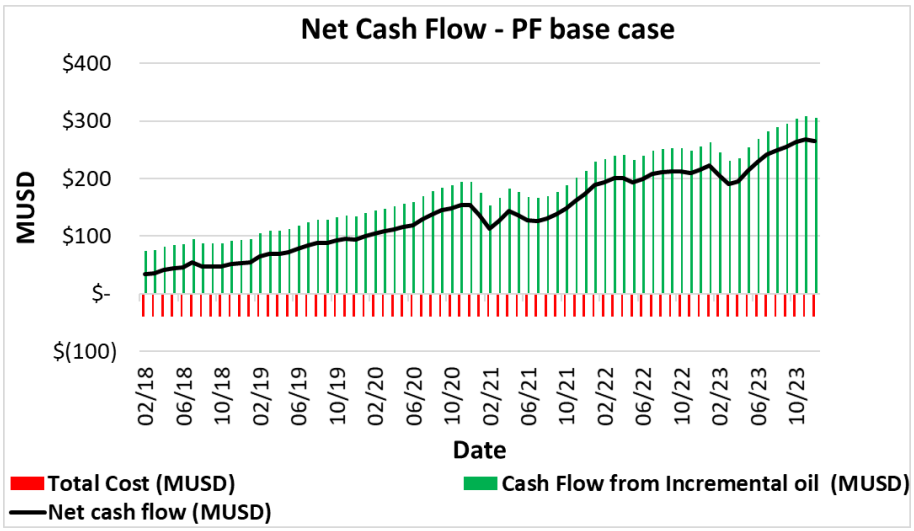

Figure 5.41. Net cash flow plot for PF base case with crude oil price of 55 USD/Bbl

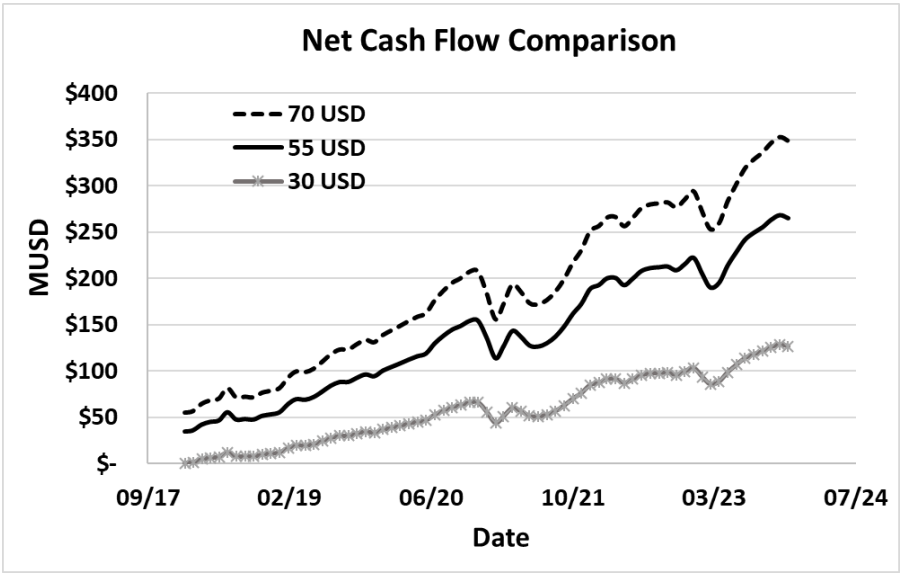

Figure 5.42. Net cash flow comparison for crude oil price of 70, 55 and 30 USD/ Bbl.

Table 5.11 reveals the NPV for each oil price scenario. Even for the lowest crude oil price the project is still profitable for more than 2.6 MMUSD. In the case of an average crude oil price the NPV is positive for 6.2 MMUSD. If the operation and the polymer costs are stable during the time, this project is profitable by 13 USD/Bbl.

Since this project is not assuming a CAPEX cost or capital cost as installations of water flooding and chemical injection or the drilling of new wells and only assumes the OPEX cost or operation cost, the project is economically beneficial for the company in all three scenarios.

NPV (MMUSD)	
WTI 70 USD/Bbl	$ 8.47
WTI 55 USD/Bbl	$ 6.27
WTI 30 USD/Bbl	$ 2.60

Table 5.12. NPV results for different crude oil prices.

5.5.2 Surfactant Polymer flooding base case evaluation

The SPF results for the base case are evaluated economically in order to rank the most applicable EOR process in the Colombian field. Table 5.12 displays the parameters used for the SP slug and polymer drive slug. The discount rate is assumed as 8% yearly. The crude oil price is assumed as a variable according to the price range shown in Figure 5.40.

Parameter	Value	Units
Crude oil price per barrel	70	USD/Bbl
Operational plant cost	320	KUSD/month
Polymer cost	3.79	USD/Kg
Polymer concentration	533 to 760	ppm
Surfactant cost	5.51	USD/Kg
Discount rate	8%	per year
	0.64%	per month

Table 5.13. Parameters for the NPV calculation for the base case of SPF.

Figure 5.43 shows the investment versus the cash flow of the incremental oil associated to the SPF. For this plot the calculation is with the average oil price of 55 USD/Bbl. The investment for this case is higher than PF for two main reasons: the surfactant product is more expensive than polymer and the surfactant concentration for this case is 1.0 wt% versus the polymer concentration that is approximately 0.04 wt%.

Additionally, the low recovery for the SP injection based on hypothetical phase behavior assumptions and injection design made the project drastically less competitive. Figure 5.44 presents the net cash flow at different crude oil prices of 30, 50, and 70 USD/Bbl. Since the polymer, surfactant and operational investment are not variables in this exercise; the cost of chemical and operations per Bbl is 137.46 USD.

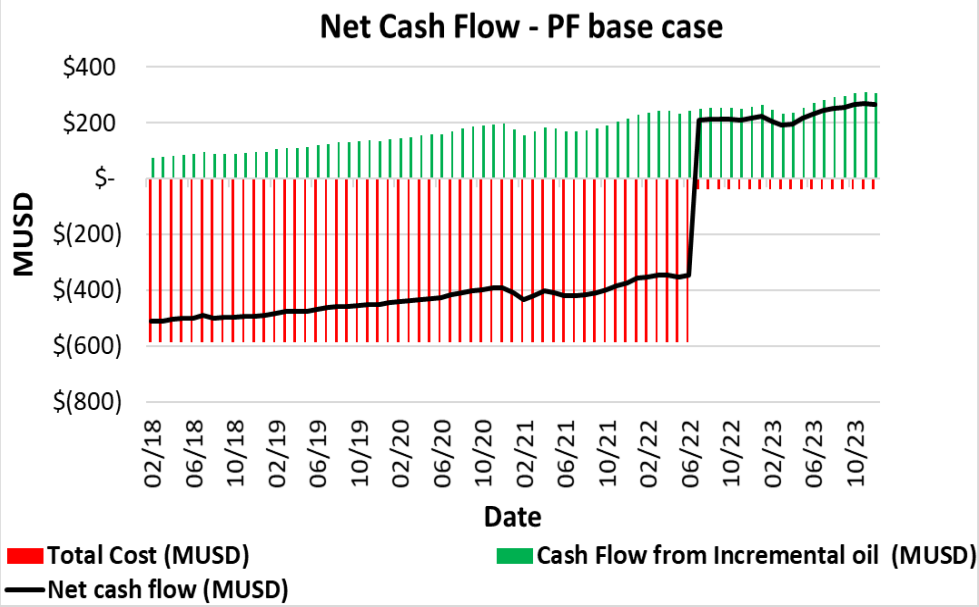

Figure 5.43. Net cash flow plot for SPF base case with crude oil price of 55 USD/Bbl

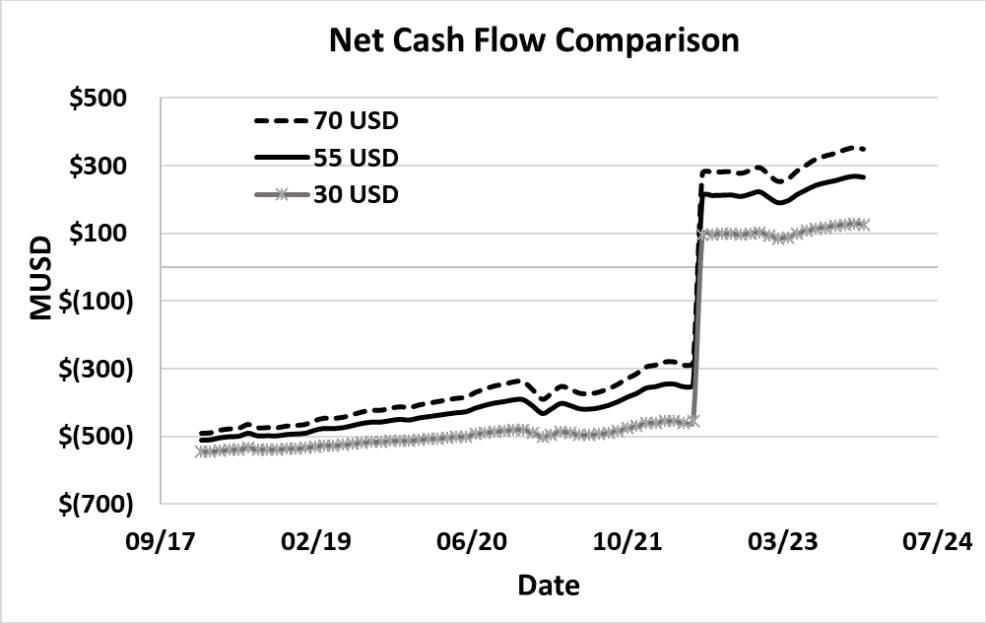

Figure 5.44. Net cash flow comparison at a crude oil price of 70, 55 and 30 USD/Bbl.

NPV (MMUSD)		
WTI 70 USD/Bbl	$	(9.90)
WTI 55 USD/Bbl	$	(12.10)
WTI 30 USD/Bbl	$	(15.77)

Table 5.14. NPV results per crude oil scenario.

Table 5.13 reveals the NPV for each oil price scenario. Even for the highest scenario of crude oil price the project is unprofitable by 9.9 MMUSD. In the case of an average crude oil price the NPV is negative by 12.1 MMUSD. If polymer and surfactant costs are stable during the SPF operation, the project tarts becomeprofitable with a crude oil price of 138 USD/ Bbl.

This project is depending on more detailed research that give us more clarity regarding to the optimum salinity to reach the lowest IFT. This could turn into an economically efficient optimization for the Colombian company. Meanwhile, the SPF project is economically adverse for the company in all three scenarios evaluated.

Chapter 6. Conclusions and Future Work

In this chapter, the work presented in this research will be summarized and concluded with more relevant findings for the optimal development of Colombian field through the EOR processes. Subsequently, recommendations for future work are presented.

6.1 Summary and Conclusions

An ECLIPSE sector model of a field case was transferred to UTCHEMRS and INTERSECT reservoir simulators. This model migration included the conversion of the reservoir geometry, reservoir properties, well locations, and well completion/perforation data. The results of three simulators were in fairly good agreement during HM and forecast for WF and PF. The close match for the base cases of three different simulators has given a confidence to build additional flood scenarios using The University of Texas at Austin UTCHEMRS 2019.2.

The simulation of a hypothetical WF case without polymer injection during HM and forecast was the reference to evaluate the effectiveness of PF pilot in A sands. According to the results from three simulators the PF in Colombian field give a significant oil recovery in the sub sands A2 and A2i of A reservoir. With an additional recovery in a range of 7.3 to 12.8%. Furthermore, the polymer injection delays the water breakthrough lowering the water cut by 2 to 5% for different simulators. The positive effect of PF on the increase in oil production makes this base case is a profitable project for the Colombian company with a positive NPV of 6.27 MMUSD.

The positive results of PF in A2 and A2i open the option of testing the same technology in a reservoir structurally lower than A sands, called B sands. The results of injecting polymer in both reservoirs simultaneously were considered as non-conclusive due to the few wells currently in B sands in the pilot area and their locations in areas with likely high water saturations. The initial results reveal that this case seems a counterproductive scenario with 3% lower recovery than the original case. Therefore, a new scenario was required to evaluate the true potential of B sands.

An additional main case was designed with the purpose of testing the PF in B sands in three new wells drilled infill the injectors 1292 and 1313 and the producer Well 443. The additional

wells reduce the spacing by half between the injector and the producer. The scenario proposes both production and the selective injection by single formation. The cases presented were: only production/injection in A sands and only production/injection in B sands. WF and PF scenarios were simulated in order to identifying the incremental oil recovery associated with PF for each reservoir. The current Well 443 was also evaluated. The oil recovery results per sand were comparable with the previous analyses for the other existing wells. For A and B sands the oil recovery computed were 7% and 2% respectively.

The new infill producers NW01, NW02 and NW04, were tested with the polymer injection in each formation A and B sands. After the analysis of UTCHEMRS results for the selective injection and single production wells, the PF influence in both sands is appreciable as areally and vertically. This causes a delay in the early arrival of water and increase oil production from layers with lower permeability. The 3D plots evidence the heterogeneous vertical permeability that influences in the early breakthrough of water. Although, it was also possible to realize that polymer is helping with a more homogenized flood front sweeping a larger region than WF. This front might cause the formation of oil bank and delays the breakthrough of water. Therefore, reducing the water cut by 3% to 10%. The oil recovery in those wells for A sand is in a range of 18.6 to 46% and for B sands of 14 to 42 % The significant oil production is likely associated with an oil bank breakthrough. The new producers were near to the oil bank created for the previous polymer injected (apply for A sands) plus the polymer injected for the forecast simulation.

The well locations are no in a drained area plus their position respect to the polymer front could be the key to formation of the oil bank. The positive response of B2c and B2d sands of the new infill drills ton the polymer injection gives prospect to extend the polymer pilot to the lower sands. However, additional simulations are needed to strengthen this interpretation.

The SPF case was tested in the A2 and A2i reservoir sands with negligible incremental oil recovery compared to PF presented above. The analysis of the results defined that although the injection water is fresh but is not enough to reach the optimum salinity defined according to the surfactant phase behavior formulation assumed. As a result, the lowest IFT was not achieved and

subsequently the ROS was not mobilized. However, a sectorized oil recovery benefit was evident due to a possible fully miscible displacement. More research and simulation cases will be needed to determine the feasibility of SPF in A sands of the Colombian field.

The vertical heterogeneity in A sands represents a challenge for any mechanism of EOR. A ME channeling was noted in Well 1159 demonstrated that A sands has considerable permeability variations layer by layer. Additionally, the possible ME fingering could be avoided by the increasing polymer viscosity in polymer drive and SP slug ensuring the stability and mobility control of the slug.

6.2 FUTURE WORK

The consistent disagreement of the three simulators with the field data at the beginning of the HM could be an indication to review the geological and dynamic model. A correct grid population of properties and an adequate hydraulic connectivity, which is crucial for the EOR processes studied in this research, may help to improve the reliability of the geomodel imported to improve the simulation results.

Considering the high complexity and heterogeneity of the reservoir o considered here, it is necessary to conduct the frequent well tests such as pressure, production, injectivity, and fluid test in strategic locations of the reservoir. This could help to better understand the nature of the reservoir. In addition, the inclusion of tracer results could help to refine the model connectivity.

The implementation of the gas phase in UTCHEMRS will strengthen the simulation capability for field cases and will guarantee more reliable results.

The positive result of this research recommends the implementation of the PF expansion in A2 and A2i reservoir sands of the Colombian field.

Laboratory tests to develop surfactant formulation tailored for the reservoir conditions of A sands are recommended. Dynamic coreflood results will aid in optimizing the injection strategy and obtain critical data of microemulsion viscosity, recovery factor, surfactant retention, polymer viscosity to use in future SPF pilot simulations.

Glossary

NOMENCLATURE/ ABBREVIATIONS

AIM	Adaptive Implicit Method
AKN	Alkane Carbon Number
Bbl	Barrel
Bbls	Barrels
Bopd	Barrels of oil per day
CAPEX	Capital Expenditure
CDC	Capillary Desaturation Curve
CDM	Capillary Desaturation Model
CEOR	Chemical Enhanced Oil Recovery
CMC	Critical Micelle Concentration
CPG	Corner Point Geometry
EOR	Enhanced Oil Recovery
HM	History Match
HPAM	Hydrolyzed Polyacrylamide
IFT	Interfacial Tension
ILT	Injection Logging Test
IMPEC	Implicit Pressure Explicit Compositions
M	Mobility Ratio
MBbls	Thousands of barrels
ME	Microemulsion
MMBbls	Millions of barrels
MMUSD	Millions of American dollars
MPB	Microemulsion Phase Behavior
MUSD	Thousands of American dollars
NE	North East
NW	North West
OPEX	Operative Expenditure
PF	Polymer Flooding
PV	Pore Volume
PVI	Pore Volume Injected
PVT	Pressure, Volume and Temperature
ROIP	Remaining Oil In Place
ROS	Residual Oil Saturation
RT	Rock Type
SE	South East
SP	Surfactant - Polymer
SPF	Surfactant Polymer Flooding
SW	South West
TVD	True Vertical Depth
USD	American Dollars
VDP	Dykstra-Parsons Coefficient
WF	Water Flooding
WTI	West Texas Intermediate

SI METRIC CONVERSION FACTORS

ft	x	3.048	e-01	=	m
ft^3	x	3.048	e-01	=	m^3
cP	x	1.0	e-03	=	$Pa * s$
psi	x	6.895	e+00	=	kPa
mD	x	1e-15	e+00	=	m^2
Bbl	x	1.6	e-01	=	m^3

Bibliography

Alusta, G. A., Mackay, E. J., Fennema, J., Armih, K., et al. 2012. EOR vs. Infill Well Drilling: Sensitivity to Operational and Economic Parameters. Society of Petroleum Engineers. SPE-143300. doi:10.2118/150454-MS.

Araktingi, U.G., Orr, F.M. 1993. A Particle Tracking Computational Technique is Applied to Investigate how Viscous Fingers Form and Grow in Heterogeneous Porous Media. SPE Advanced Technology Series, Vol. 1, No. 1.

Baran, J.R, Jr. 2000. Winsor I, III, II Microemulsion Phase Behavior of hydrofluoroethers and Fluorocarbon/Hydrocarbon Cationic Surfactants. Journal of Colloid and Interface Science 234, 117–121. https://doi:10.1006/jcis.2000.7284

Bird, R.B., Stewart, W.E., Lighfoot, E.N. 2002. Transport Phenomena, second ed. New York, John Wiley and Sons.

Bordeaux, F. R. 2016. Modelos Rápidos de simulação aplicados à injeção de polímeros em reservatórios heterogéneos. Campinas State University. MS Dissertation from Department of Mechanical Engineering and Geosciences Institute. Campinas.

Bryce, Robert. 2010. Power Hungry, Austin, TX, Public Affairs.

Chang, L., Jang, S. H., Taghavifar, M., & Pope, G. A. 2018. Structure-Property Model for Microemulsion Phase Behavior. Presented at the SPE Improved Oil Recovery Conference, Society of Petroleum Engineers. SPE-190153-MS. https://doi.org/10.2118/190153-MS

Chatzis, I., Morrow, N.R. 1984. Correlation of Capillary Number Relationships for Sandstone, New Mexico, Society of Petroleum Engineers Journal, Vol. 24, No. 5. 555–562. https://doi.org/10.2118/10114-PA

Clifford, P. J., Sorbie, K. S. 1985. The Effects of Chemical Degradation on Polymer Flooding. Presented at SPE Oilfield and Geothermal Chemistry Symposium, 9-11 March, Phoenix, Arizona. SPE-13586-MS. https://doi:10.2118/13586-MS.

Delshad, M., Pope, G.A., and Sepehrnoori, K. 1996. A Compositional Simulator for Modeling Surfactant Enhanced Aquifer Remediation, 1 Formulation. J. Contaminant. Hydrology. Vol. 23, No. 4: 303-327. https://doi.org/10.1016/0169-7722(95)00106-9

Fernandes, R. B. 2019. Development of Adaptive Implicit Chemical and Compositional Reservoir Simulators. PhD Dissertation, The University of Texas at Austin. Austin, Texas.

Gheneim, T., Azancot, A., Acosta, T., Zapata, J, F. et al. 2017. Enhanced Oil Recovery in a High Stratigraphic Complex Reservoir: Casabe Project Case Study. Presented at Abu Dhabi International Petroleum Exhibition & Conference, 13-16 November, Abu Dhabi, UAE. SPE-188555-MS. https://doi:10.2118/188555-MS

Gogarty, W. B. 1967. Mobility Control with Polymer Solutions. SPE Journal Vol. 7, No. 2. SPE-1566-B. https://doi:10.2118/1566-B

Green, D.W., Willhite, G.P., 1998. Enhanced Oil Recovery, volume 6. Richardson, Texas, SPE Textbook Series.

Guo, H., Dou, M., Hanqing, W. et al. 2015. Review of Capillary Number in Chemical Enhanced Oil Recovery. Presented at the SPE Kuwait Oil and Gas Show Conference, Mishref, Kuwait, 11–14 October. SPE-175172-MS. https://doi.org/10.2118/175172-MS

Homsy, G. M. 1987. Viscous Fingering in porous media. Ann. Rev. Fluid Mech. Vol 19, pp. 271-311.

Huh, C. 1979. Interfacial Tensions and Solubilizing Ability of a Microemulsion Phase That Coexists with Oil and Brine. Houston, Texas. Journal of Colloid and Interface Science. Vol. 71, No. 2. 408–426. https://doi.org/10.1016/0021-9797(79)90249-2

ICP. 2019. Experimental evaluation and selection of polyacrylamide base polymers, Piedecuesta, Santander.

Lake, L.W., Johns, R.T., Rossen, W.R., Pope, G.A. 2014. Fundamentals of Enhanced Oil Recovery, second ed. Richardson, Texas, SPE.

Lashgari, H.R., Pope, G.A., Taghavifar, M., et al. 2018. A new three-phase microemulsion relative permeability model for chemical flooding reservoir simulators. J. Pet. Sci. Eng.

Morrow, N.R. 1979. Interplay of Capillary, viscous and buoyancy forces in the mobilization of residual oil, Socorro, New Mexico, JCPT.

Needham, R. B.; Doe, P. H. 1987. Polymer Flooding Review. Journal of Petroleum Technology. Vol. 39, No. 12.:1503 – 1507. SPE-17140-PA. https://doi.org/10.2118/17140-PA

Omar, A. E. 1983. Effect of Polymer Adsorption on Mobility Ratio. Presented at Middle East Oil Technical Conference and Exhibition, 14-17 March, Manama, Bahrain. SPE-11503-MS. https://doi:10.2118/11503-MS

Pope, G.A., Nelson, R. C. 1978. A Chemical Flooding Compositional Simulator. SPE Journal. Vol. 18, No. 5. 339-354. SPE-6725-PA. https://doi.org/10.2118/6725-PA

Pyrcz, M., Deutsch, C.V. 2014. Geostatistical Reservoir Modeling, second ed. New York, NY. Oxford University Press.

Reed, R. L. and Healy, R. H. 1977. Some Physico-Chemical Aspects of Microemulsion Flooding: A Review, Improved Oil Recovery by Surfactant and Polymer Flooding, D.O. Shah and R.S. Schechter (eds.). New York City. Academic Press.383-437.

Sahni, A., Dehghani, K., Prieditis, J., & Johnson, S. G. 2005. Benchmarking Heterogeneity of Simulation Models. Presented at SPE Annual Technical Conference and Exhibition, 9-12 October, Dallas, Texas SPE-96838-MS. https://doi:10.2118/96838-MS

Schowalter, W.R. 1977. Mechanics of Non-Newtonian Fluids, Oxford, Pergamon Press.

Sheng, J.J. 2013. Enhanced Oil Recovery Field Case Studies, Lubbock, Texas, Elsevier.

Slater, G. E., & Ali, S. M. F. 1970. Two-Dimensional Polymer Flood Simulation. Presented at the Fall Meeting of the Society of Petroleum Engineers of AIME, 4-7 October, Houston, Texas. SPE-3003-MS. https://doi:10.2118/3003-MS

Sorbie, K. S. 1991. Polymer-Improved Oil Recovery. Boca Raton, Florida, CRC Press.

Stegemeier, G. L. 1976. Mechanisms of Oil Entrapment and Mobilization in Porous Media. Presented at the AICHE Symposium on Improved Oil Recovery By Surfactant and Polymer Flooding, Kansas City, Missouri, 12-14 April.

Tavassoli, S. 2014. Investigation of the Effects of Buoyancy and Heterogeneity on the Performance of Surfactant Floods. PhD Dissertation, The University of Texas at Austin. Austin, Texas.

U.S. EIA. 2019. Short-Term Energy Outlook. U.S. Energy Information Administration. U.S. Department of Energy. Washington, District of Columbia, November. Retrieved November 13, 2019 from https://www.eia.gov/outlooks/steo/report/prices.php

UTCHEM, University of Texas Chemical Simulator. 2017. Technical Documentation 2017. Vol. 2. Austin, Texas. Center for Petroleum and Geosystems Engineering, The University of Texas at Austin.

Winsor, P. A. 1954. Solvent Properties of Amphiphilic Compounds. Butterworths, London.

Zhang, G., Seright, R.S. 2007. Conformance and Mobility Control: Foams vs. Polymers. Presented at International Symposium on Oilfield Chemistry, Houston, 28 Febraury-2 March. SPE-105907-MS. https://doi.org/10.2118/105907-MS